AFRL-ML-WP-TR-1998-4197

INVESTIGATIONS OF THE NONLINEAR OPTICAL RESPONSE OF COMPOSITE AND PHOTONIC BAND GAP MATERIALS

ROBERT NELSON

Materials & Manufacturing Directorate
Air Force Research Laboratory
Air Force Materiel Command
Wright-Patterson AFB OH 45433-7734

NOVEMBER 1998

FINAL REPORT FOR PERIOD 09/01/93 – 09/24/98

Approved for public release; distribution unlimited

MATERIALS & MANUFACTURING DIRECTORATE
AIR FORCE RESEARCH LABORATORY
AIR FORCE MATERIEL COMMAND
WRIGHT-PATTERSON AIR FORCE BASE, OH 45433-7734

NOTICE

USING GOVERNMENT DRAWINGS, SPECIFICATIONS, OR OTHER DATA INCLUDED IN THIS DOCUMENT FOR ANY PURPOSE OTHER THAN GOVERNMENT PROCUREMENT DOES NOT IN ANY WAY OBLIGATE THE US GOVERNMENT. THE FACT THAT THE GOVERNMENT FORMULATED OR SUPPLIED THE DRAWINGS, SPECIFICATIONS, OR OTHER DATA DOES NOT LICENSE THE HOLDER OR ANY OTHER PERSON OR CORPORATION OR CONVEY ANY RIGHTS OR PERMISSION TO MANUFACTURE, USE, OR SELL ANY PATENTED INVENTION THAT MAY RELATE TO THEM.

THIS REPORT IS RELEASABLE TO THE NATIONAL TECHNICAL INFORMATION SERVICE (NTIS). AT NTIS, IT WILL BE AVAILABLE TO THE GENERAL PUBLIC, INCLUDING FOREIGN NATIONS.

THIS TECHNICAL REPORT HAS BEEN REVIEWED AND IS APPROVED FOR PUBLICATION.

Robert L. Nelson

ROBERT L. NELSON, Project Engineer
Sensor Materials Branch
Survivability & Sensor Materials Division

Robert L Denison

ROBERT L. DENISON, Chief
Sensor Materials Branch
Survivability & Sensor Materials Division

William R Woody

WILLIAM R. WOODY, Chief
Survivability & Sensor Materials Division
Materials & Manufacturing Directorate

Do not return copies of this report unless contractual obligations or notice on a specific document require its return.

REPORT DOCUMENTATION PAGE

Form Approved
OMB No. 0704-0188

1. AGENCY USE ONLY *(Leave blank)*	2. REPORT DATE	3. REPORT TYPE AND DATES COVERED
	NOV 98	final 09/01/93 - 09/24/98

4. TITLE AND SUBTITLE
INVESTIGATIONS OF THE NONLINEAR OPTICAL RESPONSE OF COMPOSITE AND PHOTONIC BAND GAP MATERIALS

5. FUNDING NUMBERS
PE: 63202F
PR: 4348
TA: IH
WU: RD

6. AUTHOR(S)
ROBERT L. NELSON

7. PERFORMING ORGANIZATION NAME(S) AND ADDRESS(ES)
MATERIALS DIRECTORATE
AIR FORCE RESEARCH LABORATORY
AIR FORCE MATERIAL COMMAND
WRIGHT PATTERSON AFB OH 45433-7734

8. PERFORMING ORGANIZATION REPORT NUMBER

9. SPONSORING/MONITORING AGENCY NAME(S) AND ADDRESS(ES)
Materials & Manufacturing Directorate
Air Force Research Laboratory
Air Force Materiel Command
Wright-Patterson Air Force Base, OH 45433-7734
POC: Robert Nelson, AFRL/MLPO, 937-255-4474 x3216

10. SPONSORING/MONITORING AGENCY REPORT NUMBER
AFRL-ML-WP-TR-1998-4200

11. SUPPLEMENTARY NOTES

12a. DISTRIBUTION AVAILABILITY STATEMENT
APPROVED FOR PUBLIC RELEASE; DISTRIBUTION IS UNLIMITED

12b. DISTRIBUTION CODE

13. ABSTRACT *(Maximum 200 words)*
This report is a doctoral thesis on the nonlinear optical properties of composite and photonic band gap optical materials. Emphasis is placed on the enhancement effect in both types of structures where the effective nonlinearity is greater than the nonlinearity of either of the constituent materials.

14. SUBJECT TERMS
nonlinear optics, electrooptics, second harmonic generation, composite optical materials, photonic band gap optical materials

15. NUMBER OF PAGES
125

16. PRICE CODE

17. SECURITY CLASSIFICATION OF REPORT	18. SECURITY CLASSIFICATION OF THIS PAGE	19. SECURITY CLASSIFICATION OF ABSTRACT	20. LIMITATION OF ABSTRACT
UNCLASSIFIED	UNCLASSIFIED	UNCLASSIFIED	SAR

Curriculum Vitae

Robert Lorne Nelson was born in Eau Claire, Wisconsin on July 3, 1965. He attended the University of Wisconsin, Eau Claire from 1983 to 1987, and graduated with a Bachelor of Science degree in physics. After working four years as an instructor for the Naval Nuclear Power School, he decided to return to school to pursue a PhD under the sponsorship of the U. S. Air Force Palace Knight program. He began his graduate studies at the Institute of Optics at the University of Rochester in 1993. His thesis work has been conducted in the field of nonlinear optics under the supervision of Professor Robert W. Boyd.

Publications

R. L. Nelson, G. Kojoian, J. Seal, and D. H. Pearson, "Accurate Optical Positions for 107 Byurakan Objects and 11 Blue Stars from the 'Second Byurakan Spectral Sky Survey [I]'," Astronomical Journal **95**, 1678 (1987).

R. L. Nelson and R. W. Boyd, "Enhanced Electrooptic Response of Layered Composite Materials," submitted to Appl. Phys. Lett. (1998).

R. L. Nelson, R. W. Boyd, J. E. Sipe, and R. E. Perrin, "Nonlinear optical response of a dense Maxwell Garnett composite material," submitted to Phys. Rev. A (1998).

R. L. Nelson and R. W. Boyd, "Enhanced third-order nonlinear optical response of photonic band gap materials," submitted to J. of Mod. Opt. (1998).

Y. K. Yoon, R. L. Nelson, and R. W. Boyd, "Measurement of the nonlinear optical susceptibility of silver," submitted to Opt. Comm. (1998).

Acknowledgments

First I would like to thank my advisor, Professor Robert Boyd, for his assistance, support, and guidance in my graduate career. Useful insights could always be obtained in our discussions regarding the subtleties of nonlinear optics. I also appreciate his enthusiasm for the subjects I chose to study.

The support of the people in the Air Force Materials Directorate was critical in the completion of this work. I am grateful for the generous offering of lab resources which enabled me to perform my work. In particular I would like to thank Mr. Bill Woody, Mr. Bob Denison, Mr. Robb Susnik, Mr. Gary Kepple, Dr. Ken Hopkins, Dr. Richard Sutherland, Dr. Frank Szmulowicz, Dr. Dave Zelmon, Mr. Gerry Landis, Mr. Ron Perrin, Mr. Tom Kensky and Mr. James Drummond for all their assistance.

I would also like to thank all my colleagues and friends at the Institute of Optics for making my time there productive and enjoyable.

Finally I want to thank all my family and friends who made this possible through their support and encouragement. I would especially like to acknowledge my undergraduate mentor, the late Dr. Gabriel Kojoian, who gave me the early guidance and encouragement necessary to pursue a career in science.

Support for this work was provided by the U. S. Air Force Materials Directorate and the Palace Knight program.

Abstract

There has been much recent interest in the development of nonlinear optical composite materials as they can posses large values of the nonlinear susceptibility. A nonlinear optical composite material is capable of enhancing the nonlinear response of its component materials due to the nonuniform electric field distribution between the constituents. For this reason the effective bulk nonlinear optical susceptibility is not typically given by the volume weighted average of the individual susceptibilities. It is the goal of the present work to investigate the enhancement effect of second-order and third-order nonlinear optical composite materials as well as third-order photonic band gap materials and also to consider the accuracy of nonlinear effective medium theory.

Layered optical composite materials can enhance the nonlinear susceptibility for electric fields polarized normal to the plane of the layers. For enhancement to occur, the dominant nonlinear constituent must posses an optical dielectric constant lower than that of the other constituent. This is the usual condition for enhancement for all composite geometries. As a test of consistency of the nonlinear effective medium theory, predictions were compared against the results of the well accepted formalism for calculating second-harmonic generation in multilayer materials. In the calculations performed, the effective medium predictions were in consistent agreement with the more exact formalism. Also a third-order electrooptic layered composite material was constructed and the third-order susceptibility was measured for both the composite material and a homogeneous film of the nonlinear dominant material. The composite susceptibility was measured to be 3.2 times the susceptibility of the homogeneous material, in reasonable agreement with the predictions of effective medium theory.

In a digression from the optical composite materials mentioned above, another type of two-component material was studied for its ability to enhance the nonlinear optical response of a given homogeneous material. One-dimensional photonic band gap structures were analyzed for their ability to enhance the third-order response of their constituents. It was found that the third-order response of either a high refractive index or a low refractive index constituent could be enhanced near the photonic band edge of the band gap material. Typical enhancement factors were in the range of 4-6. Introduction of a central "defect" nonlinear region into the middle of the photonic band gap material resulted in an enhancement factor of approximately 30 over an equivalent length of homogeneous nonlinear material.

Finally the effective third-order nonlinear susceptibility of a Maxwell Garnett optical composite was calculated for a composite material with a nonlinear host medium and the spherical inclusions arranged on a simple cubic lattice. This allowed for a calculation that was accurate for all fill fractions up the close pack limit unlike previous treatments of such composites that were restricted to dilute fill fractions only. However there was surprisingly good agreement with the dilute limit results up to moderately high fill fractions.

Table of Contents

List of Figures

Chapter 1

Introduction

The linear and nonlinear properties of optical composite materials is an interesting field of study. The effective bulk optical properties can differ significantly from those of the constituents, especially in the nonlinear case. Optical composite materials also present the possibility of engineering bulk materials properties, an example of which is the use of form birefringence in layered composites to achieve phase matched second harmonic generation.[1] The many applications of nonlinear optical materials has led to intense recent interest in developing better material systems. Nonlinear optical composite materials offer the possibility of greatly enhanced nonlinear response over their homogeneous counterparts, therefore there has also been recent activity into the investigation of these materials for their potential application. This thesis addresses the characterization and determination of the nonlinear optical properties of composite optical materials.

The central problem is the determination and measurement of the effective, or average, bulk optical properties of composite optical materials. In particular we are interested in the susceptibilities $\chi^{(1)}$, $\chi^{(2)}$, and $\chi^{(3)}$. Before discussing the details of the effective averaging we must first define what we mean by composite. For the purposes of this thesis we use the following definition: an optical composite material is a mixture of two or more constituent materials whose individual regions are characterized by bulk optical quantities (many atoms thick), but much smaller than the optical wavelength of interest. If the composite is in the form of an inclusion-host type material, then the grain sizes and spacing are constrained in the same manner. Since material variations occur on a subwavelength scale, an incident optical wave will experience an effective average of the constituent materials. Therefore the macroscopic

fields and constants that appear in Maxwell's equations describing the macroscopic properties of the composite can be quite different than the fields and constants appearing on the scale of the material variations. The analysis of the local fields, on the scale of the material variations, that make up the macroscopic average is not unlike the problem of local fields at the microscopic, or atomic, scale.

Since the susceptibilities are phenomenological constants reflecting the linear and nonlinear polarizabilities of the medium, what we seek is the relationship between the macroscopic, or averaged, polarization and the macroscopic electric field. One of the earliest such efforts was due to Maxwell Garnett[2] who developed the linear effective medium theory for the geometry that bears his name (see figure 1.2). Since then effective linear optical properties of other geometries have been analyzed, but exact analytical expressions can be difficult if not impossible for most geometries. In that case empirical or semi-empirical analysis can be attempted. The nonlinear susceptibilities of composite materials are even more difficult to obtain since they are related to the higher order moments of the material scale electric field distribution .

The usual approach to the problem begins with the consideration of the mesoscopic field distribution. Then macroscopic quantities are derived through suitable averages. Mesoscopic refers to the scale in which the material variations occur which is between the microscopic (atomic) and macroscopic (wavelength) length scales. On the mesoscopic scale we describe field quantities using the electrostatic approximation which implies that the fields can be treated using static analysis since the distances are much less than an optical wavelength. Mesoscopic field distributions are strongly influenced by composite geometry, therefore the macroscopic effective susceptibility is not a simple weighted volume average of the constituent susceptibilities. In the nonlinear effective medium analysis however, it is these inhomogeneties that are crucial in providing interesting and useful macroscopic

nonlinear properties. In other words local field effects play a larger role in the description of nonlinear optical composites than in the description of linear optical averages.

1.1 All-dielectric Effective Medium Theory in Linear Optics

Analysis of the linear response of optical composites is aided by the existence of a set of bounds on the value of the effective medium dielectric constant. First we note that the linear dielectric constant is obviously bounded by the value of the constituent materials, but a more restrictive set of bounds is possible. The most well known are the Weiner[3] limits for composites with purely real dielectric constants. The Weiner limits depend only on the volume fill fraction, f, of the constituent materials and formally are given by

$$\sum_i f_i \varepsilon_i \geq \varepsilon_{eff} \geq \left[\sum_i \frac{f_i}{\varepsilon_i} \right]^{-1}. \tag{1.1}$$

An intuitive explanation of these limits can be attempted by examining the role of screening in dielectric composites. If a static electric field is incident on the surface of a dielectric, a screening charge will develop at the surface which is simply the bound polarization surface charge. The amount of screening charge will depend on the angle between the surface normal and the incident field which is most conveniently expressed as the well known boundary conditions for the electric and displacement fields at the surface. In explicit terms these are that the normal component of the displacement, **D**, and the tangential component of the electric field, **E**, are continuous at the interface between dielectrics. If the electric field is incident from a region of lower dielectric constant onto a region of higher dielectric constant, the screening charge acts to reduce the electric field inside the higher dielectric constant material and

therefore reduces its contribution to the average of the effective dielectric constant. The cases of maximum and zero screening are illustrated below in figure 1.1.

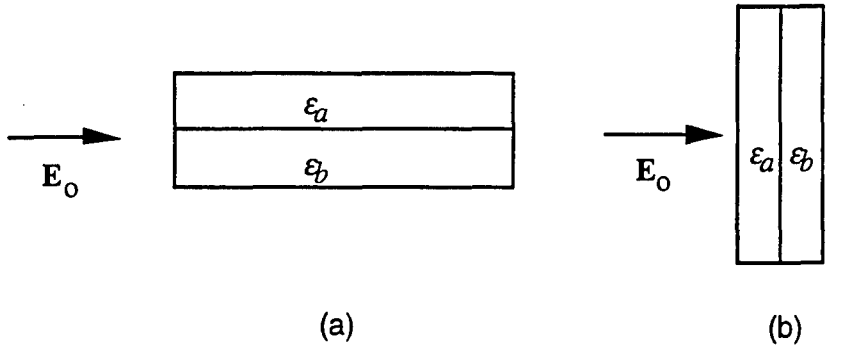

Figure 1.1 Limiting cases of screening with (a) no screening and (b) maximum screening

It is interesting to observe that with no screening we simply have the Weiner limit of ε_{eff} that is the volume weighted average ε. In the limit of maximum screening we have the other Weiner limit. Grains of composite material will have components of surface normals that are both perpendicular and parallel to the incident field, therefore a composite's effective medium dielectric constant will lie between these two limits and will always be less than or equal to the volume weighted average.

There are three well known composite geometries (figure 1.2) whose linear and to some extent nonlinear optical properties have been studied. Obviously there are an infinite number of possible geometries but these three are usually the starting point for consideration of composite materials. The layered composite geometry is unique for the following three reasons: it is not an isotropic composite like the other two, it is a composite in one of its dimensions only, and the mesoscopic fields are uniform. Also apparent is that the layered composite presents the two limiting cases of screening action described above and it will now be shown that its two principal effective dielectric constants are given by the Weiner limits. We use the electrostatic boundary

conditions requiring continuity of tangential **E** and normal component of **D** at the boundary between two dielectric media. Also by the symmetry of the layered composite we expect the effective medium to behave like a uniaxial crystal with optic axes perpendicular to the plane of the layers.

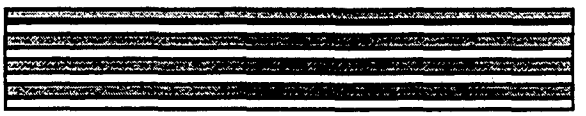

Layered Composite: The thickness of each layer is mesoscopic

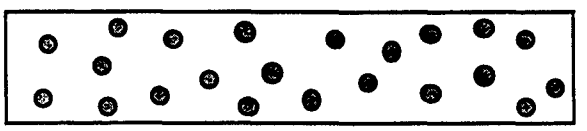

Maxwell Garnett Composite: The size and spacing of inclusions is mesoscopic

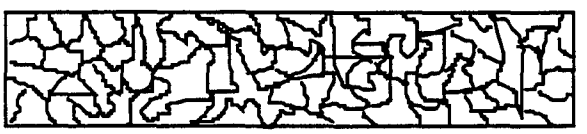

Bruggeman Composite. Each material region is mesoscopic

Figure 1.2 Three types of composite geometries, in each there are two constituents whose linear and nonlinear optical properties are generally different.

For electric fields that are normal to the plane of the layers it is seen that the displacement field will be equal in both layers as implied by the latter boundary condition stated above. By inspection it is seen that

$$\mathbf{D} = \mathbf{d}_a = \mathbf{d}_b, \quad \mathbf{e}_a = \frac{\mathbf{d}_a}{\varepsilon_a}, \quad \mathbf{e}_b = \frac{\mathbf{d}_b}{\varepsilon_b} \tag{1.2}$$

assuming that each of the layers a and b is isotropic and the fields are uniform. In all that follows we denote mesoscopic quantities in lowercase letters and macroscopic in uppercase letters. Uniformity of the fields implies that $\mathbf{E} = f_a \mathbf{e}_a + f_b \mathbf{e}_b$ and after some simple algebra using $\mathbf{D} = \varepsilon_{eff} \mathbf{E}$, it is readily seen that

$$\varepsilon_{eff_\perp} = \frac{1}{\frac{f_a}{\varepsilon_a} + \frac{f_b}{\varepsilon_b}} \tag{1.3}$$

for electric fields perpendicular to the layers. An equally simple analysis for fields parallel to the plane of the layers yields

$$\varepsilon_{eff_{//}} = f_a \varepsilon_a + f_b \varepsilon_b. \tag{1.4}$$

As expected the two principal dielectric constants of a layered composite are equal to the Weiner limits.

Analysis of almost any other geometry is more difficult due to the mesoscopic fields being nonuniform. With some simplifying assumptions however, the Maxwell Garnett geometry can be readily solved. To begin consideration of Maxwell Garnett effective medium theory we examine the limiting case of dilute inclusion volume fill fraction. The optical wavelength is considered to be very long in comparison to the interinclusion distance, therefore we may use electrostatic analysis. In this scenario the local inhomogenous field surrounding a given inclusion does not extend far enough to affect neighboring inclusions and around a single inclusion the mesoscopic field structure can be assumed to be a uniform applied field plus the dipole field added by the presence of the inclusion. At distances far from any inclusion we have simply the uniform applied field labeled $\mathbf{E}_o$ in figure 1.3. The solution of this electrostatic problem is performed[4] using Laplace's equation and appropriate boundary conditions. The resulting mesoscopic field solution is used for the macroscopic averaging.

Within an inclusion the electric field is uniform and equal to

$$\mathbf{e}_i = \frac{3\varepsilon^h}{\varepsilon^i + 2\varepsilon^h}\mathbf{E}_o \tag{1.5}$$

which also implies a uniform polarization within the inclusion. Like the metallic spheres considered by Maxwell Garnett, outside an inclusion the electric field due to the inclusion is dipolar. This field can be represented by the field of a dipole situated at the center of the spherical inclusion with dipole moment

$$\mathbf{p} = \frac{\varepsilon^i - \varepsilon^h}{\varepsilon^i + 2\varepsilon^h} r_i^3 \mathbf{E}_o \tag{1.6}$$

where r_i is the inclusion radius. To summarize the noninteracting inclusion model, we have a collection of physical dipoles with their fields superimposed onto the applied field $\mathbf{E}_o$. This mesoscopic field structure used for both linear and nonlinear[5] analysis.

Fig. 1.3 The Maxwell Garnett mesoscopic field structure: far from the inclusion is incident field $\mathbf{E}_o$ but near the inclusion is the dipole field of the inclusion superimposed onto $\mathbf{E}_o$, h and i denote host and inclusion respectively

To better enable the analysis, we use the notation of Sipe and Boyd[5] in their treatment of Maxwell Garnett nonlinear optical composites. Using the definition

$$\mathbf{p}'(\mathbf{r}) = \begin{cases} 0 & \mathbf{r} \in host \\ (\chi^i - \chi^h)\mathbf{e}(\mathbf{r}) & \mathbf{r} \in inclusion \end{cases} \tag{1.7}$$

for the mesoscopic polarization, the linear polarization is restricted to nonzero values only within the inclusion material. This transformation of variable simplifies the calculation since the mesoscopic fields are uniform there. Now that the mesoscopic field structure is established it remains to average the fields and find the constitutive relation between the macroscopic quantities $\mathbf{P}'$ and $\mathbf{E}$. Since the polarization is zero in the host and uniform in the inclusions, the averaging of the polarization is fairly simple since we then have $\mathbf{P}'=f\mathbf{p}'$ where f is the volume fill fraction of the inclusion material. Note that with our definition of $\mathbf{p}'(\mathbf{r})$, inside the inclusions we have

$$\mathbf{p}'(\mathbf{r}) = \frac{3\varepsilon^h}{4\pi}\frac{\varepsilon^i - \varepsilon^h}{\varepsilon^i + 2\varepsilon^h}\mathbf{E}_o. \tag{1.8}$$

The averaging of the mesoscopic electric field is a little more complicated. First we observe that since $\mathbf{E}_o$ is uniform, it already is a macroscopic field ($\mathbf{E}_o$ is often referred to as the cavity field in most Maxwell Garnett analysis). Averaging the field of the inclusions is performed by invoking a well known result of electrostatics[6] that gives the relation

$$\mathbf{E}_{inclusion} = -\frac{4\pi}{3\varepsilon^h}\mathbf{P}' \tag{1.9}$$

for a unit volume enclosing an inclusion. Then the total average field is the sum, or

$$\mathbf{E} = \mathbf{E}_o - \frac{4\pi}{3\varepsilon^h}\mathbf{P}'. \tag{1.10}$$

$\mathbf{E}_o$ can then be expressed in terms of $\mathbf{P}'$ by using (1.8) and the relation $\mathbf{P}'=f\mathbf{p}'$. Performing the algebra leads to the desired constitutive relation. With more manipulation and using $\varepsilon = 1 + 4\pi\chi$, the Maxwell Garnett effective medium expression is obtained,

$$\frac{\varepsilon_{eff}-\varepsilon^{h}}{\varepsilon_{eff}+2\varepsilon^{h}}=\mathrm{f}\frac{\varepsilon^{i}-\varepsilon^{h}}{\varepsilon^{\mathrm{i}}+2\varepsilon^{h}}\,. \tag{1.11}$$

In some derivations of the Maxwell Garnett effective medium relation, and in most derivations of the Lorentz local field correction in linear dielectrics[7], a fictitious cavity inside the medium is introduced to enable the calculation of the local field. The end result is identical, but by using the cavity construct it appears that neighboring inclusions (or atoms) contribute zero to the local field. Far off inclusions appear to have an influence that contributes through the surface charge induced on the imaginary cavity inner wall due to the polarization outside the imaginary sphere. It is physically unrealistic however that nearby dipoles have no contribution to the local mesoscopic electric field yet dipoles far away affect the local field at an inclusion or atom. As Aspnes[8] has pointed out, that is in fact an incorrect conclusion and a better interpretation of the relation between the macroscopic field and the cavity field ($\mathbf{E}_o$) falls naturally out of the mesoscopic perspective we have used here. The difference between the two is simply due to the effects of averaging the inclusion dipole fields which are superimposed onto the applied field.

For higher fill fractions of the inclusions, the assumption of noninteracting inclusions is untenable. Recall that a uniform incident field at an inclusion induced a uniform field and polarization inside the inclusion. This crucial assumption may be preserved to somewhat higher than dilute fill fractions in the following two cases. First if the inclusions are arranged on a simple cubic lattice, then the lattice sum of the dipolar inclusion fields is zero at any lattice site.[7] Second if the inclusions are randomly located, then it can be assumed that their net effect on each other's local field is zero in the average sense, which is the approach used in Sipe and Boyd.[5] In most nondilute Maxwell Garnett composite structures however, satisfactory description may

require a more sophisticated approach. For all-dielectric composites, the Maxwell Garnett effective medium dielectric constant is bounded by the relatively restrictive Weiner limits and as is discussed below, it may therefore remain a good approximation to higher inclusion fill fractions.

Bruggeman developed the equation bearing his name by assuming that both constituents were Maxwell-Garnett-type inclusions imbedded in a host effective medium and that neither material be given preference as the host material. Setting $\varepsilon^h = \varepsilon_{eff}$ in the Maxwell Garnett expression and adding a term for the other constituent yields the Bruggeman expression for the effective medium dielectric constant,

$$0 = f_a \frac{\varepsilon_a - \varepsilon_{eff}}{\varepsilon_a + 2\varepsilon_{eff}} + f_b \frac{\varepsilon_b - \varepsilon_{eff}}{\varepsilon_b + 2\varepsilon_{eff}}. \tag{1.12}$$

The Bruggeman expression is plotted in figure 1.4.

In figure 1.4 we plot the effective medium dielectric constants of the layered (Weiner limits), Maxwell Garnett, and Bruggeman effective medium expressions as a function of fill fraction of constituent a for two component composite (ε_a=2.25, ε_b=4). Also plotted is the average of the Weiner limits which might be considered a first approximation for an arbitrary shaped inclusion particle. In all-dielectric composites the Weiner limits provide fairly tight bounds and the three approximations for effective media are all reasonably close. Therefore even if the Maxwell Garnett linear effective medium theory was derived for sparsely distributed inclusions, it should remain a decent approximation at higher fill fractions as does the Bruggeman approximation. Metallic composite Weiner limits would not provide such tight

restrictions and the effective medium approximations also would not be as accurate over such a range of fill fractions. More discussion on metallics is presented below.

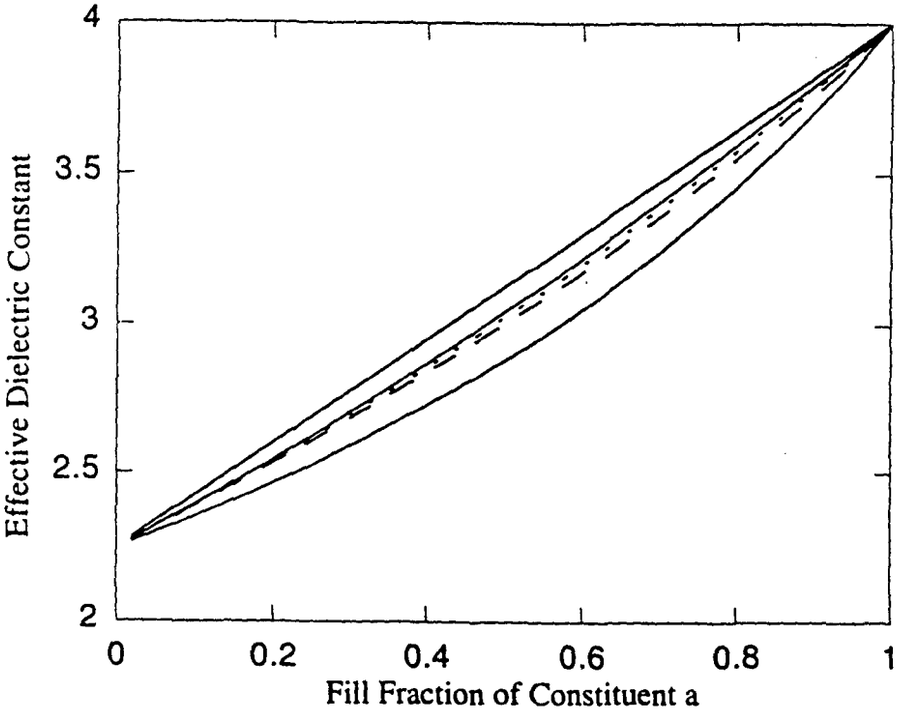

Figure 1.4 Various all-dielectric effective medium results. The upper and lower solid curves are the Weiner limits which also represent the two layered composite results. In ascending order on the plot are average of the Weiner (long dash), Maxwell Garnett (short dash) and Bruggeman (solid). In this calculation we have set the two dielectric constants as ε_a=2.25 and ε_b=4.

Investigation into composite geometries beyond the three types discussed continues since there are many interesting possibilities. A Maxwell Garnett theory of ellipsoidal inclusion particles has been developed for instance, with analytic solution possible if all the particles have the same shape. Both randomly oriented[9.11] and oriented[9.10] geometries have been investigated and there are significant differences between them. Fractal geometries have also been of recent interest. Probably a

majority of the research, both theoretical and experimental, done in composite materials has been directed at metal-dielectric type composites. Results for metallic composites are easily used for all-dielectric cases by simply making the relevant dielectric constants purely real however. Since metallic composites have drawn such great attention, we now briefly discuss some of the features of these metallic systems

1.2 Metallic Linear Optical Composites

Metallic composite effective medium behavior is qualitatively different than the above all-dielectric results since metals are characterized by complex and sometimes negative dielectric constants. For example, examination of the Maxwell Garnett expression for the case of metallic inclusions in a dielectric host indicates a possible resonance effect if $\varepsilon^{i} + 2\varepsilon^{h} = 0$. This was the phenomenon that Maxwell Garnett was investigating when he developed the theory that bears his name. The Maxwell Garnett effective medium expression qualitatively describes the absorption peaks in the visible spectrum that give stained glass its colorful properties. Therefore an interesting new set of possibilities exists when a composite contains a metal for either one or two of its constituents. Even though the primary direction of this thesis work is all-dielectric structures, it is interesting to examine the large body of work devoted to metallic composites. Formally the theoretical results for dielectrics and metals are interchangeable by simply replacing the appropriate values of the dielectric constants and the expressions for the layered, Maxwell Garnett, and Bruggeman models above retain their validity.

Metallic composites may also be conductive and much consideration has been given to this property. Of particular interest is the percolation threshold phenomenon which is a sudden onset of increasing conductivity at a particular volume fill fraction of

the metal. Physically at the threshold, the metallic constituents are beginning to form connected networks that allow for a conducting path through the composite. The various geometries give different predictions regarding this effect with the Maxwell Garnett model predicting no threshold at all. Therefore even if the Maxwell Garnett effective medium approximation may give satisfactory results at most fill fractions for all-dielectric composites, it is inadequate for metallic composites with a high volume fraction of metal. The Bruggeman equation does however predict a percolation threshold but it can be inaccurate in regard to predicting the fill fraction at onset.[12,13] The Bruggeman effective medium expression can in fact be derived by analyzing the effective conductivity,[14,15] which is not surprising since the difference with a dielectric is only that the dielectric constant is imaginary.

The interesting resonance effect mentioned above has been has been examined by a number of investigators beginning with Maxwell Garnett. Interestingly the Maxwell Garnett equation, converse to the percolation effect, is better than the Bruggeman model at describing these resonances at nondilute (>5%) fill fractions. For granular composites in general the Maxwell Garnett equation and its generalizations appear to be much better than the Bruggeman model as demonstrated by Gittleman and Abeles[16] who compared predictions to the data of Cohen et al.[10] on sputtered composites of gold and silver in glass hosts. The generalized result for the ellipsoidal Maxwell Garnett composite in their work is given by

$$\frac{\varepsilon_{eff} - \varepsilon^h}{L\varepsilon_{eff} + (1-L)\varepsilon^h} = \mathrm{f}\frac{\varepsilon^i - \varepsilon^h}{L\varepsilon^{\mathrm{i}} + (1-L)\varepsilon^h} \tag{1.13}$$

where L is a shape factor describing the departure from spherical. Sheng[12] also used the data of Cohen et al. to construct a theory that included both the percolation

prediction of the Bruggeman model and the resonances of the Maxwell Garnett theory. He had reasonable agreement with the data on gold and silver composites.

1.3 Nonlinear Effective Medium Theory

Nonlinear optical phenomena in composite materials provide a rich and interesting range of possibilities. The local field effects that control the linear effective medium averages are of even greater importance in the consideration of the nonlinear averages since effective medium nonlinear susceptibilities in general contain more than one of the local field correction factors that are related to the mesoscopic to macroscopic field averaging. Also, unlike the linear optical constant averages, effective nonlinear optical susceptibilities are influenced by inhomogeneties in the mesoscopic field distribution. This is because the effective nonlinear susceptibilities are in general proportional to the higher moments of the local electric field distribution. An important consequence of this is that the effective nonlinear susceptibility is not bounded by the individual nonlinear susceptibilities of the component materials. This is a departure from the behavior of the linear averages that are bounded by the Weiner limits. In fact, no bound on the effective medium nonlinear susceptibility has been presented up to this time although there are practical, and perhaps theoretical, considerations that should prevent an infinitely high effective nonlinear susceptibility.

Surprisingly the first investigation of nonlinear composite materials did not occur until the 1980's with the work of Ricard et al.[16] who determined the third-order susceptibility of metal colloids in water. Their result went something as follows, first the Maxwell Garnett result is taken to lowest order in fill fraction (they used very small fill fractions of metal particles),

$$\varepsilon_{eff} \approx \varepsilon_h(1+3\beta f)\ . \tag{1.14}$$

Then a Taylor expansion with respect to a small change in the inclusion dielectric constant is performed giving

$$\delta\varepsilon_{eff} = 3\varepsilon_h f \frac{\partial\beta}{\partial\varepsilon_i}\delta\varepsilon_i. \tag{1.15}$$

The change in the inclusion dielectric constant is assumed to be induced by a third-order nonlinearity, or

$$\delta\varepsilon_i = 12\pi\chi_i^{(3)}|E_{loc}|^2 \tag{1.16}$$

where E_{loc} is the field experienced by a single metallic inclusion. Using the Maxwell Garnett result that the local field at an inclusion is the cavity field in the host, they arrived at the expression

$$\delta\varepsilon_{eff} = f\left(\frac{3\varepsilon_h}{2\varepsilon_h+\varepsilon_i}\right)^2\left|\frac{3\varepsilon_h}{2\varepsilon_h+\varepsilon_i}\right|^2 12\pi\chi_i^{(3)}|E|^2 \tag{1.17}$$

for the effective change in dielectric constant with incident field strength. Interesting to note is that the Maxwell Garnett local field correction factor appears to the fourth power, one higher than the order of the nonlinearity. This is due to a correction of the linear dipole moments arising from the presence of the nonlinear dipole moments. In measurements of gold and silver colloids, Ricard et al. found phase conjugate reflectivities to be several thousand times greater on resonance than off resonance.

Much composite work since Ricard et al. has focused on third-order effects in metal and semiconductor doped glasses owing mostly to the interesting enhancements of the nonlinearity at the surface plasmon resonance and to confinement effects in semiconductors. Usually for such systems, the nonlinearity is assumed to arise primarily from the inclusion material. Second-order nonlinear optical composites have

received little attention. This may be due to the difficulty of construction of a noncentrosymmetric material in the composite geometry.

Two articles, Sipe and Boyd[5] and Boyd and Sipe,[17] have derived the first nonlinear correction to the effective medium dielectric constant for certain interactions in the layered and Maxwell Garnett geometries. They considered constituents with arbitrary linear and nonlinear susceptibilities and as a consequence were among the first to consider all-dielectric composites. Also important is the fact that the host medium, and not the inclusions, was considered the nonlinear constituent in one calculation of the Maxwell Garnett response. Their results indicate that the general form for the nonlinear response of a composite optical material (with only one constituent, material a, having a nonlinear response) may be expressed as

$$\chi_{eff}^{(n)} = f_a L_a^{n+1} g_a(f_a, \varepsilon_a, \varepsilon_b) \chi_a^{(n)} . \tag{1.18}$$

L_a is the local field correction factor expressing the factor by which the macroscopic electric field differs from the uniform background mesoscopic, or 'cavity', field in material a. The condition for this factor to be greater than unity is that the average mesoscopic field in material a be greater then the average mesoscopic field in material b (which also makes the average mesoscopic field in material a greater than the macroscopic field). This in turn will be true if $\varepsilon_a < \varepsilon_b$ at the frequency of interest. The difference between the uniform field in material a and the macroscopic field is attributable to the mesoscopic fields that arise out of induced polarizations in material b. For example if the fields produced by the induced polarizations in material b oppose the cavity field in material a on average, the macroscopic average will be lower than the cavity field in a. The geometry that presents the maximum value for L_a is the layered geometry with polarization perpendicular to the plane of the layers since it

represents the case of maximum shielding. When there is no shielding (layered composite with polarization parallel to the plane of the layers) the macroscopic average is equal to the cavity field, therefore L_a is bounded by relations that are related to the Weiner limits.

The factor $g_a(f_a,\varepsilon_a,\varepsilon_b)$ is a term that represents the inhomogeneity of the mesoscopic field distribution. In general, g_a will tend to increase for increasingly inhomogenous field distributions and therefore increase the overall nonlinearity. Physically this derives from the fact that electric field 'hot spots' can dominate the nonlinearity of the composite material as the nonlinear polarization, which is proportional to higher powers of the electric field, may be very large in such regions. Stroud and Hui[20] derived a relation that defines the cubic nonlinearity in terms of the fourth moment of the mesoscopic electric field for a composite in which only material a is nonlinear. It is given by

$$\chi_{eff}^{(3)} = \frac{f_a \chi_a^{(3)} \left\langle (\mathbf{e}_a \cdot \mathbf{e}_a^*)(\mathbf{e}_a \cdot \mathbf{e}_a) \right\rangle}{E_o^4} \tag{1.19}$$

where E_o is the macroscopic averaged field. It can be seen that if we express the mesoscopic fields in material a in terms of the cavity field in material a, then an expression equivalent to equation (1.18) would result. That would make g_a equal to the fourth moment of the mesoscopic electric field in material a, divided by the fourth power of the cavity field in material a.

For the layered composite, g_a will equal 1 since all the fields are uniform. In the Maxwell Garnett geometry, g_a will be unity for the fields inside the inclusion but greater than one for the mesoscopic distribution outside in the host material. g_a probably takes on its greatest significance in composite structures such as fractal

inclusions in a suitable host medium where the mesoscopic inhomogeneities can be large.[18,19] In chapter five of this thesis we investigate the question of whether g_a is different for a Maxwell Garnett composite with the inclusion particles arranged on a simple cubic lattice as opposed to the randomly placed, non-interacting model. Since the linear Maxwell Garnett assumptions are preserved very well to relatively high fill fractions in this situation, the factor L_a is affected little between the two models.

1.4 Summary

In this chapter we have provided a brief summary of some optical properties of a few select composite geometries that are considered most often in composite analysis. The physical interpretation of the crucial role played by dielectric shielding was discussed, as well as accompanying derivations of the linear effective medium properties of the layered, Maxwell Garnett, and Bruggeman composite geometries. This effort to emphasize and explain the physical principals underpinning the linear optical properties was made because the results are also useful to understanding the nonlinear properties of optical composite materials. Briefly discussed also was metallic composite materials. Although not directly addressed in this thesis, metallic composites have additional interesting properties due to the complex dielectric constants of metals. Finally we introduced nonlinear optical composite theory to set the foundation for what follows in this thesis.

In chapters two and three of this thesis, nonlinear effects in layered optical composites are studied. A direct calculation of second-harmonic generation in a layered composite material is performed in chapter two. It is done first by using the well known formalism that accounts for each of the layers individually and then by treating the entire composite as a monolayer with effective medium properties. Comparison

between the two predictions provides a useful test of the effective medium approximation. The third order electrooptic effect in layered composites is studied both theoretically and experimentally in chapter 3. We successfully constructed and characterized a multilayered composite consisting of alternating layers of an organic polymer-dopant system and rf sputtered $BaTiO_3$. The measured electrooptic susceptibility was 3.2 times larger than the measured susceptibility of the dominant nonlinear constituent. Chapter 4 diverges from standard composite theory for an investigation of two-component third-order photonic band gap materials. These structures are interesting for the same reason that we investigate traditional composite materials. It is demonstrated that the nonlinear response can be significantly enhanced over the response of a homogeneous film of the nonlinear constituent. Finally in chapter 5 we calculate the nonlinear response of a Maxwell Garnett composite material with the inclusions arranged on a simple cubic lattice. This enables determination of the host mesoscopic fields for nondilute fill fractions all the way to the close packing limit of such a system. We then determine the nonlinear response for the case of a nonlinear host material with inclusions possessing only a linear optical response.

1.5 References

1. A. Fiore, V. Berger, E. Rosencher, N. Laurent, N. Vodjdani, and J. Nagle, "Birefringence phase matching in selectively oxidized GaAs/AlAs optical waveguides for nonlinear frequency conversion," J. of Nonlinear Optical Phys. and Mat. **5**, 645 (1996).

2. J. C. Maxwell Garnett, "Colours in metal glasses and in metallic films," Philos. Trans. R. Soc. London **203**, 385 (1904); "Colours in metal glasses, in metallic films, and in metallic solutions - II," Philos. Trans. R. Soc. London **205**, 237 (1906)

3. see e.g. pp 415-420 of C.J.F. Bottcher, *Theory of Electric Polarisation*, (Elsevier, New York 1952).

4. J. D. Jackson, *Classical Electrodynamics*, 2nd ed., pp. 149-151 (John Wiley and Sons, New York 1975).

5. J. E. Sipe and R. W. Boyd, "Nonlinear susceptibility of composite optical materials in the Maxwell Garnett model," Phys. Rev. A **46**, 1614 (1992).

6. D. J. Griffiths, *Introduction to Electrodynamics*, pp. 150-52 (Prentice-Hall, Englewood Cliffs, NJ 1981).

7. J. D. Jackson, pp. 152-55

8. D. E. Aspnes, "Local-field effects and effective medium theory: A microscopic perspective," Am. J. Phys. **50**(8), 704 (1982)

9. R. J. Gehr, PhD dissertatation, Ch.4, Univ. of Rochester, 1997

10. R. W. Cohen, G. D. Cody, D. Coutts, and B. Abeles, "Optical Properties of Granular Silver and Gold Films," Phys. Rev. B **8**, 3689 (1973).

11. J. W. Haus, R. Inguva, and C. M. Bowden, "Effective-medium theory of nonlinear ellisoidal composites," Phys. Rev. A **40**, 5729 (1989).

12. P. Sheng, "Theory for the Dielectric Function of Granular Composite Media," Phys. Rev. Lett. **45**, 60 (1980).

13. D. M. Grannan, J. C. Garland, and D. B. Tanner, "Critical Behavior of the Dielectric Constant of a Random Composite near the Percolation Threshold," Phys. Rev. Lett. **46**, 375 (1981).

14. R. Landauer, "The Electrical Resistance of Binary Metallic Mixtures," J. Appl. Phys. **23**, 779 (1952).

15. D. Stroud, "Generalized effective medium approach to the conductivity of an inhomogenous material," Phys. Rev. B **12**, 3368 (1975).

16. D. Ricard, Ph. Roussignol, and C. Flytzanis, "Surface-mediated enhancement of optical phase conjugation in metal colloids," Opt. Lett. **10**, 511 (1985).

17. R. W. Boyd and J. E. Sipe, "Nonlinear optical susceptibilities of layered composite materials," J. Opt. Soc. Am. B **11**, 297 (1994).

18. D. Stroud and X. Zhang, "Cubic nonlinearities in small-particle composites: local-field induced giant nonlinearities," Physica A **207**, 55 (1994).

19. V. M. Shalaev, E. Y. Poliakov, and V. A. Markel, "Small-particle composites. II. Nonlinear optical properties," Phys. Rev. B **53**, 2437 (1996).

20. D. Stroud and P. M. Hui, "Nonlinear susceptibilities of granular matter," Phys. Rev. B **37**, 8719 (1988).

Chapter 2

Comparison Between Effective Medium Theory and Multilayer Exact Formalism in a Layered Optical Composite

2.1 Introduction

Layered optical composites are a special class of composites. They are composites in only one dimension, the direction that is perpendicular to the plane of the layers. Each layer is constructed with a thickness that is much less than an optical wavelength, therefore it is possible to assign an effective average value for linear and nonlinear optical constants. Implied from the fact that there are two polarization dependent dielectric constants is the anisotropic nature of layered composites. The layers form a uniaxial material with the optic axis perpendicular to the plane of the layers. It then follows that the nonlinear susceptibilities will be anisotropic and therefore dependent on the polarization of the incident radiation. The linear effective averages have been known for some time, the first nonlinear correction to the effective medium dielectric constant for several types of interactions has been derived recently in Boyd and Sipe.[1]

Our group's interest in layered composites stems not only from their interesting properties but also their relative ease of construction since other types of geometries, especially ordered geometries, are difficult to construct. Various deposition techniques for thin films allow for the type of control necessary for composite construction. There has been success in building Maxwell Garnett types of material, mostly with metallic inclusions, but they are usually restricted to certain types of host material which is

most typically glass. Composite multilayers on the other hand offer a wider range of possibilities.

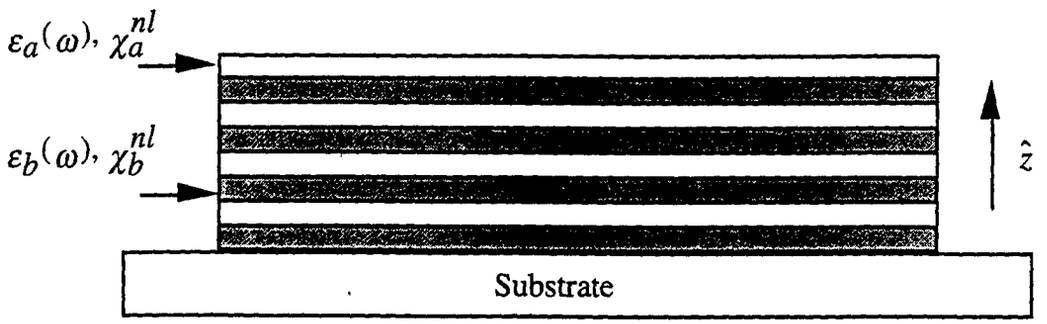

Figure 2.1 Layered optical composite geometry.

In the next section we establish the mesoscopic to macroscopic field description in the rigorous and formal setting of Sipe and Boyd[2] and Boyd and Sipe[1] which enables analysis of most nonlinear interactions in layered composites. We follow the treatment of Boyd and Sipe for the nonlinear susceptibilities with specialization to the interaction of second-harmonic generation (SHG). Then in section 2.3 the exact formalism for SHG in a radiation mode of a layered optical composite is presented, which allows for direct comparison to the nonlinear effective medium theory. This direct comparison allows for comparison of nonlinear effective medium theory against previous well established results.

2.2 Effective Medium Theory in a Layered Composite

For completeness we present the general results in references [1,2] with elaboration to SHG in layered composites. Notation is maintained as close as possible. The following mesoscopic electric field description can generally be applied to most interactions however and the above mentioned references contain examples of applications to other second and third order nonlinear effects. Exact descriptions for

specific material systems are sometimes very complicated due to the possible anisotropic nature of individual constituents.

2.2.1 Mesoscopic and Macroscopic Fields

The formal relationship between a mesoscopic field and its macroscopic counterpart is defined as[2]

$$\begin{aligned}\mathbf{E}(\mathbf{r},\omega) &= \int \Delta(\mathbf{r}-\mathbf{r}')\mathbf{e}(\mathbf{r}',\omega)d\mathbf{r}' \\ \mathbf{P}(\mathbf{r},\omega) &= \int \Delta(\mathbf{r}-\mathbf{r}')\mathbf{p}(\mathbf{r}',\omega)d\mathbf{r}'\end{aligned} \tag{2.1}$$

where $\Delta(\mathbf{r}-\mathbf{r}')$ is a smoothly varying, normalized weighting function with range $R << \lambda$, mesoscopic quantities are expressed in lowercase letters, and macroscopic in uppercase. In Ref. [2] it was shown that

$$\begin{aligned}\mathbf{e}(\mathbf{r},\omega) = \mathbf{E}(\mathbf{r},\omega) &+ \frac{4\pi}{3}\mathbf{P}(\mathbf{r},\omega) - \frac{4\pi}{3}\mathbf{p}(\mathbf{r},\omega) \\ &+ \int \tilde{\mathbf{T}}^{O}(\mathbf{r}-\mathbf{r}')c(|\mathbf{r}-\mathbf{r}'|)\cdot\mathbf{p}(\mathbf{r}',\omega)d\mathbf{r}'\end{aligned} \tag{2.2}$$

where $c(|\mathbf{r}-\mathbf{r}'|)$ is a spherically symmetric cutoff function of range R and $\tilde{\mathbf{T}}^{O}$ is the static dipole-dipole coupling tensor

$$\tilde{\mathbf{T}}^{O}(\mathbf{r}) = \begin{cases}(3\hat{r}\hat{r}-\tilde{I})/r^3 & |\mathbf{r}|>\eta \\ 0 & |\mathbf{r}|<\eta\end{cases}. \tag{2.3}$$

In equation (2.3) $\tilde{I}$ is the identity matrix and $\hat{r}$ is the unit vector in the direction of $\mathbf{r}$. We can interpret (2.2) from the mesoscopic perspective as follows. The first two terms are recognized as the applied, or cavity, field and the second two are the imhomogenous field generated by the local dipoles. The integral sums up these dipole contributions over range R but has to leave out the small cavity at location $\mathbf{r}$ to avoid the resulting singularity at the central dipole itself. To correct for the missing cavity we

add in the field of the small spherical region containing the mesoscopic polarization $\mathbf{p}(\mathbf{r})$. Since over the range of η the mesoscopic polarization can be taken as uniform, we may use the result of the field of a uniformly polarized sphere for the cavity correction (third term on the right in (2.2)).

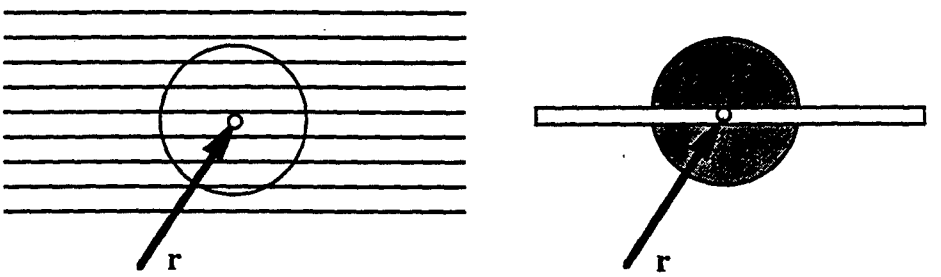

Figure 2.2 (a) The integral term in equation (2.2) is evaluated in a spherical region of radius R. (b) The region R is divided into two parts.

Evaluation of the integral term starts with considering the region of integration indicated by the large radius circle in figure 2.2 (a) above and dividing it into two parts as shown in figure 2.2 (b). The first part is the electric field due to polarization inside the layer which contains **r**, and the second part is the rest of the sphere of integration. First, consider the contribution from the layer in which **r** is located. This part of the integral yields the electric field generated by a plane of uniform polarization minus the electric field generated by a sphere of uniform polarization. These fields may be readily calculated from the laws of electrostatics[3] with the field of a uniformly polarized plane given by

$$\mathbf{e} = -4\pi\hat{z}\hat{z}\cdot\mathbf{p}, \tag{2.4}$$

and that generated by a uniformly polarized sphere is given by

$$\mathbf{e} = -\frac{4\pi}{3}\mathbf{p}. \tag{2.5}$$

Therefore the contribution from the layer containing $\mathbf{r}$ to the integral is

$$\int_{layer} \bar{\mathbf{T}}^0(\mathbf{r}-\mathbf{r}')\cdot\mathbf{p}_a(\omega)d\bar{r}' = -4\pi\hat{z}\hat{z}\cdot\mathbf{p}_a(\omega)+\frac{4\pi}{3}\mathbf{p}_a(\omega). \tag{2.6}$$

Here we have assumed that $\mathbf{r}$ is in a layer of material a and we have dropped the $\mathbf{r}$ dependence since we are integrating over range R which is much smaller than an optical wavelength. The second part of the integral comes from the contributions of the rest of the sphere of integration. For this we substitute a uniform average polarization, or the macroscopic $\mathbf{P}$. The electrostatic field generated by this polarization over a sphere minus a central layer is

$$\int_{sphere-layer} \bar{\mathbf{T}}^0(\mathbf{r}-\mathbf{r}')\cdot\mathbf{P}(\omega)d\bar{r}' = -\frac{4\pi}{3}\mathbf{P}(\omega)+4\pi\hat{z}\hat{z}\cdot\mathbf{P}(\omega). \tag{2.7}$$

Substitution of (2.7) and (2.6) into (2.2) yields an expression for the mesoscopic field in material a,

$$\mathbf{e}_a(\omega) = \mathbf{E}(\omega)+4\pi\hat{z}\hat{z}\cdot\mathbf{P}(\omega)-4\pi\hat{z}\hat{z}\cdot\mathbf{p}_a(\omega). \tag{2.8}$$

The mesocopic field in constituent b is found in an identical fashion. Equation (2.8) has interesting physical interpretation in connection with equation (2.2). The first two terms can be thought of as the layered "cavity" field , or the field inside a layer shaped cavity within a medium with $\mathbf{P}(\omega)$ and $\mathbf{E}(\omega)$. The last term represents the contribution from local dipoles in layer a in analogy with (2.2) which uses a spherical cavity.

It is necessary before performing the nonlinear analysis to generate the results for linear response of the layered composite. Even though many nonlinear optical materials have anisotropic crystal structure, to good approximation some systems can be considered isotropic in the linear susceptibility. For a specific nonlinear material we consider below, this assumption is common. The linear polarizations are then expressed as

$$\mathbf{p}_a(\omega) = \chi_a^{(1)}(\omega)\mathbf{e}_a(\omega), \quad \mathbf{p}_b(\omega) = \chi_b^{(1)}(\omega)\mathbf{e}_b(\omega) \ . \tag{2.9}$$

with substitution into (2.8) for the linear mesoscopic electric fields, it can be seen that since the second two terms contain only z components, then

$$e_{ax}(\omega) = E_x(\omega), \quad e_{ay}(\omega) = E_y(\omega) \tag{2.10}$$

which follows from continuity of tangential $\mathbf{E}$, and for the z component

$$e_{az}(\omega) = E_z(\omega) + 4\pi P_z(\omega) - 4\pi\chi_a^{(1)}(\omega)e_{az}(\omega) \tag{2.11}$$

with analogous results for material b. Uniformity of the fields implies that $P_z(\omega) = f_a p_{az}(\omega) + f_b p_{bz}(\omega)$, and substitution into (2.8) for all the polarizations yields

$$e_{az}(\omega) = \frac{\varepsilon_{eff}(\omega)}{\varepsilon_a(\omega)} E_z(\omega), \quad e_{bz}(\omega) = \frac{\varepsilon_{eff}(\omega)}{\varepsilon_b(\omega)} E_z(\omega) \tag{2.12}$$

where

$$\varepsilon_{eff}(\omega) = \frac{1}{\left(\dfrac{f_a}{\varepsilon_a(\omega)} + \dfrac{f_b}{\varepsilon_b(\omega)}\right)}, \quad \varepsilon(\omega) = 1 + 4\pi\chi^{(1)}(\omega) \ . \tag{2.13}$$

The results are identical to effective medium derivations using simpler electrostatic arguments.

2.2.2 Second-Harmonic Generation

Now we examine the case where both constituents exhibit second-order nonlinearities for second-harmonic generation. Again for simplicity we assume isotropic response in the linear susceptibility. The i'th component of the mesoscopic polarization in material a may be written as

$$p_{ai}(2\omega) = \chi_a^{(1)}(2\omega)e_{ai}(2\omega) + \sum_{jk} \chi_{aijk}^{(2)}(\omega+\omega \rightarrow 2\omega)e_{aj}(\omega)e_{ak}(\omega) \qquad (2.14)$$

with analogous expression for material b. In the evaluation of this expression to an accuracy of second order in the electric field, it is adequate to take the fields at $1\,\omega$ as given by the linear expressions in equations (2.12) and (2.10). This is because the second term is already expressed to second order in the field. Equivalently we are taking the undepleted pump, or uncoupled, approximation where the fundamental is unaffected by the nonlinear interaction. By symmetry of the composite we expect that the x and y polarizations will be identical in form.

Starting with the x-polarization, with the expression of fields in terms of their macroscopic counterparts, we have

$$p_{ax}(2\omega) = \chi_a^{(1)}(2\omega)E_x(2\omega) + \sum_{jk} L_{aj}(\omega)L_{ak}(\omega)\chi_{axjk}^{(2)}(\omega+\omega \rightarrow 2\omega)E_j(\omega)E_k(\omega) \qquad (2.15)$$

where we have defined the local field correction factors

$$L_{ax}(\omega) = L_{ay}(\omega) = L_{bx}(\omega) = L_{by}(\omega) = 1 \qquad (2.16a)$$

$$L_{az}(\omega) = \frac{\varepsilon_{eff_\perp}(\omega)}{\varepsilon_a(\omega)}, \qquad L_{bz}(\omega) = \frac{\varepsilon_{eff_\perp}(\omega)}{\varepsilon_b(\omega)}, \qquad (2.16b)$$

and where $e_{ax,y}(2\omega) = E_{x,y}(2\omega)$ by continuity of tangential electric fields. Which come directly from the linear composite effective medium expressions (2.10) - (2.13). A similar expression holds for component b. To obtain expressions for the effective susceptibility, the expression for the average given by $P_x(2\omega) = f_a p_{ax}(2\omega) + f_b p_{bx}(2\omega)$ is used to find

$$P_x(2\omega) = [f_a\chi_a^{(1)}(2\omega) + f_b\chi_b^{(1)}(2\omega)]E_x(2\omega) \qquad (2.17)$$

$$+f_a\sum_{jk}L_{aj}(\omega)L_{ak}(\omega)\chi^{(2)}_{axjk}(\omega+\omega\rightarrow 2\omega)E_j(\omega)E_k(\omega)$$

$$+f_b\sum_{jk}L_{bj}(\omega)L_{bk}(\omega)\chi^{(2)}_{bxjk}(\omega+\omega\rightarrow 2\omega)E_j(\omega)E_k(\omega)\ .$$

The effective second order susceptibility can be written down by inspection of this equation since $\chi^{(1)}_{eff}=f_a\chi^{(1)}_a(2\omega)+f_b\chi^{(1)}_b(2\omega)$ for fields parallel to the x-y plane.

The z-polarization component follows analogously but with more algebraic complexity. The full expression for the mesoscopic electric field at 2ω is now

$$e_{az}(2\omega)=E_z(2\omega)+4\pi P_z(2\omega)-4\pi p_{az}(2\omega) \tag{2.18}$$

which leads to the following expression for the mesoscopic polarization

$$p_{az}(2\omega)=\chi^{(1)}_a(2\omega)\left[E_z(2\omega)+4\pi P_z(2\omega)-4\pi p_{az}(2\omega)\right] \tag{2.19}$$

$$+\sum_{jk}L_{aj}(\omega)L_{ak}(\omega)\chi^{(2)}_{azjk}(\omega+\omega\rightarrow 2\omega)E_j(\omega)E_k(\omega).$$

Solving for the explicit term $p_{az}(2\omega)$,

$$p_{az}(2\omega)=\frac{\chi^{(1)}_a(2\omega)}{\varepsilon_a(2\omega)}\left[E_z(2\omega)+4\pi P_z(2\omega)\right] \tag{2.20}$$

$$+\frac{1}{\varepsilon_a(2\omega)}\sum_{jk}L_{aj}(\omega)L_{ak}(\omega)\chi^{(2)}_{azjk}(\omega+\omega\rightarrow 2\omega)E_j(\omega)E_k(\omega)$$

and combining with the equivalent expression for the polarization in material b, after some algebra the following expression is obtained

$$P_z(2\omega)=\frac{\varepsilon_{eff_\perp}(2\omega)-1}{4\pi}E_z(2\omega) \tag{2.21}$$

$$+\frac{f_a\varepsilon_{eff_\perp}(2\omega)}{\varepsilon_a(2\omega)}\sum_{jk}L_{aj}(\omega)L_{ak}(\omega)\chi^{(2)}_{azjk}(\omega+\omega\rightarrow 2\omega)E_j(\omega)E_k(\omega)$$

$$+\frac{f_b \varepsilon_{eff_\perp}(2\omega)}{\varepsilon_b(2\omega)} \sum_{jk} L_{bj}(\omega) L_{bk}(\omega) \chi^{(2)}_{bzjk}(\omega+\omega \rightarrow 2\omega) E_j(\omega) E_k(\omega) \ .$$

From this result and equation (2.17) we may express the general tensor component of the second order susceptibility for second-harmonic generation, with an isotropic linear susceptibility, as

$$\chi^{(2)}_{ijk_{eff}}(\omega+\omega \rightarrow 2\omega) = f_a L_{ai}(2\omega) L_{aj}(\omega) L_{ak}(\omega) \chi^{(2)}_{aijk} \qquad (2.22)$$

$$+ f_b L_{bi}(2\omega) L_{bj}(\omega) L_{bk}(\omega) \chi^{(2)}_{bijk} \ .$$

In nonlinear optics there are n+1 local field correction factors where n is the order of the nonlinear susceptibility. This fact is also evident when one considers a homogeneous nonlinear dielectric and includes consideration of local field correction factors at the atomic level. The reason for the extra factor is that to this level of approximation of the nonlinear interaction, the first two factors at 1ω are reexpressions of the linear field correcting for the linear-linear dipole interactions that modify the local field at a given point in the medium. This is the usual linear optical local field theory. The third factor accounts for nonlinear-linear dipole interactions and corrects the local field due to the generated nonlinear dipole moments in the surrounding medium. This extra local field factor gives local field considerations enhanced importance in consideration of nonlinear interactions.

It is interesting to investigate the conditions in which the effective susceptibility in (2.22) is greater than the susceptibility of either of its constituents, if at all possible. First we restrict attention to the case where only one constituent, material a, has a nonlinear response since this will probably be more common in application and has a straightforward physical interpretation. Then the relevant question is when can $f_a L_{ai}(2\omega) L_{aj}(\omega) L_{ak}(\omega)$ be greater than one. Generally we see from (2.16) that we

must consider at least one field component at the fundamental or second harmonic to be polarized in the z direction, and we must have $\varepsilon_{eff_\perp}(2\omega,\omega) > \varepsilon_a(2\omega,\omega)$, or equivalently $\varepsilon_b(2\omega,\omega) > \varepsilon_a(2\omega,\omega)$. Figure (2.3) displays the enhancement, $f_a L_{az}(2\omega) L_{az}(\omega) L_{az}(\omega)$, vs. fill fraction of the linear constituent for some values of the dielectric constant ratio, and for all polarizations along z. Significant enhancement is possible under some conditions.

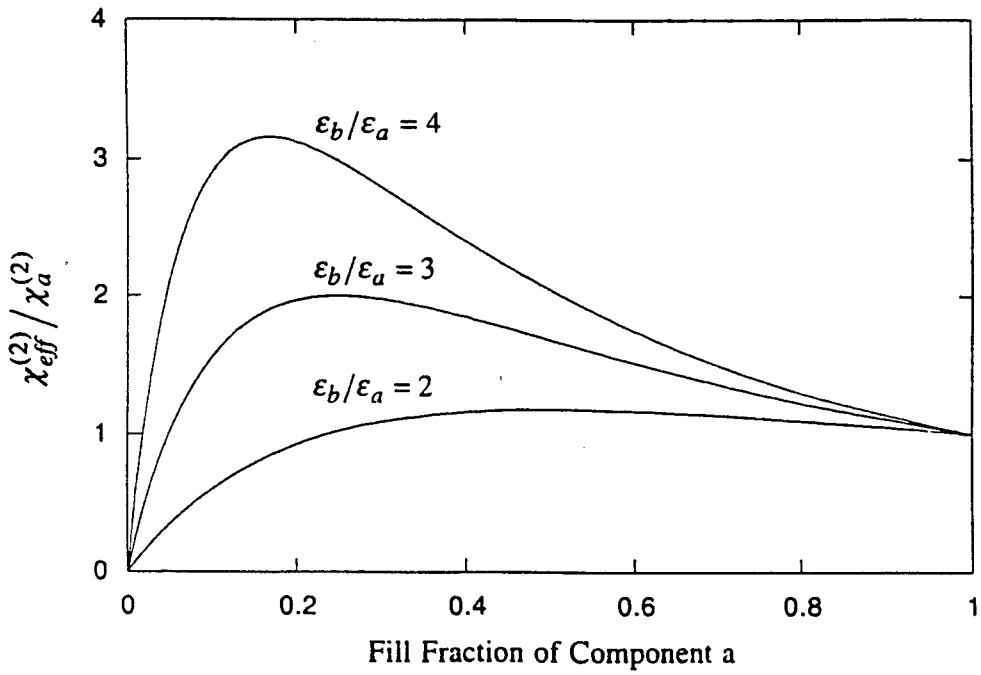

Figure 2.3 Enhancement of the layered composite susceptibility for three values of the dielectric constant ratio of the constituents. Constituent *a* is the nonlinear material, constituent *b* is considered to have only a linear response.

2.3 Second Harmonic Generation in Multilayer Composites

Using the general results of the previous section we now consider application to a specific material system. These results will then be compared to the results of an exact formalism with no effective medium approximation in the next section. In

particular we want to consider SHG on transmission through a layered composite of a radiation (nonwaveguiding) mode as shown in figure (2.4).

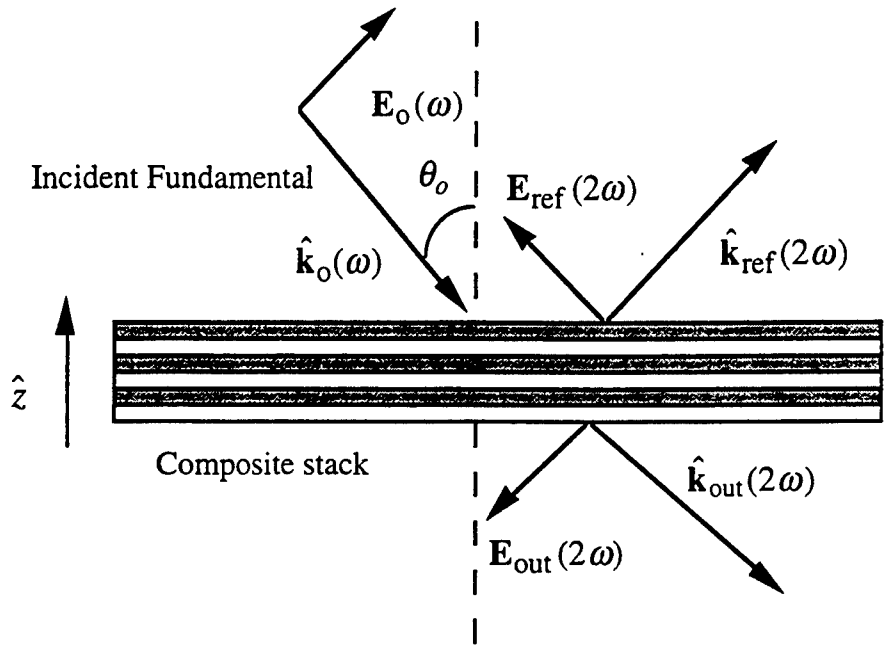

Figure 2.4 Geometry of SHG in radiation mode of composite structure.

We wish to simulate the results of a known system of materials with interesting contemporary relevance. Accordingly we choose the linear indices and nonlinear susceptibilities to represent the materials selected. The second-order nonlinear constituent is modeled as a poled polymer[4-6] and the other constituent is assumed to be a linear and isotropic dielectric. Poled polymers are an interesting class of nonlinear materials as they are centrosymmetric until transformed under the poling process. Typically the pure polymer host material (exe: poly (methyl methacrylate), poly (carbonate), or poly (imide)) does not posses a significant $\chi^{(2)}$ response. But when an orientable, that is possessing a permanent dipole moment, and high second order hyperpolarizability dopant is dissolved into the polymer matrix, the resultant guest-host system can be made to have a significant second order response. Raising the

polymer to near its glass transition temperature and applying a high dc electric field can orient the chromophores. The polymer is cooled with the dc field applied and the chromophores are frozen into a noncentrosymmetric structure. The tensor properties of this configuration are well known[4] and will be used in the composite calculation. Multilayering with another dielectric can be accomplished via spin coating, sputtering process, or some other suitable technique. Since we wish to examine the case of enhanced $\chi^{(2)}$, the linear dielectric will need to have a linear dielectric constant greater than that of the poled polymer.

Typically the second rank tensor representing the second-order poled polymer response is written in a compacted notation utilizing Kleinman symmetry.[7] We then describe the nonlinear polarization for second harmonic generation with the matrix equation

$$\begin{bmatrix} P_x(2\omega) \\ P_y(2\omega) \\ P_z(2\omega) \end{bmatrix} = 2 \begin{bmatrix} d_{11} & d_{12} & d_{13} & d_{14} & d_{15} & d_{16} \\ d_{21} & d_{22} & d_{23} & d_{24} & d_{25} & d_{26} \\ d_{31} & d_{32} & d_{33} & d_{34} & d_{35} & d_{36} \end{bmatrix} \begin{bmatrix} E_x(\omega)^2 \\ E_y(\omega)^2 \\ E_z(\omega)^2 \\ 2E_y(\omega)E_z(\omega) \\ 2E_x(\omega)E_z(\omega) \\ 2E_x(\omega)E_y(\omega) \end{bmatrix}, \qquad (2.23)$$

where the tensor $d_{ijk} = \chi^{(2)}_{ijk}/2$. The compacted notation d_{il} is a result of $\chi^{(2)}_{ijk}$ being symmetric in its last two indices due to Kleinman symmetry. Consideration of poled polymer symmetry (∞mm), Kleinman symmetry, and poling dynamics[4] gives the following form for the polymer d matrix,

$$\tilde{\mathbf{d}}_{poled\ polymer} = \begin{bmatrix} 0 & 0 & 0 & 0 & d_{31} & 0 \\ 0 & 0 & 0 & d_{31} & 0 & 0 \\ d_{31} & d_{31} & d_{33} & 0 & 0 & 0 \end{bmatrix}, \qquad d_{31} = \frac{d_{33}}{3}. \qquad (2.24)$$

The coefficient that is influenced most by composite geometry is d_{33} as it contains

three local field factors that are not unity. All other composite effective d_{il} values will be modified by one local field factor. Since we interested in the case of p-polarized incident fields as shown in figure 2.4, the value of $\chi^{(2)}_{eff}$, or d_{eff}, will be angle dependent, with the enhancement becoming larger with increasing angle of propagation inside the composite. That is the result of a larger component of electric field along the z axis. The s-polarization case is uninteresting since it provides for no enhancement of the nonlinear susceptibility. Summarizing for the composite system with poled polymer NLO constituent we have

$$\tilde{\mathbf{d}}_{composite} = f_a \cdot \tag{2.25}$$

$$\begin{bmatrix} 0 & 0 & 0 & 0 & L_{az}(\omega)d_{31} & 0 \\ 0 & 0 & 0 & L_{az}(\omega)d_{31} & 0 & 0 \\ L_{az}(2\omega)d_{31} & L_{az}(2\omega)d_{31} & L_{az}(2\omega)L_{az}(\omega)^2 d_{33} & 0 & 0 & 0 \end{bmatrix}$$

At this time we point out an important issue concerning SHG in the configuration of figure 2.4. The quantity of practical interest experimentally and theoretically is the value of output second harmonic below the composite for a given incident fundamental. We compare that quantity to the second harmonic from a homogeneous polymer film of same total thickness as the composite. Initially it might be expected that the composite sample would yield higher signal by virtue of its higher susceptibility, but closer examination of input field coupling gives a different conclusion. Examination of the fields that are actually coupled into the active regions of the samples shown in figure 2.5 (utilizing the Maxwell boundary conditions) shows that the electric field strength inside the polymer layers of the composite is not greater than the field strength coupled into a homogeneous polymer film, assuming that the dielectric properties of the incident medium is the same in both cases. Only in the case of including field localization due to propagation effects (photonic band gap structures

for instance) can higher fields be obtained in the nonlinear regions of a composite. Since we are considering layer thicknesses to be within the limits of the effective medium approximation, then that type of localization is not present unless the composite is part of some larger structure. The resulting output SHG values are actually smaller for the composite than for the homogeneous nonlinear film case, even though the effective nonlinear susceptibility is higher.

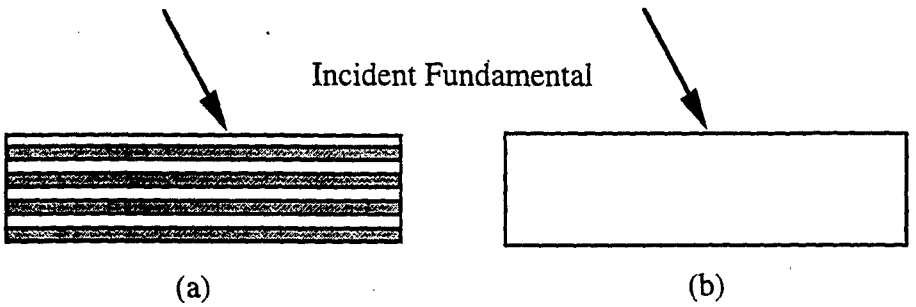

Figure 2.5 Coupling of the fundamental for a) composite and b) homogeneous layer of nonlinear constituent reveals that fields are about the same.

This situation results from the fact that the macroscopic field coupled into the composite is lower than the homogeneous film. Electromagnetic boundary conditions prevent the field coupled into the nonlinear regions of the composite from exceeding its value in other geometries. However this coupling issue is not present in a waveguide or in the configuration shown in figure 2.6. If the effective medium approximation is valid, the electric field coupled into the nonlinear layers of the composite material in fig. 2.6 is higher than the field that would be coupled into a homogenous sample of the nonlinear material and useable output enhancement may be possible.

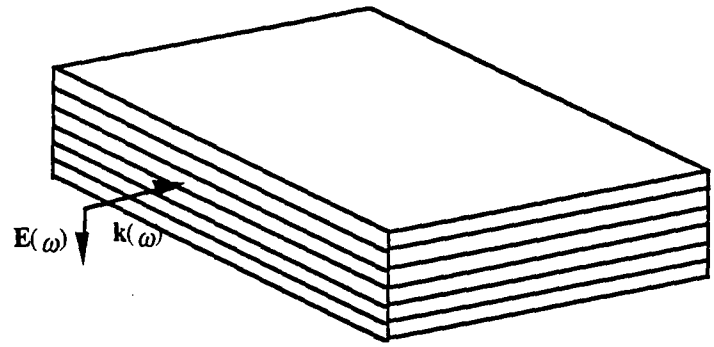

Figure 2.6 Composite coupling of fundamental where enhancement of fundamental field strength in nonlinear active layers is expected. There should actually be many layers present in the composite so that the overall dimensions of the composite is much greater than a wavelength and the composite presents itself as a bulk medium.

2.3.1 Exact Formalism

It is possible in the geometry of figure 2.4 to obtain an expression for the output second harmonic fields without utilizing the effective medium approximation. An explicit expression would be algebraically impractical but the formalism is implicitly exact and lends itself to ready calculation. We now outline such a method for the purpose of comparison to nonlinear effective medium results. Convergence of the EMT prediction to the full multilayer model in the limit of small layer thickness would provide a test of consistency for the theoretical predictions of the nonlinear effective medium results as presented in Boyd and Sipe.[1] The more exact model has been in existence for some time and has been shown to accurately model experimental results.

The formalism for calculating second-harmonic generation of thin multilayer structures began with the work of Bloembergen and Pershan[8] in 1962. Since then, there has been some expansion of that work including the important results of Jerphagnon and Kurtz[9] that set the foundation for the Maker[10] fringe measurement of nonabsorbing isotropic and uniaxial crystals. Recently Herman and Hayden[11] have

presented a more complete version of the Maker fringe technique in that they accounted for some of the approximations used by Jerphagnon and Kurtz. Sipe[12] has presented a useful new formalism for surface nonlinear optics making use of a Green-function technique and Hashizume et al.[13] combined the Green-function method of Sipe with the standard transfer matrix method that is useful for many layered structures. Our own approach resembles the original method of Bloembergen but in cases where there are possible strong counterpropagating waves, we combine the self-consistent method of Bloembergen with the Green-function formalism of Sipe, analogous to the method of Hashizume et al..

Considering the geometry of figure 2.4, we first state the driven wave equation which the second harmonic field quantities obey. From Maxwell's equations we have

$$\nabla\times\nabla\times\mathbf{E}(2\omega)+\frac{\varepsilon(2\omega)}{c}\frac{\partial^2\mathbf{E}(2\omega)}{\partial t^2}=-\frac{4\pi}{c^2}\frac{\partial^2\mathbf{P}^{nl}(2\omega)}{\partial t^2} \tag{2.26}$$

and the **H** field is determined from

$$\nabla\times\mathbf{E}(2\omega)=-\frac{1}{c}\frac{\partial\mu\mathbf{H}(2\omega)}{\partial t}. \tag{2.27}$$

We assume that only one constituent, material a, has a significant nonlinear response for second-harmonic generation. Setting up general plane wave solutions[8] for the layers a and b we have

$$\begin{aligned}
\mathbf{E}_b(2\omega)&=\hat{e}_bA_b\exp\left[i(\mathbf{k}_b(2\omega)\cdot\mathbf{r}-2\omega t)\right]+\hat{e}'_bA'_b\exp\left[i(\mathbf{k}'_b(2\omega)\cdot\mathbf{r}-2\omega t)\right]\\
\mathbf{E}_a(2\omega)&=\hat{e}_aA_a\exp\left[i(\mathbf{k}_a(2\omega)\cdot\mathbf{r}-2\omega t)\right]+\hat{e}'_aA'_a\exp\left[i(\mathbf{k}'_a(2\omega)\cdot\mathbf{r}-2\omega t)\right]\\
&-\frac{4\pi P_a^{nl}\left(\frac{4\omega^2}{c^2}\right)}{\left|\mathbf{k}_a(2\omega)\right|^2-\left|2\mathbf{k}_a(\omega)\right|^2}\left[\hat{p}-\frac{4\mathbf{k}_a(\omega)\left(\mathbf{k}_a(\omega)\cdot\hat{p}\right)}{\left|\mathbf{k}_a(2\omega)\right|^2}\right]\exp\left[i(2\mathbf{k}_a(\omega)\cdot\mathbf{r}-2\omega t)\right]
\end{aligned} \tag{2.28}$$

where

$$\mathbf{P}^{nl} = \tilde{\chi}^{(2)}(\omega+\omega \rightarrow 2\omega) : \mathbf{E}(\omega)\mathbf{E}(\omega) = \hat{p}P^{nl} \tag{2.29}$$

and a primed quantity denotes backtraveling waves. The solution for material b and the first two terms in the solution for material a can be recognized as the homogenous, or free wave solutions, and the last term in the a field solution is the bound, or driven, wave solution . For brevity, the backtraveling bound field term has been left off the above expression for the field in material a, also a cross term proportional to $\mathrm{E_a}(\omega)\mathrm{E}'_a(\omega)$ is present in the bound polarization wave but in many circumstances including our analysis, it is not significant. This cross term is easiest to handle using the Sipe Green-function formalism when it contributes significantly,[14] we found however that it did not for the particular all-dielectric composite calculations that we are considering. Present in these plane wave solutions is the undepleted pump, or uncoupled wave, approximation that was also present in the effective medium approximation. For plane waves the **H** field may be obtained from

$$\mathbf{H}(2\omega) = n(2\omega)\hat{k}(2\omega) \times \mathbf{E}(2\omega). \tag{2.30}$$

The self-consistent approach to the multilayer solution requires satisfying Maxwell's boundary conditions (continuity of $\mathbf{E}_{\tan}$ and $\mathbf{H}_{\tan}$) at each of the layer boundaries simultaneously. Mathematically we are then considering a system of 2N+2 equations and 2N+2 unknowns where N is the number of individual layers in the composite. It is possible to solve for all of the unknowns explicitly, as a practical matter however such an expression would be too cumbersome. Therefore solutions are generated through a computer algorithm. The solution output $\mathbf{E}_{free}(2\omega)$ is a vector representing the homogeneous second harmonic amplitudes in all the composite layers. It is generated from the matrix equation

$$\mathbf{A}\mathbf{E}_{free}(2\omega) = \mathbf{E}_{bound}(2\omega) \tag{2.31}$$

where $\mathbf{E}_{bound}(2\omega)$ are the bound wave amplitudes in all the composite layers as given in equation (2.28) and $\mathbf{A}$ is a 2N+2 by 2N+2 matrix representing the two boundary conditions at each interface. Both the output amplitude below the composite and the reflected second harmonic above the composite are included in the solution.

2.3.2 Comparison of Exact Formalism and Nonlinear Effective Medium Theory

Next we compare the predictions of the effective medium approach of Boyd and Sipe[3] to the predictions of the exact formalism. First it is necessary to answer the question at which layer pair thickness it is valid to assume that effective medium theory is appropriate. To satisfy this requirement we simply calculate the output for a fixed total thickness and fill fraction of the multilayer stack and vary the number of layer pairs. If the assumptions about effective medium theory are correct, there should exist a layer pair thickness size for which any smaller size will not significantly affect the output second harmonic value. Figure 2.7 displays such an effect for a fixed angle of incidence. The onset of a region of layer pair thicknesses in which smaller layer pair thicknesses have no effect on the output is clearly visible. Only the volume fill fractions can affect the response in the effective medium limit. In a suitable comparison between the exact formalism and effective medium theory, the layer thicknesses will be chosen to be well within these limits of approximation.

Once the layer optical thicknesses are set to suitably small values, the predictions for the exact and effective medium theories can be compared. To eliminate consideration of unwanted variables in evaluating a bulk effective medium average like

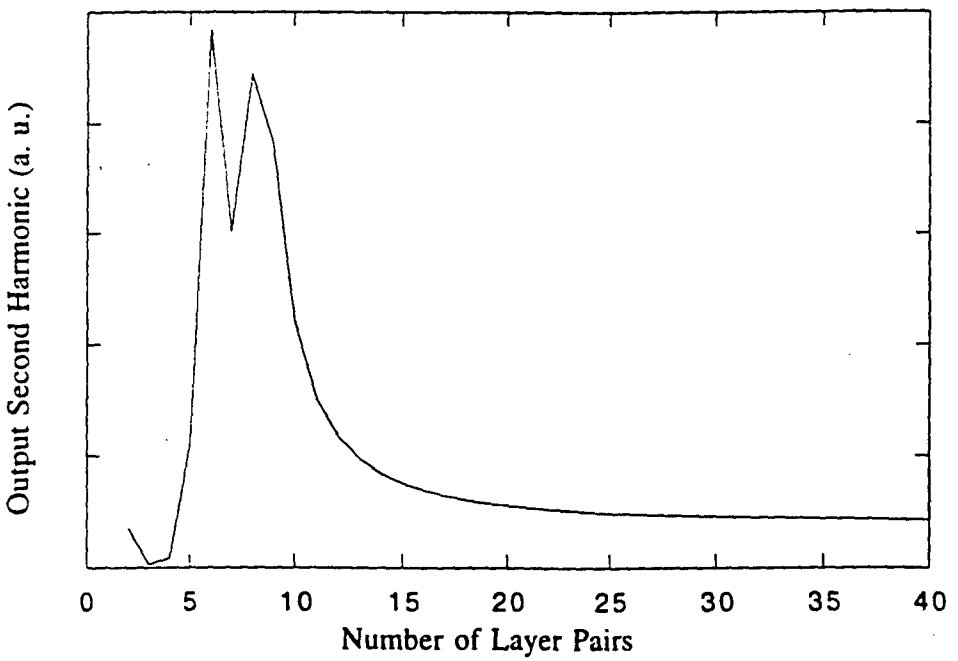

Figure 2.7 The second harmonic output from a film of fixed total thickness but variable number of layer pairs. The onset of the effective medium region of approximation is seen to occur when the number of layer pairs is about 15. The calculation assumed the following parameters: total thickness = 1 micron, incident wavelength = 1.06 microns, fill fraction = 0.6 of high index constituent, n_a=1.5, n_b=2.5, angle of incident radiation = 40°.

the susceptibility, the values of the macroscopic electric fields and the internal propagation angle should be set equal in both cases. Stated differently, we are not attempting to evaluate the ability of effective medium theory to predict Fresnel coefficients and propagation angles, but rather how well it describes the bulk average nonlinear susceptibilities. Since the results here indicated that the use of effective medium theory constants in describing the coupling of the incident field proved satisfactory with some divergence at high angles of incidence, the internal fields or propagation angles were not normalized. Each application of effective medium theory should independently consider the possible problem of inaccurate prediction of linear Fresnel coefficients however.

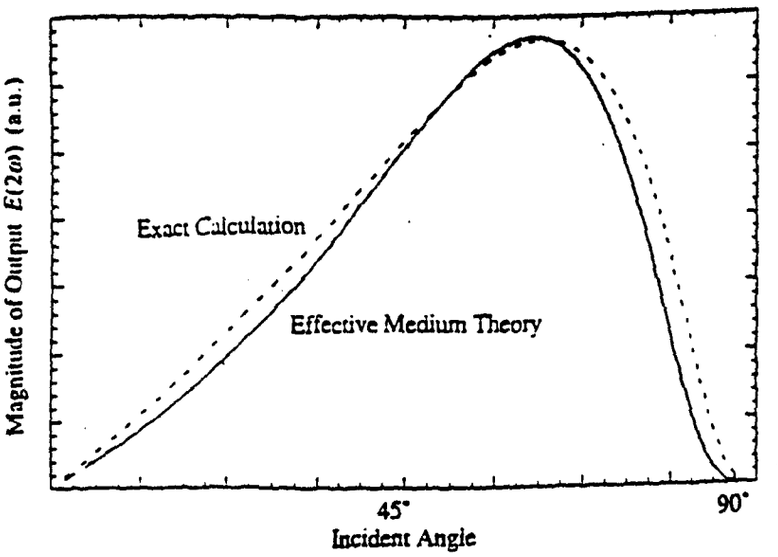

(a)

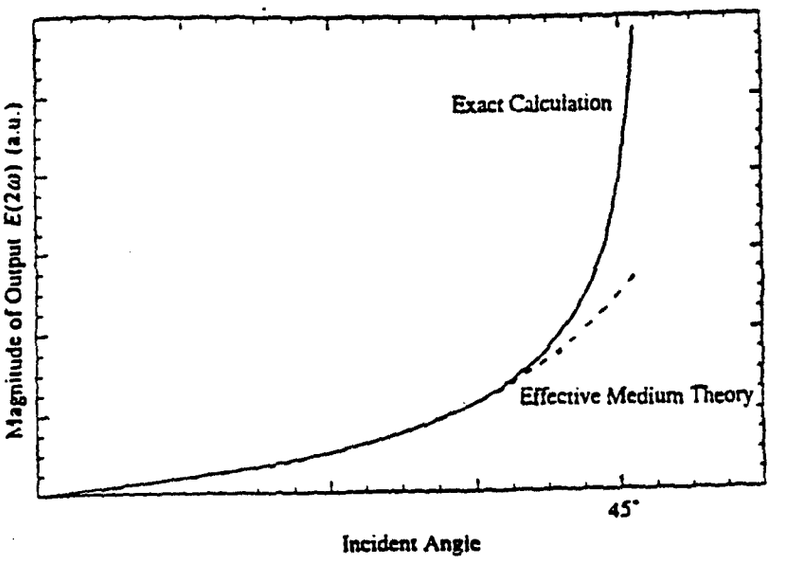

(b)

Figure 2.8 Comparisons between nonlinear effective medium theory and exact multilayer predictions. The nonlinear constituent is assumed to have n_a=1.5 and the linear dielectric has n_b=2.0. The surrounding medium has n_o=1.0 in figure (a) while n_o=2.0 in figure (b). There are 15 layer pairs, fill fraction f_b=.5819, total composite thickness = 270nm, and the incident wavelength is 3.0 microns.

Figure 2.8(a) displays the second harmonic output below the composite pictured in figure 2.4 as the angle of incidence is varied from 0 to 90 degrees. The curve has a form that is a typical response for a poled polymer system.[5] Especially since we are

utilizing effective medium predictions for the coupling of the fundamental into the composite, the effective medium result is a satisfactory representation of the composite response. Figure 2.8(b) plots the response assuming that the incident and output media have the same refractive index as the high index constituent of the composite. The significance of this configuration is that there are no waveguide modes and angles of propagation near 90° inside the composite can be realized. This would be the situation of maximum nonlinear enhancement as all polarizations are nearly in the z direction. Again the effective medium approximation proves adequate except for the high angle divergence. This is because of the error in the propagation angle prediction of effective medium theory, which has a magnified effect on the output second harmonic value due to the long propagation lengths and strong interaction in the composite. Normalization of internal angles of propagation and field magnitudes would greatly reduce the error.

2.4 Conclusions

Nonlinear effective medium theory has been shown to well represent the response of layered optical composites for second-harmonic generation in the radiation mode geometry. The predictions of the Boyd and Sipe model for layered composites was compared with the formal predictions of the well accepted formalism to calculate the SHG response in thin multilayered structures. Effective medium theory can have some difficulty in accurately predicting linear propagation properties, mostly at high angles of propagation relative to the optical surfaces. Bulk property predictions seem very accurate however.

2.5 References

1. R .W. Boyd and J. E. Sipe, "Nonlinear optical susceptibilities of layered composite materials," J. Opt. Soc. Am. B **11**, 297 (1994).

2. J. E. Sipe and R. W. Boyd, "Nonlinear susceptibility of composite optical materials in the Maxwell Garnett model," Phys. Rev. A **46**, 1614 (1992).

3. See, for example, J. D. Jackson, *Classical Electrodynamics*, (Wiley, New York, 1975).

4. R. Meredith, J. G. Van Dusen, and D. J. Williams, *Nonlinear Optical Properties of Organics and Polymeric Materials,* edited by D. J. Williams (American Chemical Society, Washington, DC, 1983).

5. D. Singer, J. E. Sohn, and S. J. Lalama, "Second harmonic generation in poled polymer films," Appl. Phys Lett. **49**, 248 (1986).

6. D. Singer, M. G. Kuzyk, W. R. Holland, J. E. Sohn, S. J. Lalama, R. B. Comizzoli, H. E. Katz, and M. L. Schilling, "Electrooptic phase modulation and optical second harmonic generation in corona poled polymer films," Appl. Phys. Lett. **53**, 1800 (1988).

7. R. W. Boyd, *Nonlinear Optics*, pp. 38-9 (Academic Press, San Diego, 1992).

8. N. Bloembergen and P. S. Pershan, "Light Waves at the Boundary of Nonlinear Media," Phys. Rev. **128**, 606 (1962).

9. J. Jerphagnon and S. K. Kurtz, "Maker Fringes: A Detailed Comparison of Theory and Experiment for Isotropic and Uniaxial Crystals," J. Appl. Phys. **41**, 1667 (1970).

10. P. D. Maker, R. W. Terhune, M. Nisenoff, and C. M. Savage, "Effects of dispersion and focusing on the production of optical harmonics," Phys Rev. Lett. **8**, 21 (1962).

11. W. N. Herman and L. M. Hayden, "Maker fringes revisited: second harmonic generation from birefringent or absorbing materials," J Opt. Soc. Am. B **12**, 416 (1995).

12. J. E. Sipe, "New Green-function formalism for surface optics," J. Opt. Soc. Am. B **4**, 481 (1987).

13. N. Hashizume, M. Ohashi, T. Kondo, and R. Ito, "Optical harmonic generation in multilayered structures: a comprehensive analysis," J. Opt. Soc. Am. **12**, 1894 (1995).

14. R. Normandin and G. I. Stegeman, "Nondegenerate four-wave mixing in integrated optics," Optics Lett. **4**, 58 (1979).

Chapter 3

Electrooptics of Layered Composite Materials

3.1 Introduction

The electrooptic response of layered composite materials presents an interesting problem as it relates to the nonlinear interaction of electrical and optical fields within a composite structure. In a layered optical composite, each layer is much less than an optical wavelength, therefore the optical wave will experience an effective average value for the linear and nonlinear optical constants. The linear effective averages have been known for some time and the first nonlinear correction to the effective medium dielectric constant for several types of interactions including the Pockels effect has been derived in Boyd and Sipe[1].

In the present chapter we investigate the quadratic electrooptic effect, also known as the Kerr effect, of layered optical composites. The theoretical portion of the following discussion is equally applicable to second-order systems however. We first derive the electrooptical properties of composite materials, both optical and electrical. We then describe the construction and measurement of a layered optical composite whose third-order susceptibility is greater than the susceptibility of either of its constituents. The $\chi_{eff}^{(3)}$ of the composite material is measured to be greater than the $\chi^{(3)}$ of the dominant nonlinear constituent by a factor of 3.2.

3.2 Theory of Electrooptic Response of Layered Composites

In order to discuss composite theory we must define what is meant by mesoscopic and macroscopic fields. Macroscopic fields, which typically are what is implied in the expression of Maxwell's equations within a material medium, are averaged fields that vary over a distance scale on the order of the wavelength of the electrical or electromagnetic field. Mesoscopic fields are quasi-electrostatic fields that vary over the distance scale of the composite constituent inhomogeneities. This distance scale is much less than the wavelength of interest but much greater than the atomic scale. The macroscopic fields are defined as suitable averages of the mesoscopic fields. A more complete description can be found in Ref. [1]. In the following discussion lowercase letters denote mesoscopic fields and uppercase letters denote macroscopic.

The electroooptic effect is a change in the refractive index of a material induced by the presence of a dc or low frequency ac electric field. The nonlinear polarizations describing such an effect up to second order in the applied electric field are[2]

$$\begin{aligned} P_i(\omega+\Omega_1) &= D^{(2)} \sum_{jk} \chi^{(2)}_{ijk}(\omega=\omega+\Omega_1) E_j(\omega) E_k(\Omega_1) \\ P_i(\omega+\Omega_1+\Omega_2) &= D^{(3)} \sum_{jkl} \chi^{(3)}_{ijkl}(\omega=\omega+\Omega_1+\Omega_2) E_j(\omega) E_k(\Omega_1) E_l(\Omega_2) \end{aligned} \tag{3.1}$$

where $D^{(2)}$ and $D^{(3)}$ are appropriate degeneracy factors. The first polarization is the Pockels electrooptic effect, and the second polarization describes the Kerr electrooptic effect. If the susceptibilities have an imaginary component, then electroabsorption will also be present. To avoid unnecessary algebra we now confine our attention first to a general layered composite geometry and then to the specific material systems we wish to investigate. A composite electrooptic geometry is illustrated in figure 3.1.

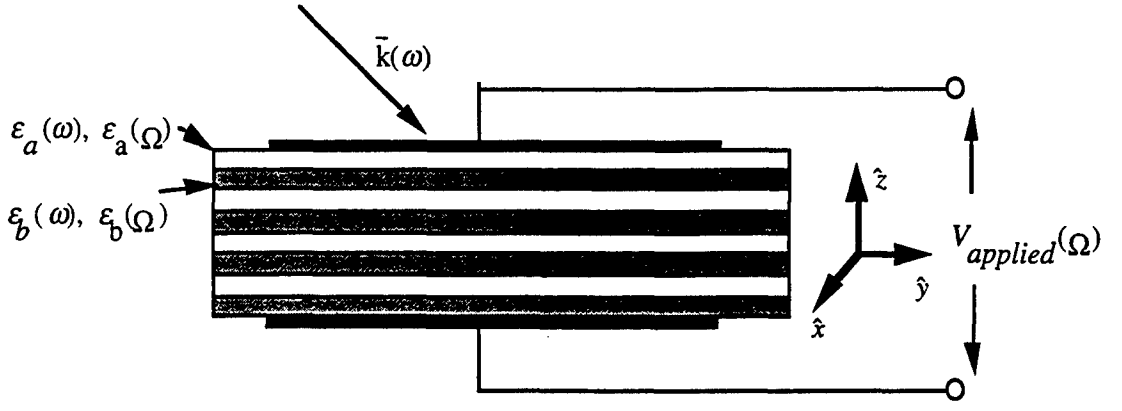

Figure 3.1 Electrooptic composite geometry. A low frequency, or dc, voltage $V(\Omega)$ is applied via electrodes surrounding the composite stack. The $E(\Omega)$ inside the composite is perpendicular to the layers, always in the z direction. The optical field enters as a radiation mode from the top.

Restriction of the electrical fields in the z direction reduces the number of tensor components we must consider in equation (3.1). Since the mesoscopic fields in a layered composite are uniform in each layer, the applied electric field will also be uniform in each layer and in the z direction. Therefore the simplification is true whether we are examining mesoscopic or macroscopic nonlinear polarizations.

We will restrict our attention to cases of isotropic constituent materials for the electrooptic effect, which is unlike the situation of poled polymers that have ∞mm symmetry in the active nonlinear layers. Isotropic constituent layers necessarily implies that we only consider the third-order Kerr effect for such materials as they will be centrosymmetric. As discussed in Boyd[3], electrooptic effects in materials are determined by their effect on the *index ellipsoid*. The index ellipsoid for an isotropic material would simply be a sphere, while for the layered composite the semimajor axis would lie along z, with the semiminor axis along x and y. The composite is uniaxial (x and y are equivalent directions) so the two semiminor axes are equal. The general expression for the index ellipsoid is given by

$$\left(\frac{1}{n^2}\right)_1 x^2 + \left(\frac{1}{n^2}\right)_2 y^2 + \left(\frac{1}{n^2}\right)_3 z^2 + 2\left(\frac{1}{n^2}\right)_4 yz + 2\left(\frac{1}{n^2}\right)_5 xz + \left(\frac{1}{n^2}\right)_6 xy = 1 . \quad (3.2)$$

If we match the x-y-z coordinates to the coordinate system of the composite, then the last three terms vanish since we are then in the principal coordinate system. It is still important to consider the last three terms for electrooptic effects since the applied electric field may effect a change on these terms even though their value is zero in the absence of the electric field. The presence of such terms would imply a rotation of the index ellipsoid under the applied field.

In the study of how the index ellipsoid is influenced by an applied electric field, it is convenient to use the impermeability tensor defined by

$$E_i = \sum_j \eta_{ij} D_j, \quad \eta_{ij} = (\varepsilon^{-1})_{ij} . \quad (3.3)$$

Relating the impermeability tensor to the optical index ellipsoid gives

$$\left(\frac{1}{n^2}\right)_1 = \eta_{11} , \left(\frac{1}{n^2}\right)_2 = \eta_{22} , \left(\frac{1}{n^2}\right)_3 = \eta_{33} , \left(\frac{1}{n^2}\right)_4 = \eta_{23} = \eta_{32} ,$$
$$\left(\frac{1}{n^2}\right)_5 = \eta_{13} = \eta_{31} , \left(\frac{1}{n^2}\right)_6 = \eta_{12} = \eta_{21} \quad (3.4)$$

Now it is assumed that the η_{ij} can be expressed as a power series in the components of the applied electric field analogous to the nonlinear polarization in equation (3.1). The resulting expression is

$$\eta_{ij} = \eta_{ij}^{(0)} + \sum_k r_{ijk} E_k(\Omega) + \sum_{kl} s_{ijkl} E_k(\Omega) E_l(\Omega) + \ldots \quad (3.5)$$

where the r and s tensor components are known as the linear and quadratic electrooptic coefficients respectively. These coefficients are not equivalent to the nonlinear

susceptibilities and effective medium expressions for these coefficients will then be different from those of the susceptibilities.

Now we consider the individual layers that were assumed isotropic and examine the nonlinear properties. As mentioned, the r values will be zero and by third order symmetry considerations[4] with an applied field in the z direction, the nonzero s components are s_{1133}, s_{2233}, and s_{3333}. Also by the symmetry of the x and y directions it is seen that $s_{2233} = s_{1133}$ leaving only two independent s coefficients. In an isotropic material, an applied electric field breaks isotropic symmetry and the medium then presents an anisotropic index of refraction to an optical wave. Equivalently stated, the applied field changes the index ellipsoid from a sphere into an ellipsoid with semimajor axis along the direction of the field. Inserting such a material into a layered composite medium and keeping the electric field oriented perpendicular to the layers preserves this symmetry since the composite also breaks the isotropic symmetry in the z direction. The composite effective medium expressions therefore define new macroscopic values for s_{1133} and s_{3333} but will not change the form of the tensor as long as the electric field is along z. Then from equation (2.36) we see that only η_{11}, η_{22}, and η_{33} will be nonzero for the composite, or that physically the index ellipsoid will only change in size along its axes and will not rotate inside the composite. Under such conditions, analysis of the electrooptic effect is simplified to consideration of index changes along the ellipse axes which in the uniaxial medium of the composite are the extraordinary and ordinary refractive indices. The changes in the principal composite indices are described by the readily derived relations

$$\Delta n_e = -\frac{1}{2} n_e^3 s_{3333} E_z^2(\Omega) , \qquad \Delta n_o = -\frac{1}{2} n_o^3 s_{1133} E_z^2(\Omega) \tag{3.6}$$

where the explicit notation $n_e = n_e(\omega)$ has been dropped with the understanding that indices of refraction are at optical frequencies.

Having established that index changes will only occur along the principal axes, the effective medium expressions for the layered composite are readily obtained. Starting with the relation $n = \sqrt{\varepsilon}$ and the well known linear effective medium expressions

$$n_e = \left(\frac{f_a}{n_a^2} + \frac{f_b}{n_b^2} \right)^{-\frac{1}{2}} , \qquad n_o = \sqrt{f_a n_a^2 + f_b n_b^2} \tag{3.7}$$

where f_a and f_b are the volume fill fractions of components a and b respectively, and considering that only one medium, constituent a, has an electrooptic response we have

$$\Delta n_e = \left(\frac{\partial n_e}{\partial n_a} \right) \Delta n_{a\perp} \quad , \qquad \Delta \mathrm{n_o} = \left(\frac{\partial n_o}{\partial n_a} \right) \Delta n_{a//} \tag{3.8}$$

$\Delta n_{a//}$ is evaluated from equation (3.2) above as mesoscopic $\Delta \mathrm{n_o}$ in material a and $\Delta n_{a\perp}$ corresponds to mesoscopic Δn_e. For a composite with two nonlinear components, identical analysis is performed for the other constituent and its effect is summed into the total Δn. In material a the electric field is the mesoscopic field, and the s coefficients are those for constituent a alone. Evaluation of the derivatives yields

$$\begin{aligned} \Delta n_e &= f_a \left(\frac{n_e}{n_a} \right)^3 \Delta n_{a\perp} = -f_a \frac{1}{2} n_e^3 s_{3333_a} e_{a_z}^2(\Omega) \\ \Delta n_o &= f_a \left(\frac{n_a}{n_o} \right) \Delta n_{a//} = -f_a \frac{1}{2} \frac{n_a^4}{n_o} s_{1133_a} e_{a_z}^2(\Omega) \end{aligned} \tag{3.9}$$

where the lower case $e_{a_z}^2(\Omega)$ emphasizes that the field in a is a mesoscopic field. This

is not the final effective medium form since we have not expressed the mesoscopic electric field in terms of its macroscopic counterpart.

The electrical portion of effective medium theory is potentially a difficult subject, especially with applied dc fields. The question is not whether effective medium theory is applicable but of how the individual media respond within the composite. When a low frequency voltage is applied to the composite as shown in figure 3.1, the electrical response can be modeled by representing the composite stack as a two terminal network of lumped circuit components. The wavelengths of such waveforms are extremely long so there is no doubt about the applicability of EMT, but the individual layer response may be complicated. The composite may then be viewed as a multilayer leaky capacitive circuit and it can be shown that the composite can be represented as a two layer element since the electric response is independent of the order in which the layers are placed.[5] The equivalent circuit for the composite is shown in figure 3.2 with the component values representing all the layers of a particular constituent.

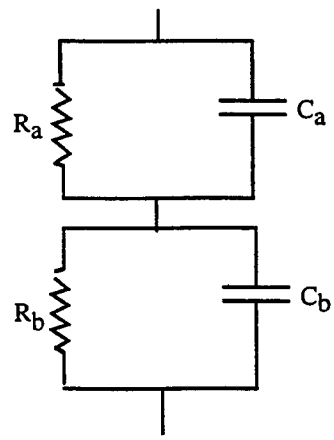

Figure 3.2 Equivalent circuit for a composite stack.

To an outside observer the composite then appears as a material of dielectric constant $\varepsilon = \varepsilon' + i\varepsilon''$[6] where

$$\varepsilon' = \varepsilon'_\infty\left[1+\frac{k}{1+\omega^2\tau^2}\right], \quad \varepsilon'' = \varepsilon'_\infty\left[\frac{\tau}{\omega\tau_1\tau_2}+\frac{k\omega\tau}{1+\omega^2\tau^2}\right], \tag{3.10}$$

ε'_∞ is the "optical" value of ε, τ refers to the time constant of either the entire stack (no subscript) or an individual layer, and ω is the angular frequency. Also for k and ε'_∞ we have[6]

$$\varepsilon'_\infty = \frac{1}{\frac{f_a}{\varepsilon_a}+\frac{f_b}{\varepsilon_b}}, \quad k = \frac{(\tau_1+\tau_2-\tau)\tau-\tau_1\tau_2}{\tau_1\tau_2}. \tag{3.11}$$

As seen from the expressions above, when the appropriate terms are small, the electric dielectric constant will average out macroscopically like the optical giving $\varepsilon'(\Omega) = \varepsilon'_\infty(\Omega)$. The distinction between electrical and optical is artificial as optical is just the $\omega \to \infty$ limit. Substitution of measured values for the time constants into the above expressions demonstrated that the composite low frequency dielectric constant could well be represented by the "optical" value, ε'_∞. A perhaps simpler way to arrive at this conclusion is to note that the RC time constant of the composite was in the 2-4 millisecond range which implies that capacitive impedances are dominating. Also determined from measurement was that $\varepsilon''(\Omega) << \varepsilon'(\Omega)$ for the composite stack .

Assuming that $\varepsilon(\Omega) = \varepsilon'_\infty(\Omega)$ is valid for the low frequency dielectric constants, expressions (3.9) may then be completed by expressing the mesoscopic electrical fields in terms of the macroscopic electric fields. The conversion factor from mesoscopic to macroscopic fields can be found in Ref. [1], but also can be regarded as a consequence of continuity of the normal component of the displacement field, $\mathbf{D}(\Omega)$, across the composite layers. The full expression for the composite is then

$$\Delta n_e = -\frac{1}{2} f_a n_e^3 s_{3333a} \left(\frac{\varepsilon_\perp(\Omega)}{\varepsilon_a(\Omega)} \right)^2 E^2(\Omega)$$
$$\Delta n_o = -\frac{1}{2} f_a \frac{n_a^4}{n_o} s_{1133a} \left(\frac{\varepsilon_\perp(\Omega)}{\varepsilon_a(\Omega)} \right)^2 E^2(\Omega) \qquad (3.12)$$

where the electrical local field factors are identical for both Δn_e and Δn_o since the applied electric field is always in the z direction. $\varepsilon_\perp(\Omega)$ is equal to $\varepsilon'_\infty(\Omega)$ from (3.11). Just as was the case for the optical wave, it is desirable for the electrical dielectric constant to be lower in the nonlinear constituent (material a in this text). This has the effect of concentrating voltage drop, and therefore electric field, across the lower dielectric constant layers. For any material placed between the electrodes, macroscopic $E(\Omega)$ is given by $V(\Omega)/\mathrm{d}$ with d being the thickness of the material. This invariance of $E(\Omega)$ leads to the fact that the low dielectric constant material within a composite will experience a higher electric field than an equivalent thickness (same thickness as composite) layer of homogeneous material since $\varepsilon_\perp(\Omega) > \varepsilon_a(\Omega)$. This is unlike the coupling of an incident optical wave where the $E(\omega)$ coupled into the structure depends on the optical dielectric constant and prevents such an enhancement of the fundamental in the low index layer for a situation such as second-harmonic generation.

The localization of the applied low frequency electric fields in addition to the optical enhancement factor of

$$f_a \frac{n_e^3}{n_a^3} \quad , \quad n_e^3 > n_a^3 \text{ if } n_b > n_a \qquad (3.13)$$

implies that a radiation mode in a layered composite can experience an enhanced Δn_e over that of an equivalent thickness layer of material a. Δn_o may be either enhanced or reduced depending on the exact material parameters. We end this section by stating the

effective medium expressions for both the quadratic electrooptic coefficients and susceptibilities for a composite with one nonlinear constituent. The quadratic electrooptic coefficients are by inspection

$$s_{3333_{eff}} = f_a\left[\frac{\varepsilon_\perp(\Omega)}{\varepsilon_a(\Omega)}\right]^2 s_{3333_a}$$
$$s_{1133_{eff}} = f_a\left(\frac{n_a}{n_o}\right)^4\left[\frac{\varepsilon_\perp(\Omega)}{\varepsilon_a(\Omega)}\right]^2 s_{1133_a} \tag{3.14}$$

and the third order susceptibilities are[1]

$$\chi^{(3)}_{3333_{eff}} = f_a\left[\frac{\varepsilon_{eff_\perp}(\omega)}{\varepsilon_a(\omega)}\right]^2\left[\frac{\varepsilon_\perp(\Omega)}{\varepsilon_a(\Omega)}\right]^2 \chi^{(3)}_{3333_a}$$

$$\chi^{(3)}_{1133_{eff}} = f_a\left[\frac{\varepsilon_\perp(\Omega)}{\varepsilon_a(\Omega)}\right]^2 \chi^{(3)}_{1133_a} . \tag{3.15}$$

3.3 Construction of Layered Electrooptic Material

The design and construction of layered electrooptic composite materials includes consideration of many variables. Most important is that the layer pair optical thickness must fall within the bounds of the effective medium theory approximation. A simple method to evaluate where those bounds are is to perform a linear optical calculation and vary the optical thickness. The layer size at which there is no significant change in the optical properties with decreasing layer size marks the point at which effective medium theory is appropriate. Also considered in composite design is the appropriate combination of constituent linear dielectric constants at both the optical and electrical frequencies. As seen in the development of the theoretical response, we would like to have the nonlinear constituent posses a lower dielectric constant at both electrical and

optical frequencies for optimum enhancement. A further consideration is the compatibility of the constituents, or the compatibility of the deposition processes.

After theoretical evaluation, construction, and testing, of several different composite systems, rf sputtered barium titanate was selected as the high dielectric constant constituent and polycarbonate doped with the AF-30 molecule as the low dielectric constant, nonlinear-dominant material. Barium titanate ($BaTiO_3$) is known for its large second order response as well as large low frequency dielectric constants. Crystalline barium titanate has a dielectric constant of 1740[19] at 1 kHz (the experimental electrical waveform frequency) while polymers such as polycarbonate are typically around 3. This is potentially a very favorable arrangement as almost all the applied low frequency electric field would appear across the polycarbonate. The $BaTiO_3$ in our sample was an amorphous rf sputtered film however, and the actual measured value of $\varepsilon(\Omega)$ was around 15. This value is large enough to provide an enhancement effect. At optical frequencies also is the favorable situation where the crystalline index of $BaTiO_3$ is around 2.4 and polycarbonate is around 1.58 at the experimental wavelength, so that optical local field factors are also greater than one. Again the $BaTiO_3$ optical dielectric constant came in lower than crystalline (1.95-2.05) due to the amorphous and probably porous nature of sputtered films.

AF-30 is an Air Force dopant developed for two photon absorption applications, however we applied it to our sample as it also displayed a measurable Kerr electrooptic response. Figure 3.3(a) displays the AF-30 molecule. Polycarbonate (figure 3.3 (b)) is a common but strong and optically clear polymer which makes it a suitable host medium. The doping level of the AF-30 in the polycarbonate was 10% weight for all samples. Influencing material selection was the fact that both the AF-30 dopant and the polycarbonate host were able to withstand the harsh environment of rf sputtering the

$BaTiO_3$. The sample temperature was estimated to approach 200 C during the rf sputter deposition in a MRC model 822 sputter system, which was cycled to avoid even higher temperatures. All samples, both composites and homogenous films, were deposited onto indium tin oxide (ITO) coated microscope slides with the ITO acting as the bottom electrode for the electrooptic sample. The top electrodes were opaque films of evaporated gold. Total sample configuration is shown in figure 3.5. The composite was composed of four layer pairs giving a total sample thickness of 800 nm.

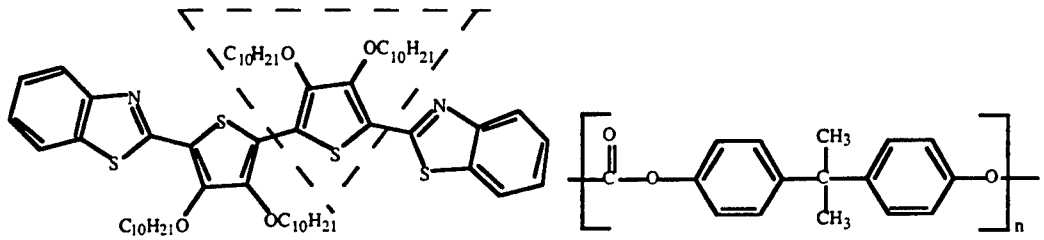

(a) (b)

Figure 3.3 (a) The AF-30, or 5-benzothiazol-2-yl-2-(5-benzothiazol-2-yl-3, 4-didecyloxy(2-thienyl))-3, 4-didecyloxythiophene, and (b) the polycarbonate monomer. AF-15 is the AF-30 molecule without the portion in the dashed triangle.

The electrooptic experiments were performed at a vacuum wavelength of 1.37 microns and simulations using conservative values for the constituent indices indicated that layer thickness of 100nm would lie in the effective medium realm of approximation. The maximum allowed layer thickness was 100 nm but also important is the ratio of constituent layer thickness as that will determine the volume fill fraction, which is an important variable in effective medium theory. Using our best measured values for both optical and electrical dielectric constants, figure 3.4 plots the expected enhancement of the nonlinear susceptibility $f_a L_a(\omega)^2 L_a(\Omega)^2$ assuming that material a (the AF-30/polycarbonate) has the dominant nonlinear response. It can be seen that maximum expected enhancement occurs when there is about 17% fill fraction of the

polymer layers which corresponds to a polymer thickness of 20.5 nm, assuming that the $BaTiO_3$ thickness is 100 nm. This thickness of a polymer layer for electrooptic materials is impractical since it will most likely electrically short out with an applied voltage and film quality would be difficult to maintain. Therefore polymer layers at the maximum 100 nm thickness were constructed in order to provide maximum electrical integrity. This implies a fill fraction of 50% which indicates an expected enhancement factor of about 2.1 for the nonlinear susceptibility.

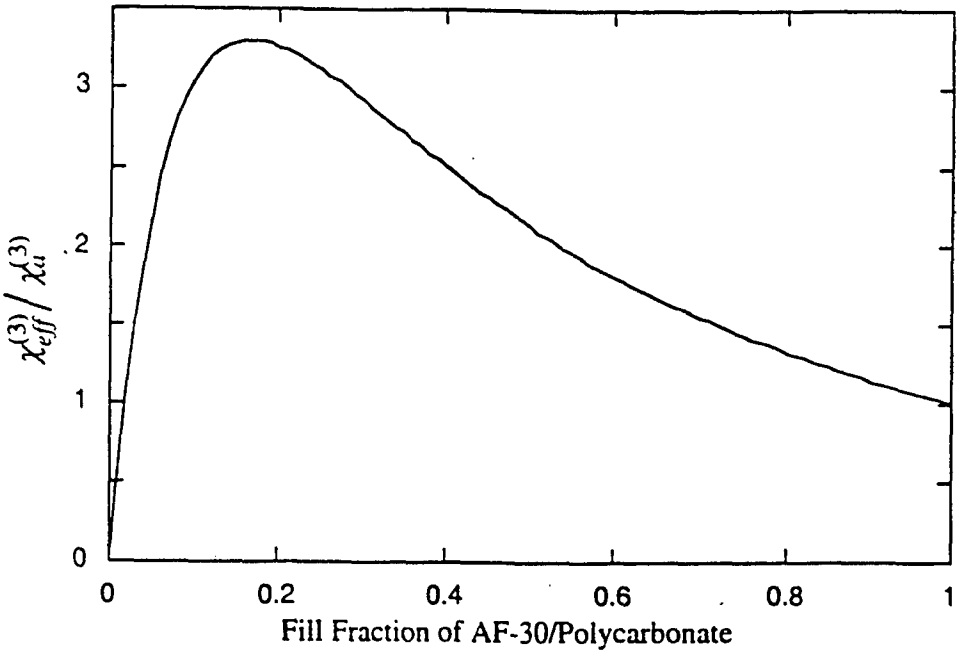

Figure 3.4 Enhancement of $\chi^{(3)}_{3333_{eff}}$ versus fill fraction of polycarbonate.

Typically several separate gold electrodes per glass slide were fabricated since usually some of the gold-sample material-ITO circuits would short out electrically. With more testing of different material systems, we feel that better alternatives could be found, especially for the nonlinear dopant material.

3.4 Electrooptic Experiment and Results

The electrooptic coefficients of electrooptic films are typically measured using the Teng and Man[20,21] reflection technique, a type of ellipsometric measurement adapted to poled polymer films, or by using interferometric techniques.[22-24] Since the Teng and Man procedure was specifically designed for the poled polymer second-order system and thus contains an assumption relating the two independent electrooptic coefficients for guest-host poled systems, it is not applicable to our Kerr electrooptic sample. Furthermore, the indium tin oxide electrode has metallic-like behavior at the wavelength of interest (n_{ITO}=0.674+0.2168i) and there are possible multiple reflection effects in the samples that would make interferometric, Teng and Man, or any other phase sensitive technique difficult to analyze. Eldering et al.[27] and Uchiki and Kobayashi[28] used modulation of transmittance though a Fabry-Pérot cavity to measure the electrooptic coefficients, which has the advantage of not being a phase sensitive measurement but requires that the sample have a Fabry-Pérot resonance. Our composite sample was not designed for such an experiment so we used simple reflectance data to characterize the electrooptic properties.

Reflectance data is influenced by the same parameters as a phase dependent signal. These include the sample thickness, index, and absorption variations. The measurement itself is simpler than the Teng and Man technique but the analysis is more complicated. Figure 3.5 gives the layout of the experiment and data collected includes the quadratic electrooptic reflectance modulation at various angles of incidence for both *s* and *p* type polarizations.

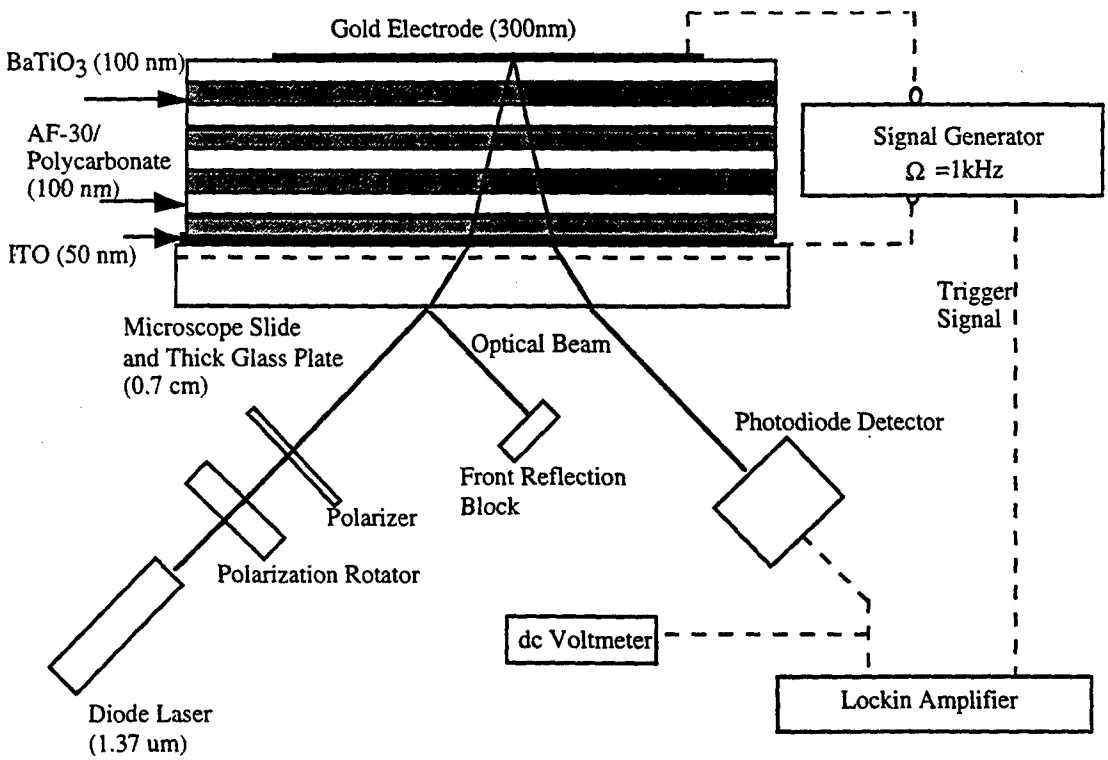

Figure 3.5 Experimental arrangement and sample geometry. The sample is rotated and the detector moved to obtain data from different angles of incidence. Front surface reflection is elimated since the diode laser has a short coherence length and there is physical seperation between reflected and transmitted beams. Index matching fluid is placed between substrate microscope slide and thick plate (0.5cm).

The signal generated from the sample is due to a modulation of the reflectance of the film due to the applied low frequency voltage that consists of a dc field superimposed onto a 1 kHz AC waveform. Thus instead of a driving electric field of form $E(\Omega)^2$ we have $E(\Omega)E(0)$. This form of applied voltage produced the strongest and most reliable electrooptic signal. A Kerr electrooptic signal will then be evidenced by shifts in the 1Ω signal with changes in the applied dc field analogous to the shift in the Teng and Man signal described in Röhl et al.[13] and as shown in figure 3.6. These can arise from changes in index (real and imaginary parts) as well as changes in film

thickness as mentioned. The front surface reflection off the sample substrate was eliminated for two reasons: first the coherence length of the laser was less than the thickness of the glass slide the sample was constructed on, therefore front reflection off that surface would have had to be accounted for with an incoherent superposition. Second, as the angle of incidence was increased a physical separation of the front reflection and the modulated beam became apparent. Therefore it was better to eliminate front surface reflection altogether utilizing a thick (0.5 cm) glass slide compressed against the glass substrate with index matching fluid in between. Data generated for the fitting procedure is the modulated *s* and *p* polarization reflected intensities as a function of angle of incidence normalized by the reflected backround intensity as displayed by a dc voltmeter. Like ellipsometric measurements that obtain the index of refraction for thin films, a fitting procedure had to be adopted to obtain the desired experimental quantities (the *s* coefficients).

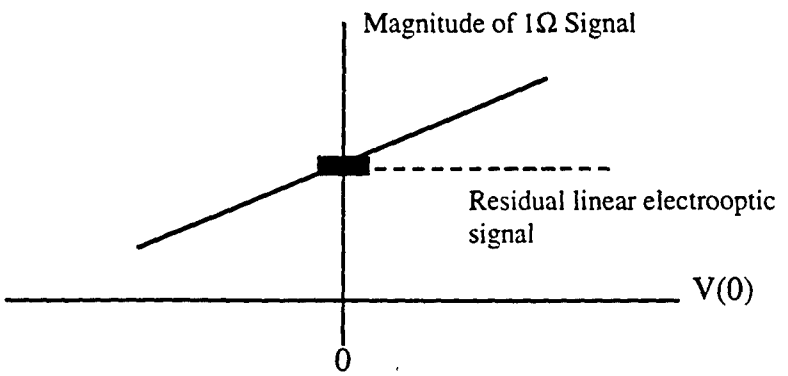

Figure 3.6 An illustrative quadratic electooptic signal with an applied voltage of form $V(0)V(\Omega)$. The 1Ω signal level detected at the lockin amplifier is linearly dependent on the applied dc voltage.

The calculated response of the sample was fitted to the experimental data by varying the appropriate parameters in the computer algorithm that simulated the quadratic electrooptic response of thin films. The calculation is accomplished by

applying homogeneous plane wave solutions to Maxwell's equations for the linear optical propagation through the sample stack with self-consistent application of boundary conditions. We were also able to investigate a composite stack with effective medium theory in the simulated results by simply treating a composite as a monolayer with effective medium properties. Thus two outputs were generated, one from an exact formalism and one assuming effective medium theory, for comparison with experiment. The calculated effective medium result is also in itself a test of effective medium approximations as it can bedirectly compared to the exact formalism.

As described in Kuzyk and Dirk[10] there are several mechanisms that can give a Kerr electrooptic response in a doped polymer film. These include electronic, orientational, orientationally induced second order (like poling), electrode attraction, electrostriction, trapped charge movement, and heating. From one perspective it does not matter what the details of the mechanism are since effective medium theory treats $\chi^{(3)}$ as a phenomenological constant and applies to any mechanism. With the experimental fitting procedure however it is important to quantify and separate thickness changes from variations in the refractive index. Also, electrode attraction is not a nonlinear optical phenomenon but rather a physical effect of the sample electret.

Thickness variations with applied voltage will derive from the electrode attraction and electrostrictive interactions. Kuzyk and Dirk[10] and Eldering et al.[11] point out that doping levels of 10% or less in polymer films do not significantly affect electrode attraction, electrostriction, trapped charge movement, and heating effects. Kuzyk and Dirk further found these effects to be insignificant in comparison to the other third order effects in their doped poly (methyl methacrylate) (PMMA) films. Uchiki and Kobayashi[12] concluded that thickness variations in their doped polycarbonate films was negligible in their Fabry-Pérot type experiment but Eldering et

al. found that thickness changes were a significant contributor to their signal in a similar type of experiment in doped PMMA. It is of course possible that these effects are stronger in PMMA than in polycarbonate. Interestingly D. Morichère et al.[15] reported that electrostriction was more important than the electronic part of the $\chi^{(3)}$ response using the Attenuated Total Reflection technique for PMMA doped with Disperse Red 1, albeit at only a 3% doping level (weight concentration).

The approach used here is to assume that electrostriction, electrode attraction, and heating (in the homogenous films) are independent of small doping levels and for trapped charge effects should be comparable in a similarly doped film. Films of polycarbonate doped with Disperse Red 1 and polycarbonate doped with AF-15 (see fig. 3.1) were measured for comparison to the AF-30 doped film. The observed signal levels in both films were much smaller than the AF-30 films even after accounting for optical effects. Electrostriction and heating are probably dominated by the polycarbonate and should have appeared in all samples if prevalent. Electrode attraction effects also should be nearly identical in all polycarbonate films, and trapped charge effects should be similar in the AF-30 and AF-15 films as they are similar molecules and the weight percent is equal in both films (therefore there is actually a higher volume concentration of the AF-15 dopant). The conclusion was that the dominant mechanism contributing to the signal in our polycarbonate samples was refractive index changes in the AF-30 doped films. As will be discussed below, we did not attempt to discern the Kerr signal mechanisms in $BaTiO_3$ since its signal was unusual in nature and was determined to be a minor part of the theoretical composite signal whether it was dominated by thickness or refractive index variations.

In order to properly fit the composite measurements, the constituent materials were characterized for both optical and electrical properties. Linear index

measurements were carried out with an automated ellipsometer and yielded indices of 1.58 ± 0.03 for the doped polymer films and 1.98 ± 0.04 for the sputtered $BaTiO_3$. Gold and ITO indices were assumed close to their published values of $n_{gold}=0.4494+8.7245i$[16] and $n_{ITO}=0.674+0.2168i$[17] with the ITO allowed to vary slightly during the fit procedure since an ellipsometric determination proved unreliable and ITO films are known to be difficult to characterize, especially at 1.37 μm which is near the ITO band edge. The available data from Ref. [17] and to some degree the attempted ellisometric fit indicated that the imaginary part of the ITO refractive index was near 0.21i but there was some discrepancy in the real part. With this uncertainty the real part of the refractive index was assumed to be in the range 0.674-1.0 as was apparent from the values in Ref. [17]. On the whole, variations of n_{ITO} over this range do not affect the conclusions of this work qualitatively but have some affect quantitatively. It was decided to use to the value 0.674 for the real part as this provided the most conservative numerical results (smallest composite enhancement) in the simulated responses.

Measurement of the electrical properties were carried out for $\Omega = 1\text{kHz}$ on a HP 4284A LCR meter. The $BaTiO_3$ dielectric constant was measured at $\varepsilon(\Omega)=15\pm1.5$ and the AF-30 doped polycarbonate film was found to have $\varepsilon(\Omega)=2.9\pm0.1$. Electrical measurements of the composite at $1\,\Omega$ yielded higher than expected values for the effective dielectric constant. The range of measured values was from 7.5 to 15 depending on which electrode on the sample composite was utilized and the expected value would be in the range 5-6 as predicted from the optical model. There was a trend of getting higher dielectric constant values from the larger electrodes on the composite, or as the area of the measuring electrode decreased the value of the measured constant also decreased. We currently have no explanation for this unusual behavior and chose

to use the theoretical (equation 3.11) value of the dielectric constant in the simulated results.

The DC electric field distribution inside the composite material is potentially a complicated issue that is determined mainly by the conductivities and not the dielectric constants of the constituents. In the steady state we expect that the dc fields would be related by

$$\frac{e_a(0)}{e_b(0)} = \frac{\sigma_b(0)}{\sigma_a(0)} \tag{3.16}$$

where the conductivity is denoted by σ. Conductivity properties also are described by effective medium theory but individual layer conductivity is difficult to determine as we have to account for nonlinear conductivity, space-charge effects, surface states, and bulk traps among other issues.[18] Also from experience in the construction and testing of polymer electrets, sample conductivity can be affected by film quality, film thickness, impurities, and the nature of the metal electrode-polymer interface, or one is almost always measuring a total sample conductivity and not necessarily a bulk material conductivity. With these complications in the application of effective medium theory to the problem of dc conductivities, the value of the static field inside the composite polymer layers was allowed to vary as a parameter of the fit procedure within physically reasonable bounds.

The electrooptic measurements were taken and fitting procedure was applied to the homogeneous films of AF-30/polycarbonate (855 nm) and $BaTiO_3$ (1.05 μm). As discussed above it was assumed that index variations were the dominant source of signal in the AF-30 films while no such assumption was made for the $BaTiO_3$. The $BaTiO_3$ signals exhibited some unusual behavior under the action of an applied dc field, at least unusual in attempting to interpret them with Kerr electrooptic behavior. Hysteresis was present in most of the signals observed but could be minimized by

cycling the sample through several changes in the dc field polarity. The *s*-polarization and low angle of incidence signals were too low for reliable interpretation so only high angle of incidence p-polarization data could be analyzed. Two of the three angles that produced good signals are shown in figure 3.7, the third angle of incidence at 75° displayed behavior like that at 70° except smaller in magnitude. As can be seen, some behavior was not Kerr-like in nature. Most likely the static field behavior of $BaTiO_3$ is complicated by issues that are beyond the scope of this work, therefore it may or may not be appropriate then to ascribe electrooptic coefficients to the sputtered $BaTiO_3$ utilizing these signals.

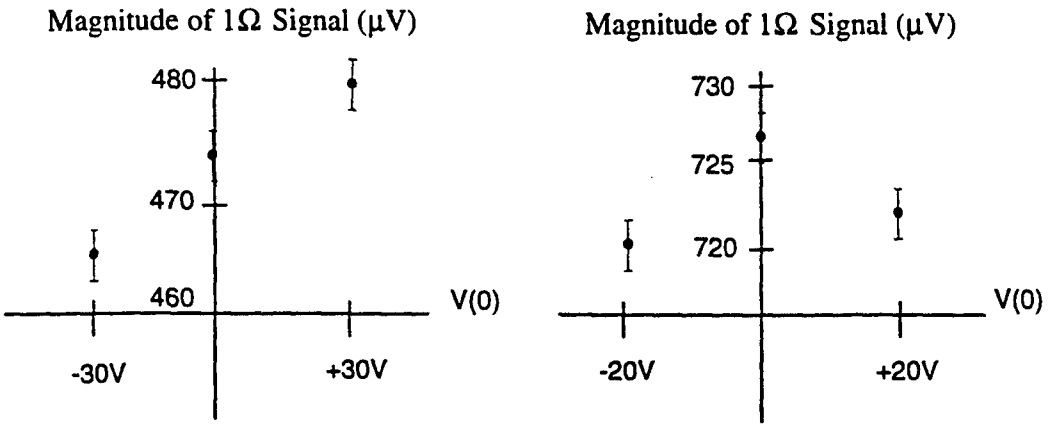

Figure 3.7 Observed $BaTiO_3$ signals with applied dc voltage. The 60° (a) angle of incidence signal appears to have some Kerr-like behavior but the (b) 70° angle of incidence signal does not.

For the sake of providing some boundaries to the analysis of the composite material however, a calculation was performed assuming a strong quadratic electrooptic response of the $BaTiO_3$. Considering the three data points while simply assigning the magnitude of signal variation at 70° and 75° as due to quadratic electrooptic effects, a fit was done for the third order electrooptic coefficients. s_{3333} was calculated to be 10%-50% of that derived for the AF30/polycarbonate depending on the exact thickness, refractive index, and ratio of s_{3333}/s_{1133}. A composite

response is then modeled using the highest value for the $BaTiO_3$ electrooptic coefficients, assuming that electrical effective medium theory assumptions at 1kHz are valid and that all of the dc field appears in the $BaTiO_3$ layers (composite response then dominated by the $BaTiO_3$). The calculated signal is only 20% of the observed composite signal at high values for the angle of incidence. Only in the improbable situation of most all of the ac voltage also appearing across the $BaTiO_3$ layers do signal strengths match those observed from the composite. We believe it more reasonable to attribute a maximum of 15% of the composite signal to the $BaTiO_3$ due to the high expected polarizability. Assuming that the $BaTiO_3$ signal is due to thickness variations it is found that the maximum contribution is again near 15%. For the rest of the analysis it is therefore assumed that the dominant source of composite signal is refractive index variations of the AF-30/polycarbonate. This conclusion is supported by measurements made on an AF-15/polycarbonate and $BaTiO_3$ composite of similar construction to the AF-30 composite. Observed signals were smaller (about 25% of the AF-30 signals at 65° angle of incidence) and non-Kerr like in nature, it is not known if there was enhancement of the AF-15 nonlinearity.

AF-30/polycarbonate *s*-coefficients were determined by a simultaneous fitting of both the composite and a homogeneous AF-30/polycarbonate film under the assumption of composite response dominated by the AF-30/polycarbonate. It was necessary to use the composite data to some degree due to the paucity of data from the homogeneous film. As with the $BaTiO_3$ data, low angles of incidence and *s*-polarized input generally provided small and unreliable signals, however the homogeneous film did provide some decent p-polarized signals at high angles of incidence and they were Kerr-like in nature. The larger composite signals though gave good p-polarization data at many angles and its distinctive shape was the attribute used as a verification on the

relative proportions of the four independant homogeneous film coefficients (real and imaginary *s*-values). The absolute magnitude of the AF-30/polycarbonate coefficients were set to match the high angle signal levels in the homogeneous film. The fitted *s* coefficients for the AF-30/polycarbonate films were $s_{3333}=(2+0.1i)\text{x}10^{-21}(\text{m/V})^2$ and $s_{1133}=(0.8+0.05i)\text{x}10^{-21}(\text{m/V})^2$. These values seem low when compared against published results for other organic systems as mentioned above, but they served mostly to calibrate the homogeneous films for comparison to the composite and internal scaling errors in the derivation would be also included in the composite fit.

The composite data was fitted assuming that the AF-30/polycarbonate was the dominant nonlinear constituent. As a consequence, the relative proportions of all four independent electrooptic coefficients were fixed. The ratio $s_{3333_{eff}} / s_{1133_{eff}}$ is given by effective medium values for the model assuming a single effective medium layer. The only variable in the composite fit is therefore a scaling factorthat determines the overall nonlinearity. Figure 3.8 displays the composite theoretical curve fit for both exact and effective medium approximations and experimental data for both the composite and the homogeneous AF-30/polycarbonate films. Errors in the data arise from signal noise as well as some spread in separately obtained measurements. The data signal levels have been scaled so that the ac and dc electric field strengths are identical between samples. This can be done since all signals scale linearly in both the applied voltages. As an example, if there is data for an applied dc voltage of 20 volts, the signal for an applied dc voltage of 10 volts is simply 50% of that. To normalize the electric fields strengths, we set

$$\frac{V_{composite}(0)}{d_{composite}} = \frac{V_{AF-30/\,polycarbonate}(0)}{d_{AF-30/\,polycarbonate}} \tag{3.17}$$

and likewise for the ac field. Setting the internal electric fields strengths equal will allow for somewhat of a basis for comparison between signal strengths as the shape of the p-polarization curve for the homogenous film is similar to the composite curve for the thicknesses of the films measured. The ratio of susceptibilities however cannot be directly extracted from the signal levels but can only be obtained through the lengthy fit algorithm that accounts for all of the involved optics. With the thickness of the homogeneous film close to that of the composite, it can be calculated that a signal from a composite film with an effective $\chi^{(3)}$ of $\chi_a^{(3)}$ would have a signal strength smaller than that of the homogeneous AF-30/polycarbonate film. The enhanced signal from that value indicates that an enhancement is occurring with field localization presumably playing a major role.

Apart from the data fitting and enhancement phenomenon is the fact that the effective medium approximation matches the exact prediction very well with some divergence at higher angles of incidence. This provides a verification of the theoretical predictions of effective medium theory. The high angle divergence is mostly due to the error in the propagation angle prediction of effective medium theory at higher angles.

The composite fit indicated a $\chi_{3333_{eff}}^{(3)}$ 3.2 times greater than the $\chi_{3333}^{(3)}$ of the AF-30/polycarbonate. The simulated response would seem to indicate an electric field localization inside the AF-30/polycarbonate greater than the expected amount based on the effective medium prediction of section 3.3. Recall that the predicted enhancement factor was 2.1, although that was derived from an all-ac applied electric field. Finally we express the effective medium coefficients and susceptibilities formally as factors of the AF-30/polycarbonate values.

$$s_{3333_{eff}} = f_a\left[\frac{\varepsilon_\perp(\Omega)}{\varepsilon_a(\Omega)}\right]\left[\frac{e_a(0)}{E(0)}\right]s_{3333_a}$$

$$\chi^{(3)}_{3333_{eff}} = f_a\left[\frac{\varepsilon_{eff_\perp}(\omega)}{\varepsilon_a(\omega)}\right]^2\left[\frac{\varepsilon_\perp(\Omega)}{\varepsilon_a(\Omega)}\right]\left[\frac{e_a(0)}{E(0)}\right]\chi^{(3)}_{3333_a} \tag{3.18}$$

$$s_{3333_{eff}} = 1.57 \cdot s_{3333_a}$$

$$\chi^{(3)}_{3333_{eff}} = 3.2 \cdot \chi^{(3)}_{3333_a} \tag{3.19}$$

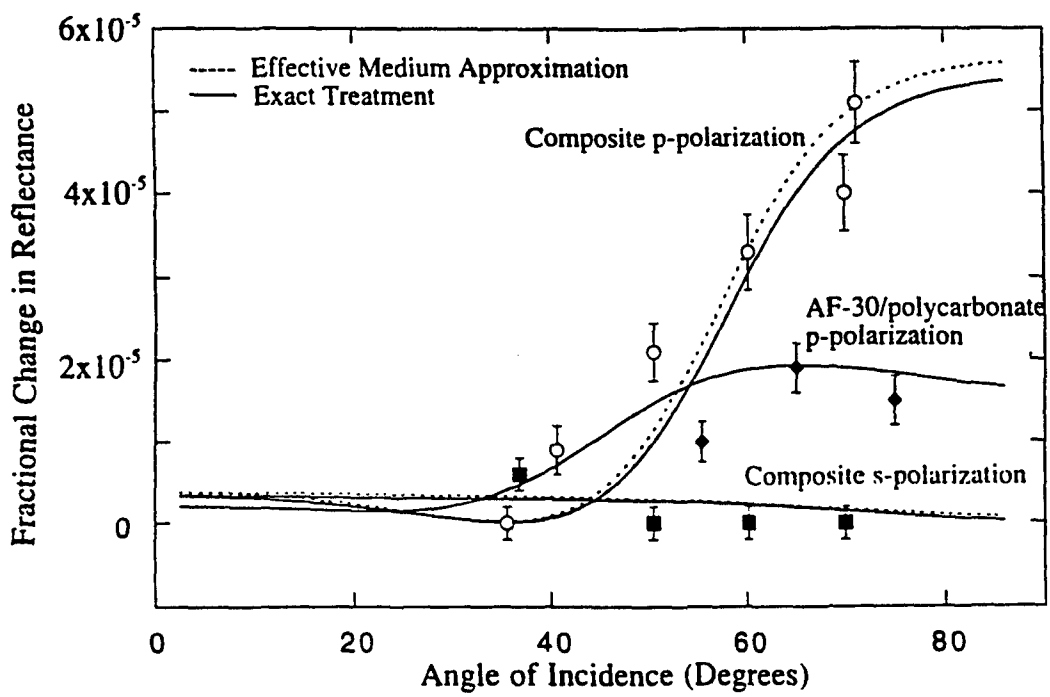

Figure 3.8 Data and theoretical curves based on fit parameters for composite and homogeneous AF-30/polycarbonate films. The electric fields were normalized based on applying 40 volts ac and dc across the 800 nm composite. Slightly higher voltages (by ratio of 855/800) would be applied across the homogeneous film since it is thicker. Unfilled circles are composite p-polarization data, filled squares are composite *s*-polarization, and filled diamonds are for the homogeneous AF-30/polycarbonate film

The relation between $\chi^{(3)}$ and the electrooptic coefficient s may be derived by utilizing the expression $n = \sqrt{1 + 4\pi\chi_{eff}}$ where $\chi_{eff} = \chi^{(1)} + 6\chi^{(3)}E(\Omega_1)E(\Omega_2)$ and the degeneracy factor of 6 arises out of the fact that there are 3 distinct applied fields including the optical field. An expression for Δn is then derived, assuming Δn is due to nonlinear effects, and set equal to equation (3.6) for a homogeneous film or (3.12) in the case of a composite to solve for a relation between the two quantities.

3.5 Conclusions

From a simple phenomenological point of view, we know that layer thicknesses are within the effective medium approximation and so the composite may be represented as a monolayer with a susceptibility of more than three times that of the homogenous polymer layers and larger than that of $BaTiO_3$ by some other factor. The large enhancement explanation lies in the details of electrical effective medium theory or in the $BaTiO_3$ response. For all-optical interactions, effective medium theory has been shown[19] to provide excellent results, so there is little reason to expect anomalies with the optical portion of the effective medium approximation. The high nonlinearity may derive from the composite acting to enhance some Kerr mechanisms in ways not explainable with the current effective medium theory such as the multilayer structure introducing an abundance of surface states for instance. There may also be some uncertainty in the measured layer sizes that could actually mean a higher fill fraction of $BaTiO_3$ than assumed. In any case it is reasonable to assume that much of the composite response is explained with the formal predictions of effective medium theory with a more complete and detailed model perhaps obtainable in the future. Higher enhancements are possible at higher fill fractions of the $BaTiO_3$ in theory.

Practically, electrooptic materials are utilized mostly in the waveguide configuration. For our material to be used as such film quality would probably have to improve or scattering losses would be large. It is very encouraging that the enhancement leads to a measurable increase in the output modulation of the reflected light. This demonstrates that composite structures may well find use in the wide variety of applications for electrooptic materials. These results are complementary to those of Fischer et al.[19] for degenerate four wave mixing in layered composites and provide further confirmation of the theoretical predictions of Boyd and Sipe[1].

3.6 References

1. R .W. Boyd and J. E. Sipe, "Nonlinear optical susceptibilities of layered composite materials," J. Opt. Soc. Am. B **11**, 297 (1994).

2. R. W. Boyd, *Nonlinear Optics*, pp. 399-400 (Academic Press, San Diego, 1992).

3. see ref. 2 p. 406.

4. A. von Hippel, *Dielectrics and Waves*, pp. 228-31 (Artech House, Boston 1995).

5. A. von Hippel, *Dielectric Materials and Applications*, p. 305 (Artech House, Boston 1995).

6. C. C. Teng and H. T. Man, "Simple reflection technique for measuring the electro-optic coefficient of poled polymers," Appl. Phys. Lett. **56**, 1735 (1990).

7. J. S. Schildkraut, "Determination of the electrooptic coefficient of a poled polymer film," Applied Optics **29**, 2839 (1990).

8. R. A. Norwood, M. G. Kuzyk, and R. A. Keosian, "Electro-optic tensor ratio determination of side-chain copolymers with electro-optic interferometry," J. Appl. Phys. **75**, 1869 (1994).

9. F. Qiu, K. Misawa, X. Cheng, A. Ueki, and T. Kobayashi, "Determination of complex tensor components of electro-optic constants of dye-doped polymer films with a Mach-Zehnder interferometer," Appl. Phys. Lett. **65**, 1605 (1994).

10. M. G. Kuzyk and C. W. Dirk, "Quick and simple method to measure third order nonlinear optical properties of dye doped polymer films," Appl. Phys. Lett. **54**, 1628 (1989).

11. C. A. Eldering, A. Knoesen, and S. T. Kowel, "Use of Fabry-Pérot devices for the characterization of polymeric electro-optic films," J. Appl. Phys. **69**, 3676 (1991).

12. H. Uchiki and T. Kobayashi, "New determination method of electro-optic constants and relevant nonlinear susceptibilities and its application to doped polymer," J. Appl. Phys. **64**, 2625 (1988).

13. P. Röhl, B. Andress, and J. Nordmann, "Electro-optic determination of second and third order susceptibilities in poled polymer films," Appl. Phys. Lett. **59**, 2793 (1991).

14. W. C. Chew, *Waves and Fields in Inhomogeneous Media*, pp. 49-53 (Van Nostrand Reinhold, New York 1990).

15. D. Morichère, M. Dumont, Y. Levy, G. Gadret, and F. Kajzar, "Nonlinear properties of poled polymer films: SHG and electrooptic measurements," SPIE **1560**, *Nonlinear Optical Properties of Organic Materials IV* (1991).

16. E. D. Palik (editor), *Handbook of Optical Constants of Solids*, p.294 (Academic Press, Orlando,1985).

17. J. A. Woollam Co., Inc. Users Manual for VASE Ellipsometer, pp. 415-425 (Oct. 1992).

18. R. Blum, M. Sprave, J. Sablotny, and M. Eich, "High-electric-field poling of nonlinear optical polymers," J. Opt. Soc. Am. B **15**, 318 (1998).

19. G. L. Fischer, R. W. Boyd, R. J. Gehr, S. A. Jenekhe, J. A. Osaheni, J. E. Sipe, and L. A. Weller-Brophy, "Enhanced Nonlinear Optical Response of Composite Materials," Phys. Rev. Lett. **74**, 1871 (1995).

Chapter 4

Photonic Band Gap Nonlinear Optical Materials

4.1 Introduction

There has been recent interest in the nonlinear optical properties of composite material systems composed of two or more constituent materials. Systems where the scale of the material variations is much less than the optical wavelength, so that the electrostatic field approximation may be applied, are generally termed composite optical materials. We studied such systems in chapters 1,2,3 and 5 of this thesis. If the scale of the material variations is increased to the extent that there are significant optical phase shifts over the material inhomogeneities, there is another interesting class of both linear and nonlinear optical phenomena that can occur.

A photonic band gap (PBG) structure is a material system that prohibits the propagation of electromagnetic radiation over a range of wavevectors. Incident radiation at these wavevectors will be almost entirely reflected because of the interference properties of radiation within the structure. PBG structures can be constructed in one, two, and three dimensions. Here we consider only the one-dimensional case as it is simplest to examine and construct yet still is potentially useful. The principles involved in one dimensional structures can be extended to higher dimensions however.

The properties of a PBG material can be engineered by selecting proper materials for the constituents and by altering the mechanical structure. A widely analyzed one dimensional structure is a periodic multilayer of two materials possessing different

linear optical properties and whose optical layer thicknesses are near a quarter-wavelength. Quarter-wavelength structures can be used for high or low reflection dielectric coatings [1]. Interesting nonlinear effects can occur in these PBG structures as will be discussed below, while others have studied spontaneous emission rates [2-5] and enhanced gain in a PBG laser [6]. Higher dimensional arrays of spheres or cylinders have been shown to have PBG behavior [2,7,8].

Enhanced nonlinear properties of periodic dielectric structures were predicted as early as 1970 by Bloembergen and Sievers [9], and later in Ref. [10], who introduced the idea of harmonic phase matching by using the optical properties of multilayers. Second-harmonic generation (SHG) has been investigated by a number of authors in various types of multilayer structures. Enhancement of the reflected second harmonic was observed experimentally in a 17-layer-pair structure [11] where the fundamental was tuned to the middle of the PBG stop band providing for strong counterpropagating beams. Enhanced SHG using a defect in an otherwise periodic structure has been investigated theoretically and experimentally [12-13], and was also experimentally demonstrated in a vertical cavity geometry of GaAs/AlAs multilayers combined with a SiO_2/TiO_2 distributed Bragg Reflector [14]. These enhancement schemes rely on a resonant cavity and our own calculations show that similar enhancement can be achieved utilizing simple partially transmitting metallic layers surrounding a single resonant layer in a Fabry-Pérot mode as suggested in [15]. The drawback of such an arrangement is the tendency of the metal layers to ablate with a strong incident fundamental. Enhancement of SHG in fiber Bragg gratings was also the subject of recent work [16].

Enhanced SHG in a one dimensional PBG structure without accompanying cavity modes was demonstrated numerically for large-index modulated structures with a pulsed incident fundamental [17] and theoretically for weakly periodic media using

multiple-scales perturbation [18]. These authors report enhancements of 2-3 orders of magnitude in power levels of the generated second-harmonic, over an equivalent length of phase-matched bulk material, near the photonic band edge of the fundamental. These results provide strong motivation for further investigation and application of such structures. Three reasons for the strong enhancement are described in the above two references. First the field amplitudes are enhanced due to resonance effects, also the transmission factor is large so that most of the fundamental energy is transmitted (also in [17] the second harmonic is tuned near the second-order band edge), and last the group velocity at the band edge is small so the fundamental field spends more time inside the structure which provides for greater conversion efficiency.

Third-order processes have also gained attention in PBG type materials with investigations into gap-soliton propagation and optical switching [19-29]. An interesting application involving a $\chi^{(3)}$ process was the nonlinear optical diode in Ref. [30,31] where optical transmission was dependent on the direction of propagation. Recently three different one-dimensional photonic band gap structures were investigated for their optical limiting abilities [32], and in their investigation of a quarter-wavelength type structure, the authors numerically found good broadband limiting properties of a 63 layer structure with modest linear index modulation but nonlinear coefficients of equal value but opposite sign in the adjacent layers. The limiting process was accomplished through strong reflectivity at high incident intensities.

In the present article we numerically further investigate the nonlinear optical properties of PBG structures with an emphasis on the question of how the nonlinear response compares to the bulk response of the nonlinear constituent. Unlike references [17,32] we will consider systems where only one of the materials possesses the

dominant nonlinear response. Also we will concentrate on deep index modulations, with relatively weak nonlinearities, where properties such as reflection and transmission are relatively unaffected by the nonlinear interactions occurring inside the structure, unlike Ref. [32].

4.2 Linear Optical Properties

The outstanding feature of linear optical propagation in PBG structures was mentioned above: There exists a range of wavevectors for which incident electromagnetic radiation will not propagate inside the PBG material, which is the band gap region. The range of frequencies over which this occurs and the strength of the reflectivity will depend on the details of the structure. For one-dimensional periodic dielectric materials these will be the values of the layer indices, the thicknesses of the layers and the number of layer pairs that are in the structure. Generally with more layers present and greater index differentials between layers, the stronger will be the band gap effects. We consider the dielectric stack shown in figure 3.1, and examine the case for 10 periods and purely real dielectric constants of $\varepsilon_a(\omega)$=2.25 and $\varepsilon_b(\omega)$=4. The resulting transmission properties are plotted in figure 3.2 for fixed layer pair thickness and as a function of incident vacuum optical wave number (no dispersion). It can be clearly seen that there is a band of incident wavelengths for which the transmission is very low while outside the band the transmission is high and is even unity for certain wavelengths. The band edge is also indicated as this will have special significance in the nonlinear investigations to follow.

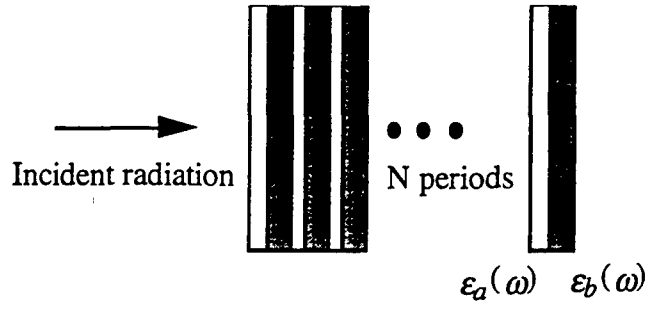

Figure 4.1 Geometry of a one-dimensional PBG structure.

Figure 4.2 would be of identical form if we plotted transmission for fixed incident wavelength and variable layer pair optical thickness. This will be the variable that will be considered in the following sections. The band edge and band gap will retain their meaning but occur at certain layer thicknesses instead of particular incident wavelengths. In fact if both constituents are kept near their quarter-wave thicknesses, then the band gap center position can be defined as the layer thicknesses where

$$\frac{[n_a d_a + n_b d_b]}{\lambda_o} = \frac{1}{2} \tag{4.1}$$

The band edge region is an interesting region in the study of both linear and nonlinear optics. As discussed in Ref. [5] the spontaneous dipole emission rate at this point is greatly enhanced due to a high electromagnetic density of states and transmittance of near unity. Alternatively spontaneous emission is suppressed inside the band gap region. It might be guessed that the driven dipole emission rate also will be enhanced as in the case of second-harmonic generation as shown in Ref. [17]. Now the question of whether third-order degenerate four wave mixing (DFWM) processes can be enhanced is addressed.

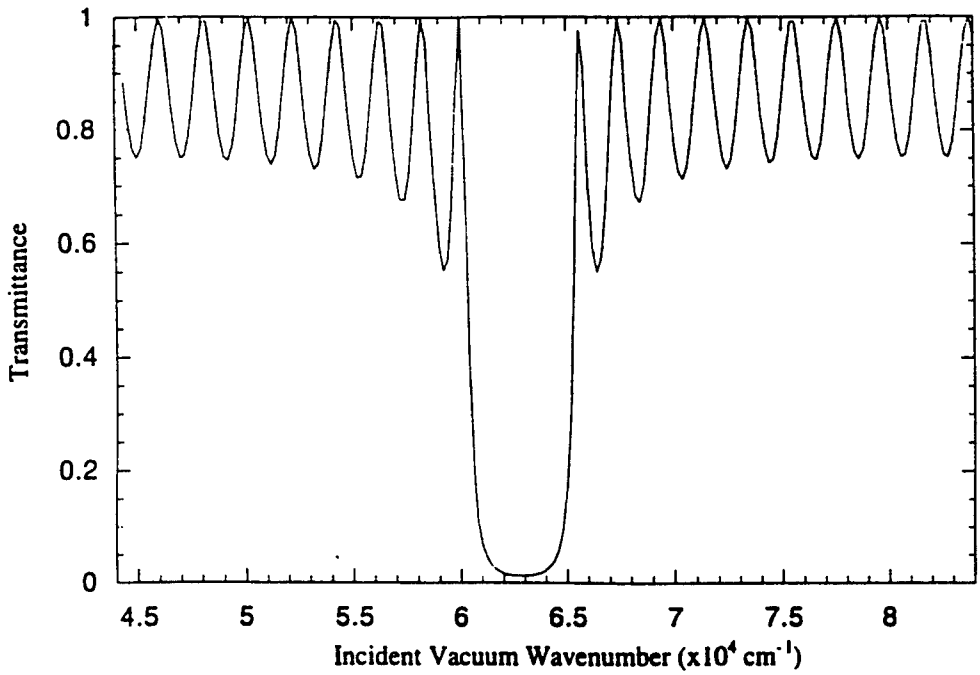

Figure 4.2 Calculated transmittance curve for a PBG structure. The surrounding medium is air, n_a=1.5, d_a=500 nm, n_b=2, d_b=375 nm, where d is the layer thickness and there are 10 layer pairs. The band gap is the region of low transmittance and the band edge is the peak of high transmittance on either side of the band gap.

4.3 The Intensity Dependent Refractive Index in PBG Structures

4.3.1 Method of Calculation

We consider plane waves of linear polarization propagating in the direction perpendicular to the plane of the layers in the multilayered PBG structure. The structures considered are composed of N layer pairs with only one of the constituents having a third-order Kerr optical nonlinearity. Initially we consider the material with only the linear response as constituent *a* and the material with the third order nonlinearity is denoted constituent *b*. The refractive index for the *b* layers is given by

$$n_b = n_{b0} + 2\bar{n}_2|\mathrm{E}(\omega)|^2 \tag{4.2}$$

where $\bar{n}_2$ is the nonlinear refractive index. Initially the zeroth order field magnitudes throughout the structure are calculated using the incident field magnitude and assuming no nonlinearities present. Also we will suppress the explicit ω notation as it is understood that all field quantities are oscillating at the same optical frequency.

The field solutions are arrived at by requiring the electromagnetic boundary conditions of continuity of the tangential components of E and H, with E and H plane wave solutions to Maxwell's equations in each layer, be satisfied simultaneously at each of the 2N+1 boundaries. Incident E and H fields are considered to have a fixed amplitude. The unknown H fields are determined from the E fields using the plane wave relation

$$\mathbf{H} = n\hat{\mathbf{k}} \times \mathbf{E} \ . \tag{4.3}$$

For the zeroth order solution this leads to the matrix equation

$$\mathbf{AF} = \mathbf{F}_0 \tag{4.4}$$

where $\mathbf{A}$ is a (4N+2) X (4N+2) matrix representing the two boundary conditions at each interface, $\mathbf{F}$ is a vector representing all the unknown electric field amplitudes including the back traveling amplitudes (2 per 2N layers plus reflected and transmitted, 4N+2 in all), and $\mathbf{F}_0$ is the vector that represents the known input amplitudes which for this case is just the incident E and H fields. This approach is equivalent to the transfer matrix technique and details may be found elsewhere [1].

Field amplitudes from the zeroth order solution are used to calculate the first order correction to the refractive indices in the nonlinear layers. Considering the field in layer j in more detail we write

$$\mathbf{E}_{oj} = \hat{\mathbf{e}}(E_{oj}e^{ikz} + E'_{oj}e^{-ikz}) \tag{4.5}$$

with prime denoting backtraveling wave quantities. The scalar amplitudes are those at the top of layer j and the exponentials describe the spatial variation within the layer. When proper account is taken of the spatial dependencies of all the terms in the full expression for $|\mathbf{E}_{oj}|^2$, it is noted that only the terms which contain the same spatial dependence of the moving wave should be retained [33]. Therefore for the forward moving wave we have

$$n_{bj} = n_{b0} + 2\bar{n}_2(|E_{oj}|^2 + 2|E'_{oj}|^2) \tag{4.6}$$

and for the backtravelling wave

$$n'_{bj} = n_{b0} + 2\bar{n}_2(2|E_{oj}|^2 + |E'_{oj}|^2) \tag{4.7}$$

as the expressions for the refractive indices. The differing indices for the two waves arises out of the unequal strengths of self and cross phase modulation. Previous work [32] seems not to have maintained the distinction. Also we use the slowly varying amplitude approximation as we are not necessarily interested in the strong nonlinear limit. Once the new n_{bj} and n'_{bj} are calculated, another self-consistent solution is achieved by a second iteration of (4.4) using the new values of the layer indices separately for the forward and backtravelling waves. This first order solution for the fields is usually accurate enough in the weakly nonlinear limit (either weak field or weak n_2) to be used as a representation for the nonlinear material response, which was the case in Ref. [32]. In some situations however we may gain accuracy by continuing the iteration process until a convergence to within specified limits is achieved. This can be noticeable at higher field strengths or nonlinearities. At higher field strengths or nonlinearities, the solution begins an oscillatory behavior with the number of

iterations, that is it does not converge to a single solution. At lower nonlinear interaction levels the solution asymptotically converges to a steady value. When there is asymptotic behavior in the solution, then it is assumed that the answer provided for the nonlinear response is satisfactory while oscillatory solutions are avoided. The oscillatory solution may indicate an underlying dynamical instability, but we have not yet verified that hypothesis.

4.3.2 Non-dissipitive PBG Structures

By using the procedure described above, the field magnitudes in all layers including the exiting field can be determined. The algorithm provides amplitudes and phases for all fields and allows for consideration of the nonlinear phase shift on passage of the incident wave through a nonlinear medium. By comparing the nonlinear phase shift between PBG structures and homogenous media, the relative effective nonlinearity of the PBG can be determined. Of particular interest is whether the nonlinear phase shift is larger on passage through a PBG material over a homogenous film of equivalent total thickness.

All calculations are performed assuming a fixed incident wavelength of $1.06\,\mu$m and all layers are assumed to be lossless dielectrics. The surrounding medium has an index of 1.0 and initially the indices of the two constituents are set at n_a=1.5 and n_b=2.0 with material *b* being the Kerr active medium. There are 10 layer pairs and as a first example the thickness of material *a* (the low index linear medium) will be varied as the independent variable. The index in the nonlinear active layer is described as

$$n_{bj} = n_{b0} + \beta(|E_{oj}|^2 + 2|E'_{oj}|^2)$$
$$n'_{bj} = n_{b0} + \beta(2|E_{oj}|^2 + |E'_{oj}|^2) \quad (4.9)$$

where β=1x10^{-6}. The value of β is not as important as its product with the field modulus squared, which had to be kept at values low enough to ensure proper solution convergence. Since the purpose of the present analysis is to compare PBG materials with homogeneous layer response, the incident field magnitude was simply set to unity.

Figure 4.3 displays three curves; the nonlinear phase shift through the PBG structure, the nonlinear phase shift through a homogenous film of material *b* of equivalent total thickness, and a scaled plot of the transmittance to qualitatively display where the band edge and band gap are located. As might be inferred from the results of Ref. [17], there is an enhancement of the nonlinear phase shift at the band edge of the PBG material over the response of the homogenous layer. Since forward DFWM is an automatically phase matched process, some features present in harmonic generation do not apply. Along with phase matching, there is no 'extra' enhancement by tuning the harmonic to a higher order band edge, therefore the maximum achievable enhancement with DFWM is probably smaller. Certainly the high transmittance and the resonantly enhanced fields inside the high index layers are contributing to the enhancement.

Further investigation shows that the size of the enhancement effect increases with increasing number of layer pairs and with depth of the index differential. The relative thicknesses of the individual layers can vary considerably around the quarter-wave thickness and still provide band gap effects. This latitude in PBG design can provide for better enhancements in PBG structures. The optimum enhancement of the nonlinear phase shift, in the ten layer pair structure described above, occurred when

the low index layer was approximately 65% of its quarter-wave thickness and the nonlinear high index layer was approximately 110% of its quarter-wave thickness.

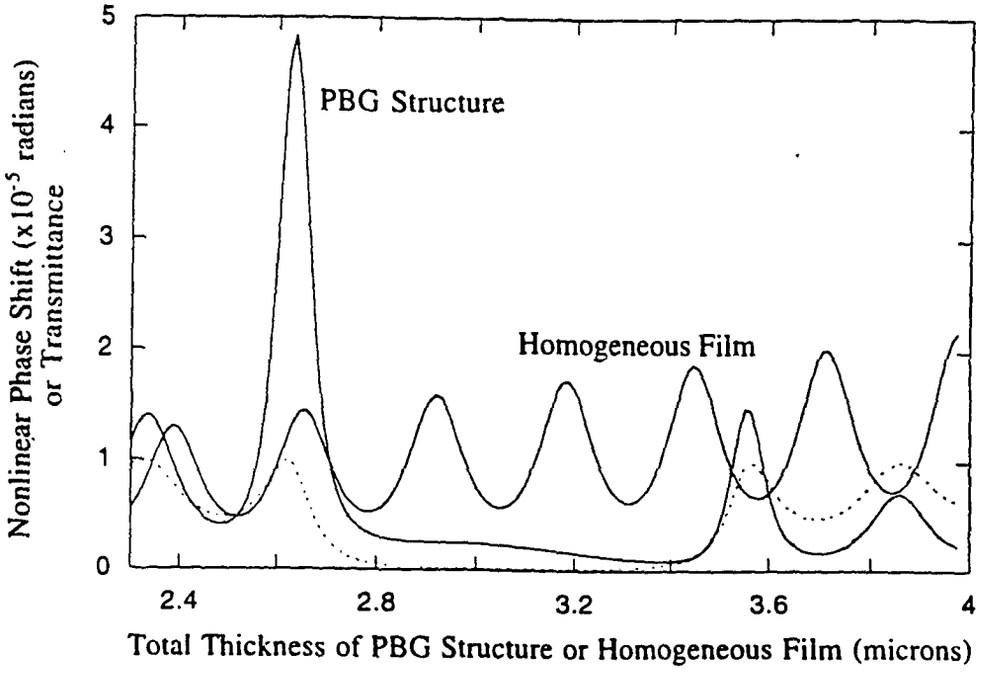

Figure 4.3 Nonlinear phase shift produced by PBG structure as compared to that of a homogenous film of the nonlinear constituent with the same total thickness as the PBG structure. The dashed line is a plot of the transmittance so that the location of the band edge is clearly visible. The thickness of the high index nonlinear component is set at the quarter-wave thickness and the low index layer thickness is allowed to vary in the PBG structure.

The next example (figure 4.4) considers the alternative situation when the nonlinear constituent is the low index dielectric layer. Now the enhancement occurs at the opposite band edge and optimization provides for a greater enhancement. With the high index passive layer at 85% of its quarter-wave thickness and the low index nonlinear layer at 140% of the quarter-wave thickness, enhancement by a factor of

approximately 6 is seen while a maximum enhancement factor of about 4 was observed when the nonlinear constituent was the high index layer.

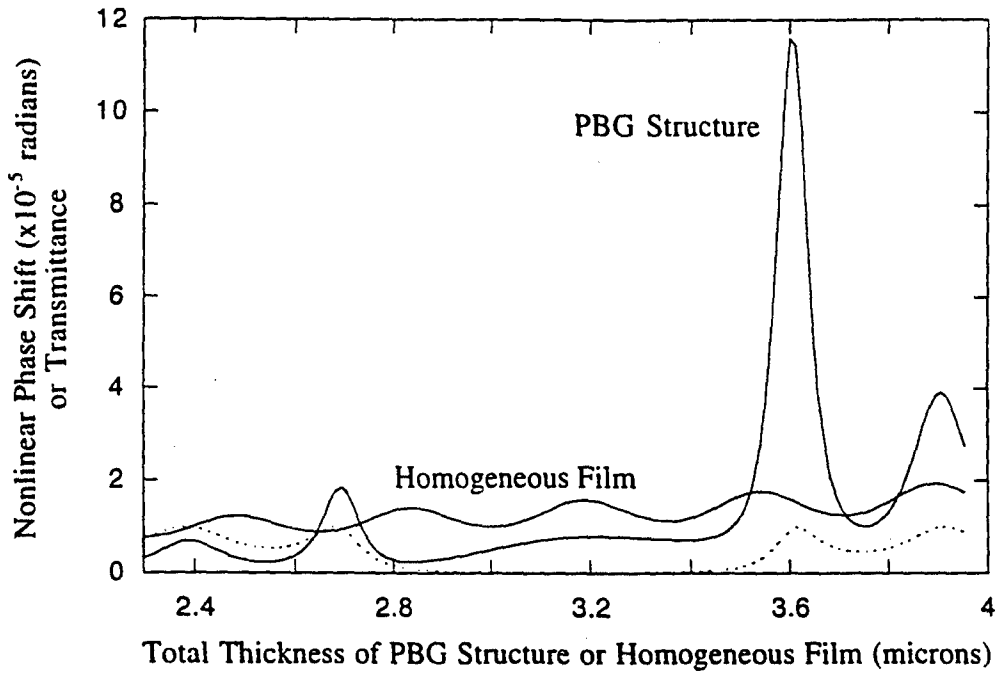

Figure 4.4 PBG nonlinear phase shift enhancement with the low index constituent as the nonlinear material, optimized for maximum enhancement. The dotted line is the transmittance. The thickness of the high index constituent is set at 85% of its quarter-wave thickness while the low index layer thickness is allowed to vary for the PBG structure. As in fig. 4.3, the homogeneous film thickness is equal to the total thickness of the PBG structure.

It is clear that PBG structures can provide for enhancements in the nonlinear phase shift in a manner similar to the reported enhancement in second-harmonic generation. This may have been an implicit result of Ref. [17,21-24,28,29,32], direct analysis was not done however as those articles were directed at other issues

surrounding PBG materials. The optimization may not be complete and further investigation may provide for better performance.

4.3.3 Nonlinear Absorption in PBG Structures

Band edge enhancements in lossless dielectric structures can be large and potentially useful. Alternatively there has been interest in nonlinear absorbing materials, especially in the application of optical limiting. We would expect that since nonlinear absorption is described by an imaginary $\chi^{(3)}$, or n_2, there is reason to expect similar enhancement of the nonlinear absorption. Two photon absorption materials hold promise as a means for optical limiting and are modeled as a positive imaginary contribution to the nonlinear refractive index. The action of a two photon absorber is then to provide an intensity dependent absorption coefficient that increases with intensity. We now investigate if a PBG-type material can also enhance the intensity dependent absorption.

The nonlinear layers (low index layers) have indices represented by the equation

$$\begin{aligned} n_{aj} &= n_{a0} + \gamma(\left|E_{oj}\right|^2 + 2\left|E'_{oj}\right|^2) \\ n'_{aj} &= n_{a0} + \gamma(2\left|E_{oj}\right|^2 + \left|E'_{oj}\right|^2) \end{aligned} \tag{4.9}$$

where γ is a complex number, the imaginary part of which describes nonlinear absorption. In order to avoid the possibility that the real part of γ (nonlinear index) could affect the magnitude of the output field, it is set to zero in order to isolate the effects of nonlinear absorption. Calculations are performed as before with several iterations done in order to ensure convergence of the solution. In this case however it will be the magnitude of the output field and not the phase that is of interest. The linear indices of the constituent layers are assumed to be purely real, possibly modeling a

nonresonant nonlinearity, and set at n_a=1.5 and n_b=2.0 and again there are 10 layer pairs. As expected (fig. 4.5), there is a band edge enhancement of the nonlinear absorption. The enhancement factor is about the same as in the nonlinear phase shift example.

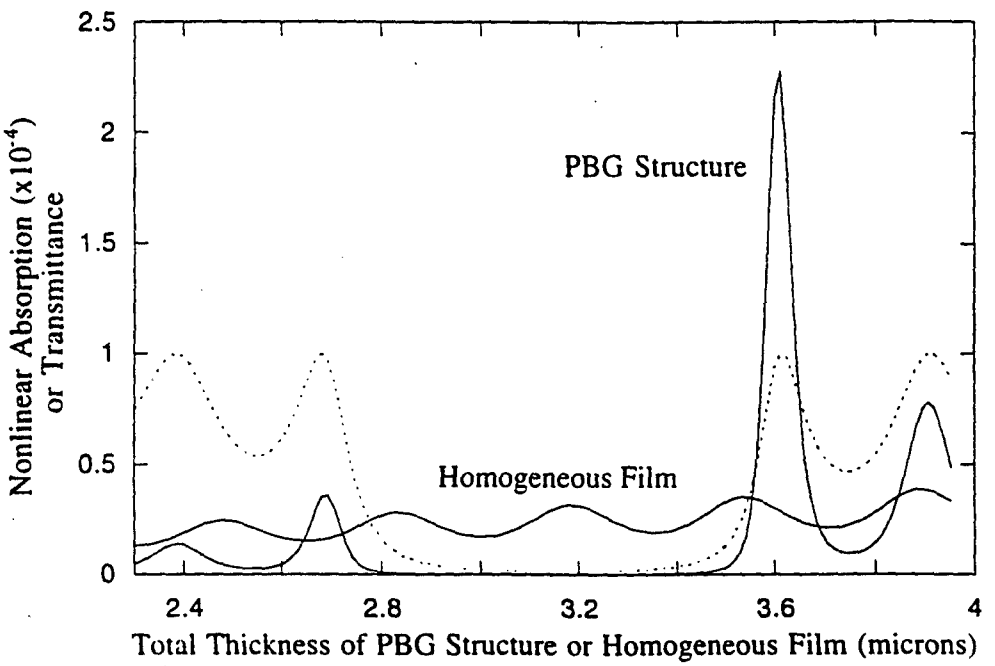

Figure 4.5 The nonlinear absorption plotted here is the change in the transmittance due to the nonlinear absorption in the sample. The low index layer is the nonlinear constituent and the high index layer thickness is held constant at 85% of its quarter-wave thickness in the PBG structure. Thickness of the homogeneous layer is as described in the previous two figures.

4.3.4 PBG Structures With a Central Phase Slip

There have been previous investigations into PBG structures containing a central region of thickness different from that of the other layers [11-13, 28, 29] with reported enhancements of second-harmonic generation in particular [11-13]. It is

interesting to ask how the calculation we have performed above is affected by the introduction of a central nonlinear active layer that is of different thickness than the other nonlinear layers. For consideration we take again the nonlinear constituent to be the lower refractive index layer and introduce a 0.5 micron low index nonlinear active central layer surrounded on either side by 5 layer pairs of PBG-type material. The high index layer thickness was set at 85% of its quarter-wave thickness and as can be seen from figure 4.6, maximum enhancement occurs when the low index nonlinear material is at approximately 120% of its quarter-wave thickness. Also apparent is that the magnitude of the enhancement has increased to a factor of about 30 over an equivalent thickness homogeneous layer of material a. The largest enhancement occurs at the new propagation mode introduced into the band gap. The enhancement here is analogous to the enhanced SHG reported in Ref. [12-13] and related to the results in Ref. [29,30]. Note that there is still an enhancement at the right band edge.

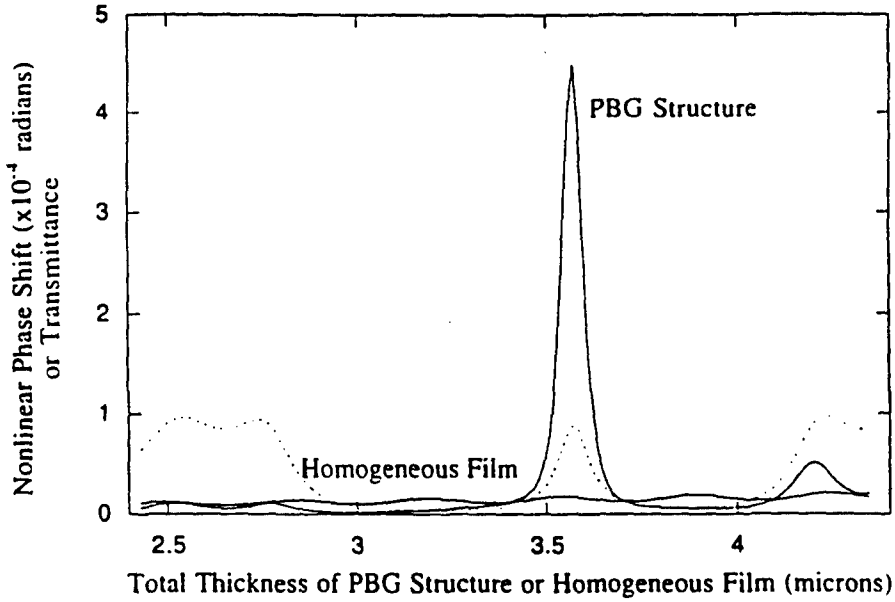

Figure 4.6 Response of a PBG structure with a central nonlinear layer. The dashed line is the transmittance. In the PBG material surrounding the central active region, the high index layers were held fixed at 85% of their quarter-wave thickness and the low index nonlinear layers were allowed to vary in thickness.

It appears that if an attempt is made to provide for maximum possible enhancement over a PBG-type structures' homogeneous counterpart, the best situations may not be limited to strictly periodic materials. The optimization problem here is more complex since there are more degrees of freedom in the design.

4.4 Conclusions

Photonic band gap optical materials are potentially useful materials for the development of material systems with enhanced nonlinear response. We have numerically demonstrated a considerable enhancement in the nonlinear refractive index at the photonic band edge over equivalent homogeneous materials. Band edge enhancements have also been shown to exist for second-harmonic generation [17,18]. Greater enhancements in the third-order nonlinearity seem possible in PBG structures with a central phase slip, or defect mode. Our results indicate a factor of 30 enhancement, with no attempt to optimize all of the physical parameters involved, in such a structure. It seems likely that greater application for theses structures will be found in future work.

4.5 References

1. M. Born and E. Wolf, *Principles of Optics*, sixth ed. (Pergamon, New York 1980).

2. E. Yablonovitch, "Inhibited Spontaneous Emission in Solid-State Physics and Electronics," Phys. Rev. Lett. **58**, 2059 (1987).

3. M. D. Tocci, M. J. Bloemer, M. Scalora, J. P. Dowling, and C. M. Bowden, "Measurement of spontaneous-emission enhancement near the one-dimensional photonic band edge of semiconductor heterostructures," Phys. Rev. A **53**, 2799 (1996).

4. J. P. Dowling and C. M. Bowden , "Atomic emission rates in inhomogenous media with applications to photonic band structures," Phys. Rev. A **46**, 612 (1992).

5. M. Scalora, J. P. Dowling, M. Tocci, M. J. Bloemer, C. M. Bowden, and J. W. Haus, "Dipole emission rates in one-dimensional photonic band-gap materials," Appl. Phys. B **60**, S57 (1995).

6. J. P. Dowling, M. Scalora, M. J. Bloemer, and C. M. Bowden, "The photonic band edge laser: A new approach to gain enhancement," J. Appl. Phys. **75**, 1896 (1994).

7. E. Yablonovitch and T. J. Gmitter, "Photonic Band Structure: The Face-Centered Cubic Case," Phys. Rev. Lett. **63**, 1950 (1989).

8. E. Yablonovitch, T. J. Gmitter, and K. M. Leung, "Photonic Band Structure: The Face-Centered Cubic Case Employing Nonspherical Atoms," Phys. Rev. Lett. **67**, 2295 (1991).

9. N. Bloembergen and A. J. Sievers, "Nonlinear optical properties of periodic laminar structures," Appl. Phys. Lett. **17**, 483 (1970).

10. C. L. Tang and P. P. Bey, "Phase matching in second-harmonic generation using artificial periodic structures," IEEE J. Quant. Elect. **QE-9**, 9 (1973).

11. J. P. van der Ziel and M. Ilegems, "Optical second harmonic generation in periodic multilayer GaAs-$Al_{0.3}Ga_{0.7}As$ structures," Appl. Phys. Lett., **28**, 437 (1976).

12. J. Martorell and R. Corbalán, "Enhancement of second harmonic generation in a periodic structure with a defect," Opt. Comm. **108**, 319 (1994).

13. J. Trull, J Martorell, R. Vilaseca, and R. Corbalán, "Second-harmonic generation in local modes of a truncated periodic structure," Opt. Lett. **20**, 1746 (1995).

14. S. Nakagawa, N. Yamada, N. Mikoshiba, and D. E. Mars, "Second-harmonic generation from GaAs/AlAs vertical cavity," Appl. Phys. Lett. **66**, 2159 (1995).

15. A. Ashkin, G. D. Boyd, and J. M. Dziedzic, "Resonant optical second harmonic generation and mixing," IEEE J. Quantum Electron. **QE-2**, 109 (1966).

16. M. J. Steel and C. Martijn de Sterke, " Second-harmonic generation in second-harmonic fiber Bragg gratings," Appl. Optics **35**, 3211 (1996).

17. M. Scalora, M. J. Bloemer, A. S. Manka, J. P. Dowling, C. M. Bowden, R. Viswanathan, and J. W. Haus, "Pulsed second-harmonic generation in nonlinear, one-dimensional, periodic structures," Phys. Rev. A **56**, 3166 (1997).

18. J. W. Haus, R. Viswanathan, M. Scalora, A. Kalocsai, J. D. Cole, and J. Theimer, "Enhanced second-harmonic generation in media with a weak periodicity," Phys. Rev A **57**, 2121 (1998).

19. W. Chen and D. L. Mills, "Gap Solitons and the Nonlinear Optical Response of Superlattices," Phys. Rev. Lett. **58**, 160 (1987).

20. N. D. Sankey, D. F. Prelewitz, and T. G. Brown, "All-optical switching in a nonlinear periodic-waveguide structure," Appl. Phys. Lett. **60**, 1427 (1992).

21. J. He and M. Cada, "Optical Bistability in Semiconductor Periodic Structures," IEEE J. Quantum Electron. **27**, 1182 (1991).

22. M. Cada, J. He, B. Acklin, M. Proctor, D. Martin, F. Morier-Genoud, M.-A. Dupertuis, and J. M. Glinski, "All-optical reflectivity tuning and logic gating in a GaAs/AlAs periodic layered structure," Appl. Phys. Lett. **60**, 404 (1992).

23. J. He and M. Cada, "Combined distributed feedback and Fabry-Perot structures with a phase-matching layer for optical bistable devices," Appl. Phys. Lett. **61**, 2151 (1992).

24. J. He, M. Cada, M.-A. Dupertuis, D. Martin, F. Morier-Genoud, C. Rolland, and A. J. SpringThorpe, "All-optical bistable switching and signal regeneration in a semiconductor layered distributed-feedback/Fabry-Perot structure," Appl. Phys. Lett. **63**, 866 (1993).

25. A. Kozhekin and G. Kurizki, "Self-Induced Transparency in Bragg Reflectors: Gap Solitons near Absorption Resonances," Phys. Rev. Lett. **74**, 5020 (1995).

26. D. N. Christodoulides and R. I. Joseph, "Slow Bragg Solitons in Nonlinear Periodic Structures," Phys. Rev. Lett. **62**, 1746 (1989).

27. C. Martijn de Sterke and J. E. Sipe, "Envelope-function approach for the electrodynamics of nonlinear periodic structures," Phys. Rev. A **38**, 5149 (1988).

28. S. Radic, N. George, and G. P. Agrawal, "Optical switching in $\lambda/4$-shifted nonlinear periodic structures," Opt. Lett. **19**, 1789 (1994).

29. S. Radic, N. George, and G. P. Agrawal, "Theory of low-threshold optical switching in nonlinear phase-shifted periodic structures," J. Opt. Soc. B **12**, 671 (1995).

30. M. Scalora, J. P. Dowling, C. M. Bowden, and M. J. Bloemer, "The photonic band edge optical diode," J. Appl. Phys. **76**, 2023 (1994).

31. M. D. Tocci, M. J. Bloemer, M. Scalora, J. P. Dowling, and C. M. Bowden, "Thin-film nonlinear optical diode," Appl. Phys. Lett. **66**, 1 (1995).

32. Y. Zhao, D. Huang, C. Wu, and R. Shen, "Comparitive study of one-dimensional photonic bandgap structures using multilayer nonlinear thin films," J. of Nonlinear Opt. Phys. and Mat. **4**, 1 (1995).

33. R. W. Boyd, *Nonlinear Optics,* (Academic Press, San Diego 1992).

Chapter 5

Nonlinear Optical Response of a Dense Maxwell Garnett Optical Composite Material

5.1 Introduction

Composite optical materials have recently been an area of intense research interest[1-10] because of the promise that these materials hold for displaying desireable nonlinear optical properties. Typically a composite material is comprised of two or more component materials which are mixed together on a mesoscopic distance scale, that is, a distance scale which is much larger than a typical atomic dimension but much smaller than an optical wavelength. The propagation of light through such a material can then be described at a macroscopic level by effective values of the linear refractive index and the nonlinear susceptibilities which are obtained by performing suitable volume averages. Interest in composite materials stems in part from the fact that the effective nonlinear susceptibility of a judiciously constructed composite material can exceed those of its constituent materials, as has been demonstrated both theoretically[6,9] and experimentally.[10]

One of the earliest investigations into optical composites was by Maxwell Garnett[1] who developed a linear effective medium theory to explain the behavior of metal-doped glasses. His theory was successful in at least qualitatively explaining the surface plasmon resonance phenomenon associated with such composites. The

Maxwell Garnett Geometry is shown in figure 5.1. Nonlinear work in Maxwell Garnett composites did not begin until the 1980's with the work of Ricard et al.[2] who determined the $\chi^{(3)}$ of metal colloids in water. Others[3-8] since then have also presented work regarding Maxwell Garnett composites. So far most effort has focused on metallic or semiconductor inclusion particles at low fill fractions. While these systems can provide for large nonlinearities, especially near a resonance, there can also be large absorption values associated with these nonlinearities. In this type of work, the host medium is usually assumed to posses a linear response only.

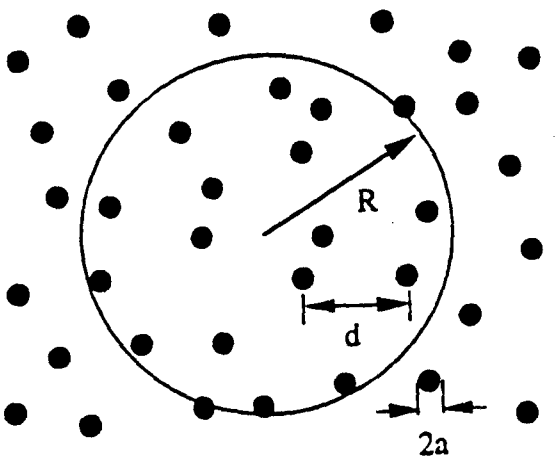

Figure 5.1 Maxwell Garnett geometry where R is the range over which the averaging of the susceptibilities is performed and a,d<<R<<λ. λ is the optical wavelength.

Sipe and Boyd[6] presented the theoretical prediction of the first nonlinear correction to the effective medium dielectric constant for third-order Maxwell Garnett[1] composites (see figure 5.1) with arbitrary linear optical dielectric constants in both constituents and randomly distributed inclusions. For the situation of a composite with both constituents possessing purely real linear dielectric constants (no surface plasmon resonance possible), they found that the effective third-order nonlinearity for a

nonlinear host medium containing linear inclusion particles can be enhanced over that of the host. The converse situation with nonlinear inclusions showed no enhancement.

The Sipe and Boyd model assumed in the nonlinear averaging of the host fields that the contribution to the nonlinear polarization by the neighboring inclusions' dipole fields was small or averaged to zero when considering the fields near a given inclusion. For dilute fill fractions of the inclusions, it is certainly true that near a given inclusion, inhomogeneities in the host electric field are due almost entirely to the dipole field of the given inclusion. At higher fill fractions proximity effects between the inclusions may become significant in both the host and inclusion electric fields. In linear effective medium theory these field distortions average out as $\chi_{eff}^{(1)}$ is determined by a linear averaging of the mesoscopic electric field distribution. This linear average is bounded by the Weiner limits[7] for the linear dielectric constant that become more restrictive at fill fractions above 50% since the value for any composite must approach the dielectric constant of the high fill fraction component. Therefore there are no possibilities for anomalous behavior and the Maxwell Garnett equations still represent a good approximation to the linear dielectric constant even though the mesoscopic fields may become very inhomogeneous at high fill fractions.

For nonlinear effective medium averaging however, the mesoscopic field inhomogeneities play a larger role than in the linear case. The nonlinear averages can vary dramatically since the χ_{eff}^{nl} can be considered to be proportional to higher moments of the mesoscopic electric field distribution,[8] which are more sensitive to the details of the mesoscopic field distribution. This fact may lead to differing predictions for the nonlinear response of high inclusion fill fraction Maxwell Garnett composites from the single inclusion field model of Sipe and Boyd since the host mesoscopic field distribution may become much unlike the dilute fill fraction case. It should be noted

that their calculation was not intended to necessarily represent these higher fill fraction composites.

In the present calculation we emphasize approaching the effective medium first from the mesoscopic perspective then procede to the macroscopic by appropriate averaging in the same vein as presented by Aspnes.[9] The mesoscopic field structure in the host can be considered to be comprised of a uniform background field onto which is superimposed the inhomogeneities generated by the mesoscopic material variations. We denote the uniform field in the host as the cavity field. In the Maxwell Garnett model the host field is the cavity field plus the dipole fields associated with the inclusions. The field inside the inclusions is assumed uniform which results if the field incident on the inclusion is uniform.

The effective third order nonlinearity for Maxwell Garnett all-dielectric composites (nonlinear host material) may be expressed as[6]

$$\chi_{eff}^{(3)} = (1-f)L_h^4 g_h(f,\varepsilon^h,\varepsilon^i)\chi_h^{(3)} \tag{5.1}$$

where f is the fill fraction of inclusions, L_h is a factor relating the cavity field in the host to the macroscopic average field (see equation 3.6 below), and g_h is a factor that represents the degree of inhomogeneity of the host fields due to the presence of the inclusions. In the developement of Maxwell Garnett composite response, it follows naturally that the mesoscopic field calculations are expressed in terms of the cavity field. Only when it is desired to cast $\chi_{eff}^{(3)}$ in terms of the macroscopic electric fied does the conversion factor L_h appears in the effective average. Since L_h is a factor relating two uniform field quantities, the order to which the cavity field is expressed does not affect the mesoscopic to macroscopic conversion and L_h depends only on the linear averaging of the mesoscopic fields. This interpretation of L_h explains a factor of

L_h^3 since the nonlinear polarization is proportional to the third power of the electric field and to the level of approximation used in the derivation of (5.1), the nonlinear polarization is expressed in terms of the linear field distribution. Not as simple to interpret is the fourth power of L_h which derives from the effect of $\mathbf{P}^{nl}$ on the factor relating the averaging from $\mathbf{E}^c$ to $\mathbf{E}$. $\mathbf{P}^{nl}$ is itself obtained by assuming no nonlinearity, but to ensure that the linear polarization is correct to the same order as $\mathbf{P}^{nl}$, the effect of $\mathbf{P}^{nl}$ on the linear polarization is accounted for. Electrostatically we treat the nonlinear polarization the same as the linear polarization and its effects on the relation between the cavity field and the macroscopic field is expressed by writing

$$\mathbf{E} = \mathbf{E}^c + \frac{4\pi}{3}\left[\mathbf{P}^{linear} + \mathbf{P}^{nl}\right]. \tag{5.2}$$

As can be seen, the correction due to $\mathbf{P}^{nl}$ will be of identical form as the factor describing how the linear polarization influences the ratio $|\mathbf{E}^c|/|\mathbf{E}|$.

In contrast to L_h, g_h does not depend on linear averages but on the higher order moments of the mesoscopic field distribution. We can think of no obvious bounds on g_h but it seems unreasonable to assume that there can be an infinite field localization inside of a composite material, especially an all-dielectric composite. Like the correction to the linear polarization described above for the nonlinear-linear dipole coupling, g_h will also contain a term for such a correction. But unlike the fourth local field factor of L_h, this term for g_h will not in general resemble the part of the nonlinearity derived from the linear distribution. This results in part from the geometric asymmetry of the host and inclusion material on the mesoscopic scale. For the case of nonlinear inclusions in the Maxwell Garnett model, inclusion fields are uniform which implies that $g_i = 1$. Large g_h values could be expected in composite materials where

there are strongly localized 'hot spots' in the electric field such as in a composite with metallic fractal clusters.

It is interesting to ask how χ_{eff}^{nl} may be affected by the modified interinclusion host fields in higher fill fractions of Maxwell Garnett composites. In the present chapter the effective third-order nonlinearity for a Maxwell Garnett system of spherical inclusions placed on a cubic lattice is calculated. Full account is taken of the effects of neighboring inclusions on the host mesoscopic electric field distribution near a given inclusion. The new calculation will account for changes in both the factors L_h and g_h due to proximity effects of neighboring inclusions.

5.2 Background

This work utilizes the general method presented in Ref. [6]; the reader is directed there for a more complete presentation of this background material. The notation will be kept nearly identical for ease of referencing. The interaction we wish to investigate is degenerate four wave mixing in response to incident linearly polarized radiation. The macroscopic direction of polarization will be taken as the z direction in all that follows. A formal connection between mesoscopic and macroscopic quantities is given by

$$\begin{aligned} \mathbf{E}(\mathbf{r},\omega) &= \int \Delta(\mathbf{r}-\mathbf{r}')\mathbf{e}(\mathbf{r}',\omega)d\mathbf{r}' \\ \mathbf{P}(\mathbf{r},\omega) &= \int \Delta(\mathbf{r}-\mathbf{r}')\mathbf{p}(\mathbf{r}',\omega)d\mathbf{r}' \end{aligned} \tag{5.3}$$

where $\Delta(\mathbf{r}-\mathbf{r}')$ is a smoothly varying, normalized weighting function with range $R << \lambda$. In the present paper mesoscopic quantities are expressed in lowercase letters and macroscopic in uppercase.

It is useful to define

$$\mathbf{p}'(\mathbf{r}) = \begin{cases} (\chi^{\mathrm{i}} - \chi^{h})\mathbf{e}(\mathbf{r}) & \mathbf{r} \in inclusion \\ 0 & \mathbf{r} \in host \end{cases} \tag{5.4}$$

for the mesoscopic linear dipole moment per unit volume where superscripts i and h denote inclusion and host respectively. We consider fields oscillating harmonically, in which case Maxwell's equations can be written as

$$\begin{aligned} &\nabla \cdot \left[\varepsilon^{h}\mathbf{e}(\mathbf{r})\right] = -4\pi\nabla \cdot \mathbf{p}^{s}(\mathbf{r}), \\ &\nabla \cdot \mathbf{b}(\mathbf{r}) = 0 \\ &\nabla \times \mathbf{e}(\mathbf{r}) - i\tilde{\omega}\mathbf{b}(\mathbf{r}) = 0, \\ &\nabla \times \mathbf{b}(\mathbf{r}) + i\tilde{\omega}\varepsilon^{h}\mathbf{e}(\mathbf{r}) = -4\pi i\tilde{\omega}\mathbf{p}^{s}(\mathbf{r}) \end{aligned} \tag{5.5}$$

where $\tilde{\omega} \equiv \omega/c$, $\mathbf{p}^{s}(\mathbf{r}) \equiv \mathbf{p}'(\mathbf{r}) + \mathbf{p}^{nl}(\mathbf{r})$, and $\mathbf{p}^{nl}(\mathbf{r})$ is the mesoscopic nonlinear polarization. All the macroscopic counterparts to the field quantities and equations given above are found through taking the average given in (5.3). The macroscopic Maxwell's equations are then found to be identical in form to the mesoscopic expressions in (5.5).

The operational relationship between mesoscopic and macroscopic fields in a Maxwell Garnett composite dominated by dipole fields is given by[6]

$$\mathbf{e}(\mathbf{r}) = \mathbf{E}(\mathbf{r}) + \frac{4\pi}{3\varepsilon^{\mathrm{h}}}\mathbf{P}^{s}(\mathbf{r}) + \int \tilde{T}^{o}(\mathbf{r}-\mathbf{r}')c(\mathbf{r}-\mathbf{r}')\cdot\mathbf{p}^{s}(\mathbf{r}')d\mathbf{r}' - \frac{4\pi}{3\varepsilon^{h}}\mathbf{p}^{s}(\mathbf{r}) \tag{5.6}$$

Where $c(\mathbf{r})$ is a spherically symmetric cutoff function of range R ($a, d << \mathrm{R} << \lambda$, see figure 5.1) and $\tilde{T}^{o}(\mathbf{r})$ is defined using the static dipole-dipole coupling tensor in the following way

$$\tilde{T}^{o}(\mathbf{r}) = \begin{cases} \tilde{T}(\mathbf{r}), & r > \eta \\ 0, & \mathrm{r} < \eta \end{cases} \tag{5.7}$$

$$\tilde{T}(\mathbf{r}) = \frac{3\hat{\mathbf{r}}\hat{\mathbf{r}} - \tilde{U}}{\varepsilon^h r^3} \tag{5.8}$$

with $\hat{\mathbf{r}} = \mathbf{r}/r$ and $\tilde{U} = \hat{\mathbf{x}}\hat{\mathbf{x}} + \hat{\mathbf{y}}\hat{\mathbf{y}} + \hat{\mathbf{z}}\hat{\mathbf{z}}$. The first two terms on the right in (5.6) represent the cavity field and the second two terms are the contribution to the local field from dipoles near the field point $\mathbf{r}$. In materials where higher-order multipole fields are significant, the integral term in equation (5.6) must be modified to include interactions between higher-order multipole moments. In this work, the local fields involve such interactions, therefore equations (5.6)-(5.8) as used in Sipe and Boyd are no longer adequate.

As has been shown in calculations of the effective conductivity of cubic array Maxwell Garnett composites,[11-13] proximity effects at high volume fill fractions imply that the inclusions' electric octupole and higher-order moments can become significant contributors to the effective medium response. These multipole effects scale with the ratio of inclusion and host dielectric constants. For our particular calculation we find that including effects of multipoles of order 2^5 (same order as Ref. [12]) gives an estimated error in the calculated results of 15% at the maximum packing fraction of $\pi/6$. In calculating the multipole host fields of the cubic lattice, the electrostatic potential is derived using an expansion in odd Legendre polynomials about each inclusion[11,12]

$$V^{host} = -E^c z + \sum_{n=1}^{\infty}\sum_{i=1}^{\infty} c_{2n-1} r_i^{-2n} P_{2n-1,i}(\cos\theta_i) \tag{5.9}$$

with the cavity field E^c in the +z direction (see fig. 5.2), 2n-1 is the order of the Legendre polynomial, and the summation over $\mathbf{i}$ represents summation over the inclusions. Subscript $\mathbf{i}$ is taken to mean that we are considering a spherical polar coordinate system centered on inclusion $\mathbf{i}$ with θ_i measured from the +z axis. $-E^c z$

represents the potential contribution from the uniform applied background field. Only odd order terms of the Legendre polynomials appear in the multipole expansion (5.9) as a consequence of the fact that the potential V must be an antisymmetric function of θ, about $\theta = \pi/2$. Also the potential must be symmetric in the azimuthal coordinate ϕ, about $\phi = \pi/4$, which implies that only terms with m divisible by 4 can contribute (in the $Y_{lm}(\theta,\phi)$ notation [14] for spherical harmonics). For this calculation we will consider n=1,2,3 only which implies that the only term with nonzero m is the n=3, m=4 term. We do not include this term since it was shown to have negligible impact in the calculation of Ref. [11] and appears in the highest order term of (5.9). Electric fields are obtained from the usual $\mathbf{E} = -\nabla V$ relation.

5.3 Calculation Method

Since the inclusions are arranged on a cubic lattice (see figure 5.2), we can numerically compute the interinclusion host field by simply adding the inclusion multipole contributions of all the inclusions inside of a suitably large sphere (in the calculation, a distance equal to 20 times the inclusion radius which also ensures a convergent solution). The multipole expansion of the mesoscopic electric field near a given inclusion is

$$\mathbf{e}(\mathbf{r}) = -\nabla\left[-E^c z + \sum_i c_1 \frac{\cos\theta_i}{|\mathbf{r}_i - \mathbf{r}|^2} + c_3 \frac{1/2(5\cos^3\theta_i - 3\cos\theta_i)}{|\mathbf{r}_i - \mathbf{r}|^4} + c_5 \frac{1/8(63\cos^5\theta_i - 70\cos^3\theta_i + 15\cos\theta_i)}{|\mathbf{r}_i - \mathbf{r}|^6}\right] \quad (5.10)$$

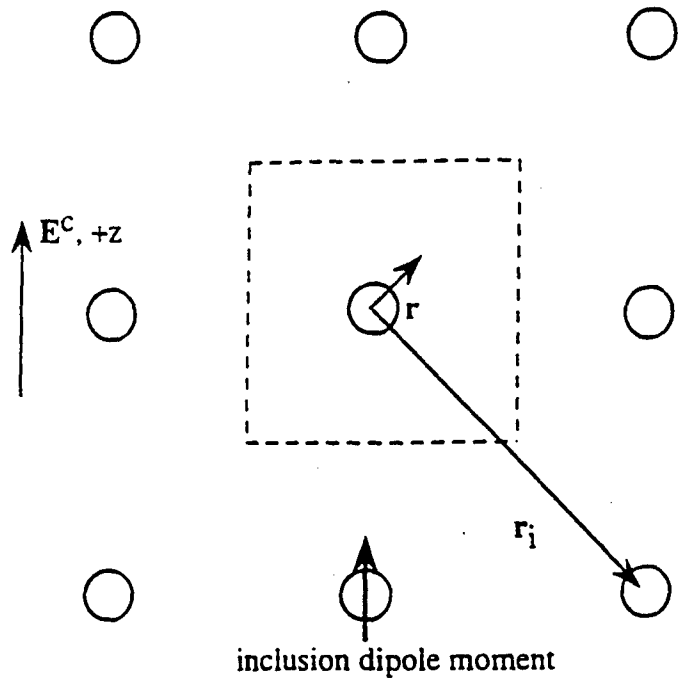

Figure 5.2 The geometry (two dimensional cross section) of the Maxwell Garnett calculation. The inclusions are arranged on a cubic lattice and the incident field is linearly polarized in the z direction. The unit cell is outlined with a dashed line.

where $\mathbf{r}$ and $\mathbf{r}_i$ are field and inclusion location vectors as shown in figure 5.2. The sum is over inclusions inside of a suitably large sphere surrounding the point $\mathbf{r}$. In the determination of the c coefficients, which are directly proportional to the multipole moments, we use the results of Ref. [12] slightly modified for the present situation. The c values to the level of approximation used here are given by

$$c_5 = 3.456 \frac{\varepsilon^i - \varepsilon^h}{(\varepsilon^i + 6/5\varepsilon^h)} \frac{a^{11}}{d^7} c_1 \tag{5.11}$$

$$c_3 = \frac{12.44 c_1 / d^5}{\left[\frac{\varepsilon^i + 4/3\varepsilon^h}{\varepsilon^i - \varepsilon^h} \frac{1}{a^7} - \frac{11.52}{d^7} \right]} \tag{5.12}$$

$$\frac{\varepsilon^i + 2\varepsilon^h}{\varepsilon^i - \varepsilon^h}\frac{1}{a^3}c_1 - \frac{12.44}{d^5}c_3 - \frac{3.456}{d^7}c_5 = E^c \tag{5.13}$$

where the lattice sums are evaluated in the given references and the last equation is solved for c_1 by substitution of the first two into the third. In writing equation (5.13) in the form shown, we have made use of the fact that the dipole-dipole coupling term sums to zero. In particular, at each lattice site, the total field of all the other dipoles vanishes as a consequence of the fact that the dipoles are placed on a cubic array and that the averaging procedure is carried out over a spherical volume. To the degree of approximation used in the present paper, it can be seen that octupole-octupole interactions are included in c_3, however 2^5 pole-2^5 pole interactions are not included in c_5.

We now calculate the mesoscopic polarization given by

$$\mathbf{p}^{nl}(\mathbf{r}) = A^h[\mathbf{e}(\mathbf{r})\cdot\mathbf{e}(\mathbf{r})^*]\mathbf{e}(\mathbf{r}) + \frac{B^h}{2}[\mathbf{e}(\mathbf{r})\cdot\mathbf{e}(\mathbf{r})]\mathbf{e}(\mathbf{r})^*. \tag{5.14}$$

In this calculation we assume linearly polarized radiation with purely real dielectric constants implying that when the mesoscopic polarization is considered, the quantities $[\mathbf{e}(\mathbf{r})\cdot\mathbf{e}(\mathbf{r})^*]\mathbf{e}(\mathbf{r})$ and $[\mathbf{e}(\mathbf{r})\cdot\mathbf{e}(\mathbf{r})]\mathbf{e}(\mathbf{r})^*$ are then identical and are collinear. The two terms in (5.14) may then be combined into a single term with coefficient (A+B/2). The c coefficients, and therefore the mesoscopic electric fields, are determined as functions of the cavity field. Ultimately however we wish to express the macroscopic nonlinear polarization in terms of the macroscopic electric field. Since the nonlinear polarization is cubic in the electric field, it is satisfactory to use the linear expression for the relationship between the cavity and macroscopic electric field which is given by

$$\mathbf{E}^c = E^c\hat{\mathbf{z}} = \left[\frac{\varepsilon + 2\varepsilon^h}{3\varepsilon^h}\right]E\hat{\mathbf{z}}\,. \tag{5.15}$$

where the cavity to macroscopic field relationship is still the same as in the Maxwell Garnett usual derivation but the effective medium dielectric constant, ε, is not. An explicit expression for ε can be found in Ref. [11,12] or the expression

$$\varepsilon = \varepsilon^h + \frac{4\pi c_1}{d^3 E} \tag{5.16}$$

may be used where c_1 from the expressions above is recognized as the inclusion dipole moment.

The mesoscopic electric field (5.10) is calculated at 26^3 points in the unit cell surrounding each inclusion. By symmetry of the cubic lattice, the field distribution in each unit cell is identical, and the field needs to be determined only in one octant of the unit cell as the rest of the cell can be determined via symmetry. The mesoscopic nonlinear polarization is then calculated using the single-term form of (5.14). The macroscopic nonlinear polarization is the simple average of the mesoscopic polarization over all the points in the unit cell, that is

$$\mathbf{P}^{nl} = \frac{1}{N}\sum_{j=1}^{N} \mathbf{p}_j^{nl} \ . \tag{5.17}$$

At a point within the unit cell that is also within an inclusion boundary, the mesoscopic nonlinear polarization is set to zero. By symmetry considerations, the x and y components of all macroscopic quantities will average to zero.

The next step is to calculate the effect of the nonlinear mesoscopic polarization on the linear polarization within the inclusions. This is necessary to obtain the linear polarization correct to third order. It is accomplished by summing the contributions to the electric field at a lattice site due to all nonlinear polarizations inside of a suitably large sphere (19 times the inclusion radius) surrounding the lattice site. In order to perform this calculation, a volume element (ΔV) equal to the unit cell volume divided

by N is assigned to each nonlinear polarization in order to convert it to a dipole moment. That dipole moment is then used to calculate the nonlinear contribution to the electric field at the given lattice site,

$$\Gamma = \sum_n \frac{3(\boldsymbol{\mu}^{nl}(\mathbf{r}_n)\cdot\hat{\mathbf{r}}_n)\hat{\mathbf{r}}_n - \boldsymbol{\mu}^{nl}(\mathbf{r}_n)}{r_n^3} \tag{5.18}$$

where

$$\boldsymbol{\mu}^{nl}(\mathbf{r}_n) = \mathbf{p}^{nl}(\mathbf{r}_n)\Delta V, \tag{5.19}$$

and $\mathbf{r}_n$ is a vector from the host nonlinear dipole to the given inclusion site. The sum is over points inside the host and is performed in a manner similar to the mesoscopic electric field calculation.

Since the correction to the linear polarization involves the nonlinear polarization, the total material response is expressed in terms of the displacement field in order to avoid confusion between the linear and nonlinear contributions. The macroscopic displacement is calculated starting with the expression

$$\begin{aligned}\mathbf{D} &\equiv \mathbf{E} + 4\pi\mathbf{P} \\ &= \varepsilon^h\mathbf{E} + 4\pi\mathbf{P}' + 4\pi\mathbf{P}^{nl} \\ &= \varepsilon\mathbf{E} + 4\pi(A + B/2)_{eff}(\mathbf{E}\cdot\mathbf{E}^*)\mathbf{E}\ .\end{aligned} \tag{5.20}$$

Next using [6]

$$4\pi\mathbf{P}' = 3\varepsilon^h \frac{\varepsilon - \varepsilon^h}{\varepsilon + 2\varepsilon^h}(\mathbf{E}^c + \Gamma) \tag{5.21}$$

where f is the inclusion fill fraction (we have used the generalized expression for nondilute fill fractions), and

$$\mathbf{E}^c = \mathbf{E} + \frac{4\pi}{3\varepsilon^h}\mathbf{P}' + \frac{4\pi}{3\varepsilon^h}\mathbf{P}^{nl} \tag{5.22}$$

we eliminate $\mathbf{E}^c$ from (5.21) by substitution of (5.22) into (5.21). The resulting equation is solved for $\mathbf{P}'$ and substituted into (5.20). Doing the simple algebra yields

$$\mathbf{D} = \varepsilon\mathbf{E} + 4\pi\frac{\varepsilon + 2\varepsilon^h}{3\varepsilon^h}\mathbf{P}^{nl} + (\varepsilon - \varepsilon^h)\mathbf{\Gamma} \ . \tag{5.23}$$

After substitution of the computed quantities $\mathbf{P}^{nl}$ and $\mathbf{\Gamma}$, we may examine the ratio of $(A+B/2)_{eff}$ over (A+B/2) in the pure host material. This is the ratio of the second two terms in the displacement field (5.23) to the same quantity in a homogeneous material,

$$\mathbf{D}^{nl} = 4\pi(A + \frac{1}{2}B)(\mathbf{E}\cdot\mathbf{E}^*)\mathbf{E} \ . \tag{5.24}$$

5.4 Results and Discussion

Figure 3 plots the resulting ratio of $(A+B/2)_{eff}/(A+B/2)$ mentioned above vs. the inclusion fill fraction ($\varepsilon^h = 2.25$ and $\varepsilon^i = 8$) for both the cubic lattice and Sipe and Boyd models. The result ends at the maximum packing fraction of $\pi/6$ and displays an enhancement in the nonlinear response over all inclusion fill fractions. As expected, the two results match very closely at low inclusion fill fractions. The cubic lattice results rise slightly above the Sipe and Boyd results for fill fractions of about 20%-35%. Above 45% inclusion fill fraction, the host volume displacement by the inclusions begins to reduce the enhancement. This is not predicted in the single inclusion model of Sipe and Boyd.

The fact that the new calculation does not deviate from the Sipe and Boyd prediction in any significant way up to about 45% fill fraction is probably because the dominant source of enhancement is the linear scaling between the macroscopic electric field and the cavity field given in equation (5.15) and that dipole effects dominate (the first term in the sum of equation (5.10)). This conclusion is supported by noting that the dotted line in figure 5.3, which represents the Sipe and Boyd result with L_h set

equal to 1, lies well below the full Sipe and Boyd result. Differences would then be expected only when the effective medium dielectric constant deviates significantly from the Maxwell Garnett result which does not occur until the inclusion fill fraction reaches approximately 40%. Increased inhomogeneities of the electric fields on the mesoscopic scale that can increase the amount of enhancement apparently were not significant enough in the present calculation to provide for additional enhancement over the Sipe and Boyd result. Most likely it is difficult to obtain large g_h values in an all-dielectric composite material.

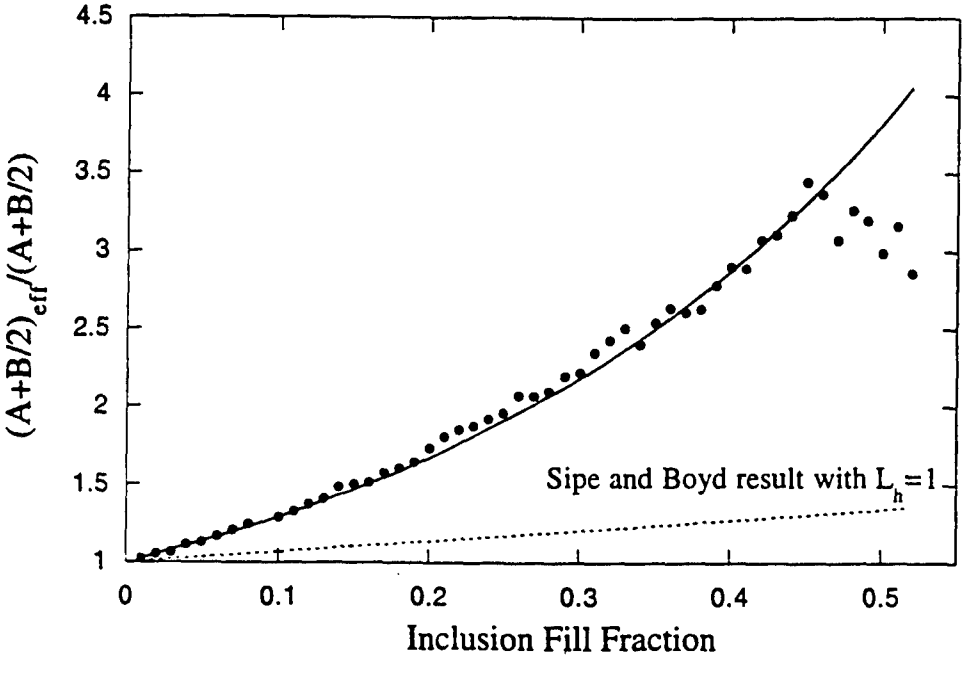

Figure 5.3 Comparison of cubic lattice calculation and the Sipe and Boyd Maxwell Garnett models with $\varepsilon^h = 2.25$ and $\varepsilon^i = 8$. Plotted is the enhancement in the quantity (A+B/2). The solid line represents the Sipe and Boyd result. Oscillations in the calculated points at higher fill fractions are probably artifacts of the calculation program. The dotted line is the Sipe and Boyd result with $L_h = 1$ to illustrate the magnitude of the cavity to macroscopic field scaling.

5.5 References

1. J. C. Maxwell Garnett, "Colours in metal glasses and in metallic films," Philos. Trans. R. Soc. London **203**, 385 (1904); "Colours in metal glasses, in metallic films, and in metallic solutions - II," Philos. Trans. R. Soc. London **205**, 237 (1906).

2. D. Ricard, Ph. Roussignol, and C. Flytzanis, "Surface-mediated enhancement of optical phase conjugation in metal colloids," Opt. Lett. **10**, 511 (1985).

3. R. W. Cohen, G. D. Cody, D. Coutts, and B. Abeles, "Optical Properties of Granular Silver and Gold Films," Phys. Rev. B **8**, 3689 (1973).

4. J. W. Haus, R. Inguva, and C. M. Bowden, "Effective-medium theory of nonlinear ellisoidal composites," Phys. Rev. A **40**, 5729 (1989).

5. P. Sheng, "Theory for the Dielectric Function of Granular Composite Media," Phys. Rev. Lett. **45**, 60 (1980).

6. J. E. Sipe and R. W. Boyd, "Nonlinear susceptibility of composite optical materials in the Maxwell Garnett model," Phys. Rev. A **46**, 1614 (1992).

7. D. Stroud and P. M. Hui, "Nonlinear susceptibilities of granular matter," Phys. Rev B **37**, 8719 (1988).

8. G. S. Agarwal and S. Dutta Gupta, "T-matrix approach to the nonlinear susceptibilities of heterogeneous media," Phys. Rev. A **38**, 5678 (1988).

9. R. W. Boyd and J. E. Sipe, "Nonlinear optical susceptibilities of layered composite materials," J. Opt. Soc. Am. B **11**, 297 (1994).

10. G. L. Fischer, R. W. Boyd, R. J. Gehr, S. A. Jenekhe, J. A. Osaheni, J. E. Sipe, and L. A. Weller-Brophy, "Enhanced Nonlinear Optical Response of Composite Materials," Phys. Rev. Lett. **74**, 1871 (1995).

11. R. C. McPhedran and D. R. McKenzie, "The conductivity of lattices of spheres I. The simple cubic lattice," Proc. R. Soc. London Ser. A **359**, 45 (1978).

12. R. E. Meredith and C. W. Tobias, "Resistance to Potential Flow through a Cubical Array of Spheres," J. Appl. Phys. **31**, 1270 (1960).

13. S. *Y.* Sheu, S. Kumar, and R. I. Cukier, "Simulation of the dielectric constant of a composite material," Phys. Rev. B **42**, 1431 (1990).

14. J. D. Jackson, *Classical Electrodynamics*, pp. 136-38 (2^{nd} ed. Wiley and sons, New York 1975)

Chapter 6

Conclusions

In this thesis both theoretical and experimental investigations into nonlinear optical composite materials have been presented. The outstanding feature of these materials is that the effective nonlinear susceptibility of the composite structure can be significantly larger than the individual susceptibilities of the constituents forming the composite. This useful phenomenon was also found in the investigation of third-order photonic band gap materials. The reason composite materials are able to produce an enhanced nonlinear response is that there can be a very inhomogeneous electric field distribution on the mesoscopic scale that has large effects on the nonlinear response of the bulk. Nonlinear susceptibilities are in general proportional to the higher-order moments of the local field distribution, which tend to increase with increasingly inhomogeneous field distributions, and composite field distributions can be engineered to concentrate the mesoscopic fields in the nonlinear constituent. The accuracy of effective medium theory in describing the nonlinear susceptibilities and investigation of the enhancement phenomenon were the central considerations of this thesis.

The thesis contained four distinct portions. In chapter 2 we compared the predictions of second-order effective medium theory against available exact formalisms for second-harmonic generation in multilayered composites. The system modeled was a composite comprised of alternating layers of a second-order poled polymer and a second material with a higher linear refractive index but no second-order response. Effective medium theory performed very well in predicting an accurate bulk nonlinear response, which is what we expect, but had difficulty with high angle of incidence

linear propagation properties. This difficulty does not diminish the utility or success of the theory however. When the layer pair thickness of an optical composite material is within the bounds of the effective medium approximation, it can be assumed with confidence that the medium may be treated as a single bulk medium with properties described by nonlinear effective medium theory.

Chapter 3 was a continuation of the study of second-order nonlinear layered optical composites with the electrooptic response of such structures examined both theoretically and experimentally. The electrical response of these materials can be complicated and possibly contains new and difficult to describe properties not found in homogeneous materials. However, we found some degree of success in using electrical effective medium theory as presented in describing the electrooptic response of the composite constructed. A third-order composite material composed of alternating layers of a spin cast polymer host with a third-order nonlinear organic dopant and a higher index buffer material (rf sputtered $BaTiO_3$) was constructed. In measurements of both the composite material and individual homogeneous films of each of the constituents, it was found that the composite material had a third-order susceptibility equal to 3.2 times the susceptibility of the doped polymer material, which was the dominant nonlinear constituent. The best prediction available from theory predicted an enhancement of a factor of 2.1 but given the uncertainties and the difficulty of establishing an electrical effective medium theory, the results were in reasonable agreement with effective medium theory. What is more significant however is that the enhancement represents a large and possibly useful increase in the nonlinear response. The many uses of electrooptic materials and the continuing search for better systems provides motivation for further research into these types of composites.

In chapter 4 we moved away from the standard definition of composite materials and considered two-component photonic band gap materials. Again the

motivation was the possibility that a material could be constructed which provided an enhanced nonlinear response over an equivalent amount of homogeneous material composed of either constituent. For radiation incident normally to the surface of a one-dimensional periodic multilayer photonic band gap material, it was found that the third-order response could be enhanced by a factor in the range of 4-6. The band gap structure was composed of two materials of refractive indices 1.5 and 2.0 respectively whose layer sizes were varied around a thickness near a quarter-wavelength and only one constituent was considered to have a nonlinear response. The enhancements were found to occur near the photonic band edge and either the high or low index material's response could be enhanced with slightly better results if the low index material was considered as the nonlinear constituent. Also considered was the situation where a central nonlinear 'defect,' or phase slip, region was introduced whose thickness was larger than the other layers in the otherwise periodic structure. In this case the enhancement factor was found to be approximately 30, representing a significant performance increase. Here again we find that these modeling results provide strong motivation for further theoretical and experimental research.

Chapter 5 considered third-order Maxwell Garnett composites with high fill fractions of the inclusion material. Previous work with Maxwell Garnett composites has only considered dilute fill fractions as the inclusions were assumed to be far apart and therefore were noninteracting in the sense that the field inhomogeneities produced by a given inclusion did not extend to it's nearest neighbors. In the present calculation we arranged the inclusions on a simple cubic lattice and treated the mesoscopic fields in a manner accurate enough to consider inclusion fill fractions all the way up to the close pack limit for such an arrangement. Results from previous work on the conductivity properties of cubic arrays of conducting spheres was utilized to determine the multipole expansions necessary to obtain the interinclusion host fields. The host

medium was considered to be the nonlinear constituent as this arrangement was determined previously to enhance the host nonlinear susceptibility. Our results indicated surprising accuracy of the previous noninteracting inclusion model, which may be due to the fact that we considered all-dielectric composites and the typical dielectric constant differential may not be large enough to introduce significantly larger field inhomogeneities. As a result however, we may with more confidence attempt to construct a moderately high fill fraction Maxwell Garnett composite and expect enhanced nonlinear properties.

The important conclusions of this thesis are that effective medium theory is a valid approximation to the nonlinear optical response of the composite materials investigated, the enhancement of the nonlinear susceptibility under suitable conditions can be a significant multiple of the nonlinear response of the corresponding constituent materials, and that previous all-dielectric Maxwell Garnett results are valid to significantly higher fill fractions than previously thought. Most future work in nonlinear optical composites will probably be directed at the enhancement effect as there are many applications of nonlinear optical materials. The largest obstacles in this field of study are likely to become materials processing issues as in can be very difficult to engineer these materials on the mesoscopic scale.